Integrated Multicore Fibre Devices for Optical Trapping

Ashleigh Louise Barron

A dissertation submitted for the degree of Doctor of Philosophy

Institute of Photonics and Quantum Sciences

School of Engineering and Physical Sciences

Heriot-Watt University

May 2014

Abstract

The work described in this thesis details the development of a multicore fibre device that can be used to optically trap multiple cells and particles. The optical trapping of multiple cells at close proximity allows for cell-to-cell interactions to be studied. Current methods available for creating arrays of traps are free space optical systems that use diffractive optics, laser scanning techniques or the interference of multiple beams to create the multiple traps. A fully integrated, fibre optic based, multiple particles, optical trapping device could be used in non-optical research facilities such as biological laboratories to aid with their research into cellular processes.

In order to create the multiple traps, the distal end of the multicore fibre needs to be modified to induce a lensing effect. The multicore fibre device presented in this thesis was lensed in a fusion splicer; this refracts the outputs from the four cores to a common point in the far field where interference fringes are formed. The initial investigation demonstrated one-dimensional interferometric optical trapping through coupling light into two of the diagonal cores of the lensed multicore fibre. This produced linear interference fringes approximately 250 ± 25 μm from the end of the fibre with a fringe spacing of 2 ± 0.3 μm. The linear interference fringes were used to optically trap polystyrene microspheres with diameters of 1.3 μm, 2 μm and 3 μm in the high intensity regions of the fringes.

Coupling into all four cores using a diffractive optical element produced an array of intensity peaks across the interference pattern with high visibility fringes greater than 80 %. Each intensity peak, spaced 2.75 μm apart could trap a single particle in two dimensions. The optical trapping of multiple microspheres and *Escherichia coli* bacterial cells was demonstrated proving that the lensed multicore fibre has the potential to be used to trap cells in biological experiments. The active manipulation of trapped 2 μm microspheres was also demonstrated through the rotation of the input polarisation to the multicore fibre.

Finally, work towards creating a “turn-key” optical trapping device was demonstrated through the fabrication of a fully integrated multicore fibre device using an ultrafast

laser-inscribed fan-out to couple light into each core. Single mode operation of the device was demonstrated at 1550 nm, using a weaker lensed MCF device. The two dimensional trapping of 4.5 μm polystyrene microspheres was shown in an array of peaks spaced 11.2 μm apart at a distance of 400 ± 25 μm from the end of the fibre.

In memory of my grandparents

Acknowledgements

Firstly I would like to thank my supervisor Professor Ajoy Kar for his guidance and continuous support throughout the duration of my PhD. I am forever grateful for him for giving me the opportunity to carry out the work described in this thesis and also for the many trips he has organised for me. My memories from Japan and India are something I will cherish for a long time.

I would also like to thank my second supervisor Dr Henry Bookey for training me in all aspects of this project. Without his guidance and support I would not have achieved most of the results detailed in this thesis. I would also like to thank Dr Graeme Brown for the training and help he provided me in ultrafast laser inscription and Dr Thomas Aspray for the useful insight into the biological aspects of this project.

My thanks go to all the other members of the nonlinear optics group both past and present in particular Dr John Macdonald, Dr Debaditya Choudhury and Rose Mary for insightful discussions and support throughout the duration of my studies. Special thanks go to my office companions Rose Mary, Peter Kremer and Anusha Keloth for much needed distractions and encouragements that helped me complete this thesis.

I would also like to thank Dr Bill MacPherson for all the outreach opportunities he has given me. It has been a pleasure to go around the country teaching physics to school children. My thanks also go to William Ramsay and David MacLachlan for making these trips even more enjoyable.

I am also grateful to my friends, in particular Martin Smith whom I am fortunate to have had support from him throughout my university career. To Greg McKay for his encouragement and friendship and to Becky O'Hagan for her support and much needed diversions. I am truly grateful to have such amazing friends.

Finally, my family deserve special thanks especially my parents Linda and John Barron, and my siblings Lisa, Graeme and Craig for their encouragement and support. Extra special thanks goes to my sister Lisa for proof reading this thesis for me.

Publications by the author

Peer reviewed journal articles by the author

1. A. L. Barron, A. K. Kar, and H. T. Bookey, "Dual-beam interference from a lensed multicore fiber and its applications to optical trapping." Opt. Express **20,** 23156-23161 (2012). This paper is the cover image of the issue and was Optics InfoBase image of the week commencing 5th November 2012.

2. A. L. Barron, A. K. Kar, T. J. Aspray, A. J. Waddie, M. R. Taghizadeh, and H. T. Bookey, "Two dimensional interferometric optical trapping of multiple particles and *Escherichia coli* using a lensed multicore fiber," Opt. Express **21,** 13199-13207 (2013). This paper was highlighted in The Virtual Journal of Biomedical Optics, **8**(11), (1st Aug. 2013). This was a paper was also Optics InfoBase image of the week commencing 3rd June 2013.

Conference papers by the author

1. H. Bookey, A. Barron, A. Kar, R. Stepien, D. Pysz, and R. Buczynski, "Multicore fibre probes for nonlinear optical measurements," *European Conference on Nonlinear Optical Spectroscopy (ECONOS),* University of Twente, Enschede, Netherlands (2011). Paper O30.

2. A. L. Barron, A. K. Kar and H. T. Bookey, "Lensed Multi-core Fiber for Interferometric Optical Tweezing Applications," *Conference on Lasers and Electro-Optics (CLEO),* San Jose, California (2012). Paper CTh1G.7.

3. A. L. Barron, A. K. Kar and H. T. Bookey, "Multi-beam interference from lensed multicore fibre probes," *Fibre Optic and Waveguides symposia, Photon 12*, Durham University, UK (2012).

4. A. L. Barron, G. Brown, A. K. Kar, and H. T. Bookey, "Lensed multicore fiber for interferometric optical trapping," *Photonics 2012,* Chennai, India (2012). Paper T2A.5.

5. A. L. Barron, A. K. Kar, A. J. Waddie, M. R. Taghizadeh, and H. T. Bookey, "Two dimensional trapping using four core interference from a lensed multicore fiber," *CLEO-PR&OECC/PS 2013,* Kyoto, Japan (2013). Paper ThL1-4.

6. A. L. Barron, A. K. Kar, G. Brown, T. J. Aspray, A. J. Waddie, M. R. Taghizadeh, and H. T. Bookey, "Optical trapping using a lensed multicore fiber," *Workshop on specialty optical fiber and their applications (WSOF),* Sigtuna, Sweden (2013). Paper T1-3.

7. A. L. Barron, A. K. Kar, G. Brown, T. J. Aspray, A. J. Waddie, M. R. Taghizadeh, and H. T. Bookey, “Interferometric Optical Trapping using a Lensed Multicore Fibre,” *Aston Institute of Photonic Technologies Student Conference 2013*, Aston University, Birmingham, UK (2013).

8. A. L. Barron, and A. K. Kar, “Multicore fibres - Applications in optical trapping” *International Conference on Optics and Optoelectronics, ICOL 2014*, Dehradun, Uttarakhand, India (2014).

Contents

List of Figures

List of abbreviations

ASE	Amplified spontaneous emission
CW	Continuous wave
DFB	Distributed feedback laser
DOE	Diffractive optical element
E. coli	*Escherichia coli*
EDFA	Erbium doped fibre amplifier
FBG	Fibre Bragg grating
FMF	Few mode fibre
GFP	Green fluorescent protein
IR	Infra-red
LED	Light emitting diode
MC-EDFA	Multicore Erbium doped fibre amplifier
MCF	Multicore fibre
MFD	Mode field diameter
MIMO	Multiple-input multiple-output
MMF	Multimode fibre
MOPA	Master oscillator power amplifier
NA	Numerical aperture
PDM-QPSK	Polarization-division-multiplexed quadrature-phase-shift-keying
PROFA	Pitch reducing optical fibre array
RF	Radio frequency
SDM	Space division multiplexing
SLM	Spatial light modulator
SMF	Single mode fibre
TA-MCF	Trench assisted multicore fibre
TLS	Tuneable laser source

ULI	Ultrafast laser inscription
UV	Ultraviolet
WDM	Wavelength division multiplexing

Chapter 1. Introduction

1.1. Motivation

There is currently a lot of interest in developing multicore fibres and expanding their applications in a variety of different fields including data communications, fibre lasers and sensors. Research into the use of multicore fibre for data communications has developed fibres that either enhance or reduce crosstalk that have found uses in other applications such as phase locked fibre lasers. The use of fibres has advantages over free space optics such as flexibility, integration and their compact nature. Where multiple beams are used, multicore fibres have advantages over fibre bundles, such as increased stability, as each core will undergo the same environmental changes like temperature increases, vibrations and pressure changes. The overall size is also decreased as multiple cores can be designed in a fibre the same width as a single core fibre. The core separations throughout the fibre are constant in comparison to fibre bundles that are made by inserting multiple single core fibres into a capillary, adding extra functionality to MCF's is less difficult and more repeatable than for a fibre bundle. Integrating multicore fibres with optical components such as diffractive optical elements and fan-out devices allows light to be coupled evenly into each core. An application where this would be advantageous is in optical trapping. A completely integrated probe could be created that will have increased flexibility over standard optical traps that use free space optics, allowing *in vivo* trapping studies to be carried out. The use of multicore fibre also allows us to explore interferometric optical trapping for the manipulation of multiple particles. Interferences fringes in the far field output are used to form either one dimensional or two dimensional traps. Trapping multiple particles at equally spaced sites in two dimensions could be advantageous for cell separation where an optical tweezer could be used to remove single particles from the two dimensional array. Trapping cells at equally spaced distances will also allow cell to cell interactions to be examined such as the formation of biofilms, quorum sensing, floc formation and metabolic cooperation studies.

1.2. Background

Modern optical fibres were born in the 1950's with fundamental research focusing on applications in medicine to replace rigid endoscopes with flexible fibre bundles [1, 2]. After the invention of the laser in 1960 [3], the application of optical fibres for long distance communication started being investigated as a replacement for copper wires [4]. At that time they showed promise for low loss transmission with the potential for higher data transmission rates. However it wasn't until 1966 when Kao and Hockham proposed that the fundamental limit on glass transparency is low enough for use in communications [5]. Kao won the 2009 Nobel prize in physics for ground breaking achievements concerning the transmission of light in fibres for optical communication [6]. By the 1970's low loss optical fibres were being commercially produced by Corning. Optical fibres were seen as the much needed replacement for coaxial cables to provide communication links across the Atlantic, with losses as low as 0.16 $dB.km^{-1}$ at 1550 nm [7], fewer repeaters would be needed resulting in lower costs compared to coaxial cables. In December 1988, the first transatlantic fibre optic cable, TAT-8 began service using 1310 nm light. 1310 nm is the zero dispersion wavelength for single mode silica fibres where the material dispersion and the waveguide dispersion cancel out. TAT-8 was able to carry 35,000 phone calls equivalent to 9 times that of its coaxial cable predecessor TAT-7 [8]. Fibre optics had shown they were more than capable of replacing coaxial cable for world-wide communications, the transatlantic telecommunications cables that followed TAT-8 operated at 1550 nm, where fibre loss is at its lowest, this provided even higher data rates [8]. The invention of the Erbium doped fibre amplifier (EDFA) in 1987 [9] allowed the signal to be optically amplified rather than converted into an electrical signal before amplification. The EDFA has a large gain bandwidth of tens of nanometers from 1525 – 1565 nm for the C-band and from 1570 – 1610 nm for the L-band. EDFA's can simultaneously amplify data channels at different wavelengths across the gain bandwidth due to inhomogeneous broadening of the linewidth of the Erbium dopant ions. This technique is useful in wavelength division multiplexing (WDM), where the data capacity of the fibres can be increased by using different wavelengths along the same fibre. WDM allows for the data capacity expansion of the networks without the need to lay more fibres. The first transatlantic cable to utilise WDM was TAT-12/13, originally deployed in 1995 as the first commercial transatlantic system that made use of EDFA technology [10]. It had a

bit rate capacity of 5 Gbit.s^{-1} using a single wavelength. In 1999, the TAT-12/13 was upgraded with WDM technology to allow for a 20 Gbit.s^{-1} capacity. This was followed in 2001 with the deployment of TAT-14 that uses 16 wavelengths and provides a total data capacity of 1.87 Tbit.s^{-1} from four fibres [11]. TAT-14 was the last publicly owned transatlantic communications cable owned by a consortium of companies from the different countries it connected. Since it was deployed there has been privately owned companies working on transatlantic communication cables. Hibernia networks are currently working on Project Express, the first transatlantic cable in over a decade [12]. Originally scheduled for completion in summer 2012 this has been delayed due to problems with vendors. When complete the cable will provide sub 60 ms latency and will initially be deployed with 40G technology with the ability to be upgrade to 100G in the future [12].

Since the 1980's the data capacity of optical fibre has increased 10 fold every four years [13]. It is expected that within the next decade networks will reach their data capacity limit [14]. The data capacity limit of standard single mode fibres (SMF) is 100 Tbit.s^{-1}, defined by the nonlinear Shannon capacity limit. The Shannon limit for SMF corresponds to filling the C and L bands of the EDFA at 10 bit.s^{-1}.Hz^{-1} spectral efficiency. Optical fibre is a Kerr nonlinear medium, when the power transmitted inside the core is increased, the capacity of the fibre also increases, however high power also causes the refractive index of the core to change through the Kerr nonlinear effect. The change of refractive index of the core distorts the WDM channel which cannot be fully compensated resulting in a limit of the data capacity carried along the fibre. The nonlinear refractive index (n_2) of SMF-28 is (2.53 ±0.09) x 10^{-20} m^2 .W^{-1} at 1550 nm [15].

A solution to this data capacity limit is to use space division multiplexing (SDM). SDM will not only increase the data capacity of each fibre but will also increase the energy efficiency and reduce the cost per unit [16]. There are two main approaches to implementing SDM by using different modes within multimode fibre (MMF) or by using multicore fibre (MCF). The multiple modes technique requires multiple-input multiple-output (MIMO) techniques to be used at the receiver to account for crosstalk between the modes as they travel along the fibre. MMF's can be designed to carry only

a small number of modes, known as few mode fibres (FMF's). In FMF's the mode coupling is significantly reduced compared to standard MMF. FMF's have been shown to be practical for long distance transmissions by transmitting a distance of 1050 km in a recirculating loop without modal dispersion [17]. Recently, speciality FMF's have been designed to minimise mode coupling, such as fibres capable of transmitting orbital angular momentum modes [18]. Bozinovic et al., demonstrated the transmission of 400 Gbit.s^{-1} over a 1.1 km fibre using four angular momentum modes operating at a single wavelength and a transmission of 1.6 Tbit.s^{-1} using two orbital angular momentum modes operating over ten different wavelengths. The fibre supports the first order antisymmetric modes: one transverse electric mode (TE_{01}), one transverse magnetic mode (TM_{01}) and two orbital angular momentum modes of opposite topological charges $l = \pm 1$ in addition to the two degenerate polarisation states of the fundamental mode ($LP_{01}^{\pm}$) that is supported by conventional SMF's. The FMF used in this experiment is known as a vortex fibre that has a high refractive index ring surrounding the core designed to lift the near degeneracy between the optical angular momentum modes and the parasitic TM_{01} and TE_{01} modes. This minimises the crosstalk between the modes [18].

MCF's are single optical fibres with multiple cores. The main disadvantage of MCF's is crosstalk. This is the transferal of light between cores due to interactions between each core mode. To reduce crosstalk, the cores are spaced well apart and variations of the core diameter and refractive index can also help to reduce the crosstalk [19]. Core-to-core coupling can also be reduced by incorporating a trench of lower refractive index around each core to confine the mode [20]. The use of MCF has increased the data capacity limit above that of single mode fibre, the highest data transmission reported so far is 1.01 Pbit.s^{-1} [21]. In 2012 the highest data transmission achieved thus far was demonstrated using a fibre that combines both MCF and FMF techniques. A capacity of 1.05 Pbit.s^{-1} was transmitted using a hybrid MCF with single and few mode cores [22]. These results show that MCF's are a viable solution to overcome the data capacity limit for use in future networks.

The research into MCF for data communications has broadened their use in a variety of different applications. Core to core coupling in MCF's can be exploited for use in fibre

lasers. MCF could be useful for high power single frequency lasers through the production of supermodes. Supermodes are formed when all the single mode cores of the MCF are locked together in the same phase. This is due to interactions between the evanescent fields of the single mode cores of the MCF. The supermode produced has a mode field diameter (MFD) five times bigger than the fundamental mode showing that these lasers could be useful for compact, high power single frequency lasers [23]. MCF lasers can also be fabricated with different dopants in each core giving the prospect of multi-band lasers when pumped from a common source [24]. Similarly to fibre lasers, the compact nature of MCF's is advantageous over bulk laser systems. With the added ability of different core dopants, MCF's have further advantage over fibre lasers in creating compact multi-band sources.

Optical fibres have proven useful as fibre sensors; their small size allows for the embedding inside mechanical structures such as aircraft wings, or buildings. Optical fibres have an advantage over electrical strain gauges as they are immune to electrical interference and are safe to use in hazardous environments. Bragg gratings written in the cores can act as strain gauges, these can be used for curvature measurements; MCF's have been shown to be able to provide both transverse and longitudinal axes measurements simultaneously by having Bragg gratings written into three cores of a four core MCF [25]. This use of MCF's is beneficial over SMF's as they can provide two dimensional bend measurements. MCF's have further advantages over fibre bundles as their shared cladding means each core will be under the same temperature changes, mechanical strain, vibrations and other environmental influences. MCF's can have the same diameter size as a SMF's, allowing for the use in applications where space and weight limit is paramount such embedding in aircraft wings.

Optical fibres provide greater flexibility over free space optics, allowing for the creating of compact devices. MCF's have also proven beneficial over fibre bundles for ultra-high resolution endoscopy [26]. The end of fibres and fibre bundles can be functionalised for use in biophotonics such as optical tweezing [27, 28] and optical transfection [29]. The use of MCF's in optical trapping will eradicate the limitations of optical trapping using bulky free space microscope systems. Optical trapping of multiple particles has so far only been achievable using free space optics and a variety

of techniques such as computer generated holograms to produce multiple beams [30], using diffractive optics to create arrays of optical traps [31], and also using interferometric techniques [32]. This thesis will present work on using a lensed multicore fibre for interferometric optical trapping for both one and two dimensions. A lensed muticore fibre is a MCF that's end has been modified to refract the output beams to a common crossing point in the far field where interference fringes are produced that are suitable for optical trapping and manipulation.

1.3. Aims and objectives of the project

The aims and objectives of the project on multicore fibre optical trapping devices are stated below. The results and details of the research working towards these aims are described in this thesis.

- To modify (functionalise) the end of a multicore optical fibre to induce an optical trapping region at the output.
- To create an interferometric optical trapping device using a multicore optical fibre and demonstrate the trapping and manipulation of multiple particles.
- To design and create a compact, cost effective trapping device using readily available equipment in a laboratory.
- To demonstrate two dimensional optical trapping of multiple biological cells using a multicore optical fibre trapping device.
- To create a fully optically integrated "turn-key" multiple particle optical trapping device, which would be suitable for use in non-optical based laboratories such as biological laboratories.

1.4. Thesis outline

The work in this thesis addresses the optical trapping of multiple particles by interferometric techniques using a lensed multicore fibre. Both one and two dimensional trapping is demonstrated. Work is presented using a variety of coupling techniques such as a diffractive optical element (DOE) and a fully integrated fan-out device fabricated using ultrafast laser inscription (ULI).

In Chapter 2, the various applications of MCF's are presented such as their use in data communications, fibre lasers and sensors. Different designs of MCF's are discussed for their uses in these different technologies.

Chapter 3 gives an introduction into optical trapping and particle manipulation. Multiple particle manipulation techniques and the various methods used to generate multiple optical traps are reviewed. The advantages of fibre based traps over free space optical traps are discussed.

The functionalisation of the lensed fibre probe is discussed in Chapter 4. One dimensional interferometric optical trapping using the lensed MCF device to produce linear interference fringes by coupling light into two of the diagonal cores is also demonstrated.

Two dimensional interferometric optical trapping is demonstrated in Chapter 5. A custom made DOE is used to couple light evenly into all four cores of the MCF. The optical trapping and manipulation of multiple microspheres and biological particles is presented.

Chapter 6 presents work towards creating a fully integrated trapping probe using an ULI inscribed, three dimensional fan-out device to individually address each core of the lensed MCF probe. Trapping at a high water absorption wavelength of 1550 nm is demonstrated using a single mode fan-out device.

Finally, Chapter 7 draws conclusions from the research and discusses future work prospects in this research field.

1.5. Summary

The development of multicore fibre has concentrated on next generation data communication systems. Space division multiplexing using a MCF allows for the data capacity of a single fibre to break through the boundary currently set by the Shannon

limit of 100 Tbit.s^{-1} for SMF. The development of MCF for data communications has been exploited for other applications such as fibre lasers [23] and sensors [25]. The compact nature of MCF provides greater flexibility over free space optics. The work presented in this thesis will demonstrate how MCF can be used as an alternative to free space optics for creating a "turn-key" multiple particles, optical trapping device which could be used in non-optics based laboratories such as biological laboratories.

Chapter 2. Multicore Fibres: Design and Applications

In this review chapter the design and applications of multicore fibres will be discussed. Current research into multicore fibres for data communications, sensing applications and fibre lasers will be reviewed highlighting their significance to the work detailed in this thesis.

2.1. Optical fibres

The most common type of optical fibre is SMF with a step index refractive index profile. The fibre has a central core with a refractive index, n_{core}, surrounded by a cladding layer with a lower refractive index of n_{clad}, as shown in Figure 2.1. Light is guided in the core by total internal reflection from the core cladding interface.

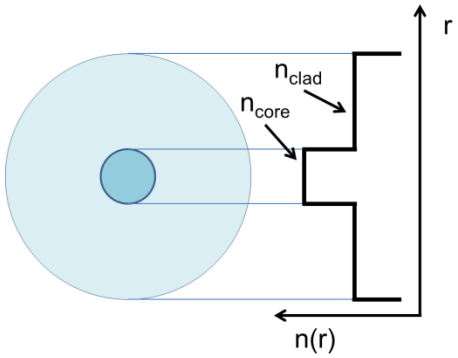

Figure 2.1. Cross section of an SMF with its refractive index profile.

2.2. Single mode fibre propagation

Single mode propagation in a step index fibre can be described by the following wave equation derived from Maxwell's equations [33-35], where ψ can represent the electric field, E or the magnetic field, H.

$$\nabla^2\psi = \varepsilon_0\mu_0 n^2 \frac{\partial^2\psi}{\partial t^2} \qquad (2.1)$$

ε_0 is the vacuum permittivity, μ_0 is the vacuum permeability, n is the refractive index and $\varepsilon_0\mu_0 = \frac{1}{c^2}$. Solutions of the wave equation for fibres with cylindrical symmetry and propagating in the z direction are in the form:

$$\psi = \psi_0(r, \phi)\exp(-i\omega t + i\beta z) \tag{2.2}$$

where β is the propagation constant and ω is the angular frequency. Substituting this equation into equation (2.1) gives the following:

$$\frac{\partial^2\psi_r}{\partial r^2} + \frac{1}{r}\frac{\partial\psi_r}{\partial r} + \left(k_0^2 n^2 - \beta^2 - \frac{l^2}{r^2}\right)\psi_r = 0 \tag{2.3}$$

k_0 is the free space wave number given by $k_0 = \frac{\omega}{c} = \frac{2\pi}{\lambda_0}$, l is a constant and r is the cylindrical coordinate. For a step index fibre where the refractive index changes monotonically across the core cladding interface the solutions of equation (2.3) leads to a range of allowed discrete values of β when $k_0^2 n_c^2 > \beta^2 > k_0^2 n_{cl}^2$ that correspond to guided modes, where n_{cl} is the refractive index of the cladding and n_c is the refractive index of the core. For step index fibres there is a small difference of index of refraction between the core and the cladding leading to weak guiding. We can substitute in a dimensionless transverse propagation constant for the core, $U = r^{1/2}\psi_r$ for the when 0 < r < a and the dimensionless transverse propagation for the cladding of $W = r^{1/2}\psi_r$ for when r > a, where a is the core radius. This gives the following equations:

$$U = a(k_0^2 n_c^2 - \beta^2)^{1/2} \tag{2.4}$$

$$W = a(\beta^2 - k_0^2 n_{cl}^2)^{1/2} \tag{2.5}$$

Using equations (2.4) and (2.5), the normalised frequency parameter V can be defined as the following:

$$V = (U^2 + W^2)^{1/2} = k_0 a(n_c^2 - n_{cl}^2)^{1/2} \tag{2.6}$$

For single mode step index fibres there is a cut off frequency of V = 2.4048 corresponding to the shortest wavelength where only single mode propagation is supported by the fibre typically in the form of the LP_{01} mode.

2.3. Multicore fibres

MCF's are single optical fibres with multiple cores as shown in Figure 2.2. These cores can be arranged in a variety of patterns to suit the application.

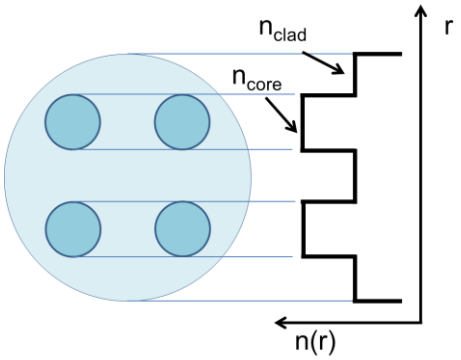

Figure 2.2. Cross section of a 4 core MCF with its refractive index profile.

The above illustration is an example of a MCF showing a single fibre with multiple cores in a shared cladding. MCF's are available in a variety of different designs to suit individual applications. In data communications the most common MCF's have hexagonal arranged cores with either 7 or 19 cores. For creating two dimensional interference patterns as demonstrated in this thesis, 4 cores with a square arrangement is sufficient.

2.4. Crosstalk

Crosstalk is the coupling of light from one core to another due to interactions between each core with another core's cladding mode. This can be desirable for some applications such as fibre lasers. However for applications such as data transmission, crosstalk in MCF's is seen as their greatest disadvantage. Crosstalk in data transmission

reduces the capacity of the MCF, the crosstalk can be reduced by spacing the cores further apart however this reduces the number of cores per fibre and thus limiting the total capacity of the fibre. The practical limit of the number of cores that can be used for communication is a much debated topic at conference discussions. The limit is generally thought to be 19 cores allowing the crosstalk to be low enough to allow for long distance transmissions and limiting the diameter size of the MCF before the flexibility is reduced and it behaves like a glass rod [36].

Cores arranged in a hexagonal pattern are used for high capacity data transmission due to their greater packing density. It has been reported that for practical limits of crosstalk of < 50 $dB.km^{-1}$, step index MCF's should have a core-to-core distance of at least 45 µm to allow a low crosstalk transmission with a large effective area, A_{eff}, and single mode operation [37]. The same study showed that for trench assisted MCF (TA-MCF) the core-to-core distance can be lowered to 35 µm [37]. Trench assisted MCF's are MCF's with a lower refractive index around the core in the cladding region of the fibre as shown in Figure 2.3. The trench around the cores reduces the crosstalk between the cores by supressing the electric field distribution in each core due to the refractive index difference.

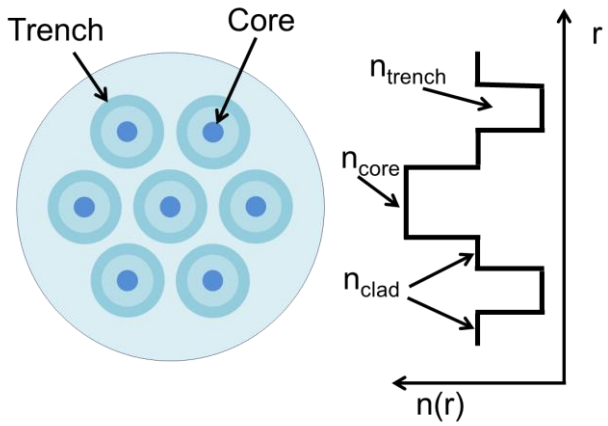

Figure 2.3. Cross section of a 7 core TA-MCF with its core refractive index profile.

Another technique for reducing the crosstalk in MCF's is by using heterogeneous cores. Small changes in the refractive index of the cores or the diameters of the cores have

been shown to reduce crosstalk in comparison to MCF's with homogeneous cores [19]. The MCF contains identical and non-identical single mode cores arranged so that the crosstalk between adjacent cores becomes small. The power transferred between non-identical cores is lower than between identical cores allowing the cores to be positioned closer together as they have reduced core to core interactions. Researchers at Hokkaido University and Yokohama, Japan found that the higher the difference of refractive index between the core and the cladding, the closer the cores can be arranged [19]. They proposed heterogeneous MCF's with three difference core refractive indices. The MCF with core-cladding refractive index differences of 0.38%, 0.39% and 0.40% were shown to have a core-to-core spacing of 40 µm to achieve crosstalk of < -30 $dB.km^{-1}$. They proposed heterogeneous MCF's with higher core-cladding refractive index differences of 1.15%, 1.20% and 1.25% with core-to-core spacing of 23 µm. Both fibres were designed to have single mode operation at 1550 nm and are shown schematically in Figure 2.4.

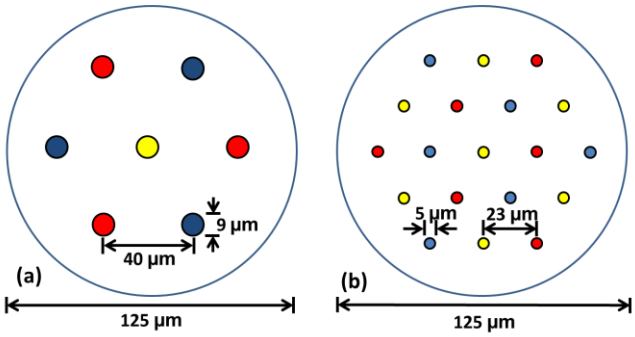

Figure 2.4. Heterogeneous MCF with (a) low core-cladding refractive index differences and, (b) high core-cladding refractive index differences. This figure has been taken from [19].

2.5. Data transmission applications

Research into MCF's has been driven, in recent years, by their potential use in data transmission applications. The use of MCF's allow the data capacity per fibre to increase over the fundamental limit of SMF's of 100 $Tb.s^{-1}$ determined by the Shannon capacity limit [14].

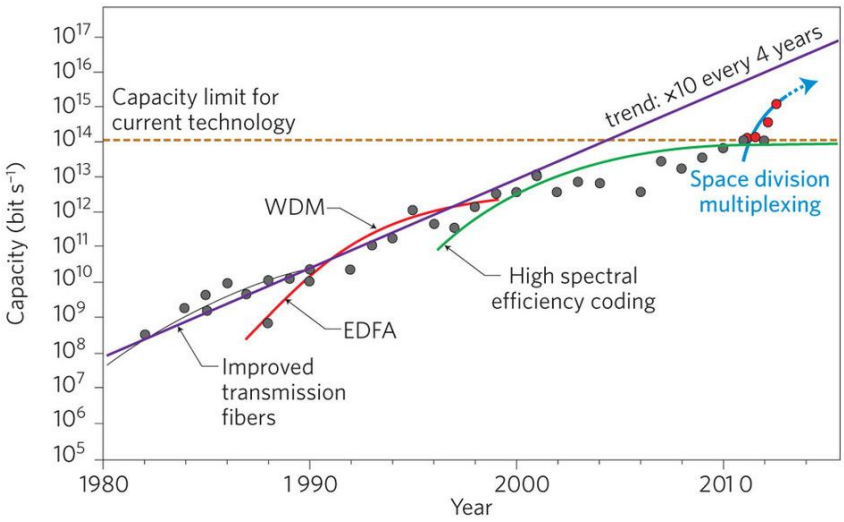

Figure 2.5. The evolution of transmission capacity in optical fibres over the past 30 years due to technological breakthroughs. This figure has been taken from [13].

The orange line in Figure 2.5. represents the Shannon limit for SMF's. Recent advances using MCF's for SDM have shown to break this limit, making them viable to cope with the high capacity demand of future communication networks. In 2012, the data capacity of MCF's surpassed 1 P.bit.s^{-1}, Takara et al., demonstrated 1.01 P.bit.s^{-1} transmission over 52 km using a 12 core TA-MCF [21]. The 12 cores of the TA-MCF are arranged in a single ring with a core pitch of 37 µm and a cladding diameter of 225 µm as shown in Figure 2.6. The cores are arranged in such a way, that each core has two nearest neighbours and experience the same level of crosstalk of -57 dB.km^{-1}, in comparison to hexagonal arranged cores where the centre core has a higher level of crosstalk than the outer cores [13].

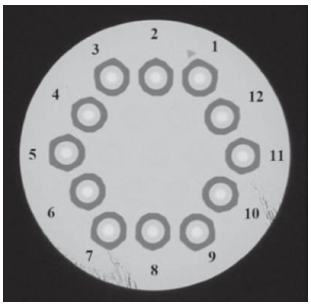

Figure 2.6. Cross section of the 12 core TA-MCF used to transmit 1.01 P.bit.s^{-1}. This figure has been taken from [21].

Techniques for expanding the data capacity of fibres such as using WDM can also be used in MCF's. For example for the above fibre the data was transmitted using 222 WDM channels, filling the C and extended L bands of the EDFA with a spacing of 50 GHz [21].

The longest transmission distance over an MCF so far is 6160 km, as demonstrated by Takahashi et al., using a 7 core MCF [38]. This paper was also the first to report Multicore Erbium-doped Fibre Amplifiers (MC-EDFA's) for long haul transmissions capable of crossing oceans. The MCF has a cladding diameter of 200 µm and a core pitch of 56 µm as shown in Figure 2.7.

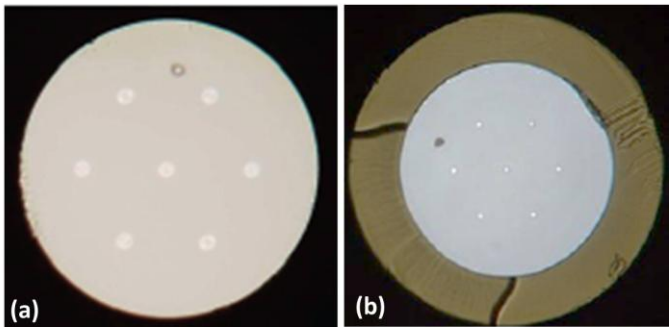

Figure 2.7. (a) Cross section of the 7 core MCF, and (b) cross section of the 7 core MC-EDFA used for long haul transmission. This figure has been taken from [38].

The transmission distance of 6160 km was reached using a 55 km length of MCF, where the transmission line was created in a loop with the cores linked in series. The output of core 1 of the MCF connected to input of core 1 of the MC-EDFA, the output of core 1 of the MC-EDFA was then connected to the input of core 2 in the MCF and so on for all 7 cores of the fibre. This loop was repeated 16 times to reach the reported 6160 km transmission distance. Using this fibre, 40 WDM channels of 128 G.bit.s^{-1} polarization-division-multiplexed quadrature-phase-shift-keying (PDM-QPSK) signals were transmitted along each core of the MCF. The total net capacity of the fibre is 28.8 T.bit.s^{-1}; a capacity distance product of 177 P.bit.s^{-1}.km^{-1} per fibre was achieved [38]. This work shows that MCF's can be used in long distance communication networks of the future and are capable of reaching the high data capacity demand that will exist for internet traffic and future data communication systems.

The research into MCF for data communications has impacted the work described in this thesis by providing affordable low loss fibres. This is just one of many examples where new fabrication processes of MCF are having an impact in an area other than data communications. In particular the development of optical interconnects for coupling light into and out of the fibre cores has eased the difficulty of integration of the MCF device described in this thesis.

2.6. Optical interconnects

The main disadvantage of using MCF's is the difficulty of coupling light into and out of their cores due to their close proximity and geometrical arrangement. There are a variety of different techniques used to fabricate devices suitable for coupling light into MCF's with companies such as Chiral [39] and Optoscribe [40], offering custom made fan-out devices to address each core of the MCF individually.

Researchers at the National Institute of Information and Communications Technology (NICT), Japan have created a free space optical device based on prisms to couple light into each core of their 19 core fibre as shown in Figure 2.8. [41, 42].

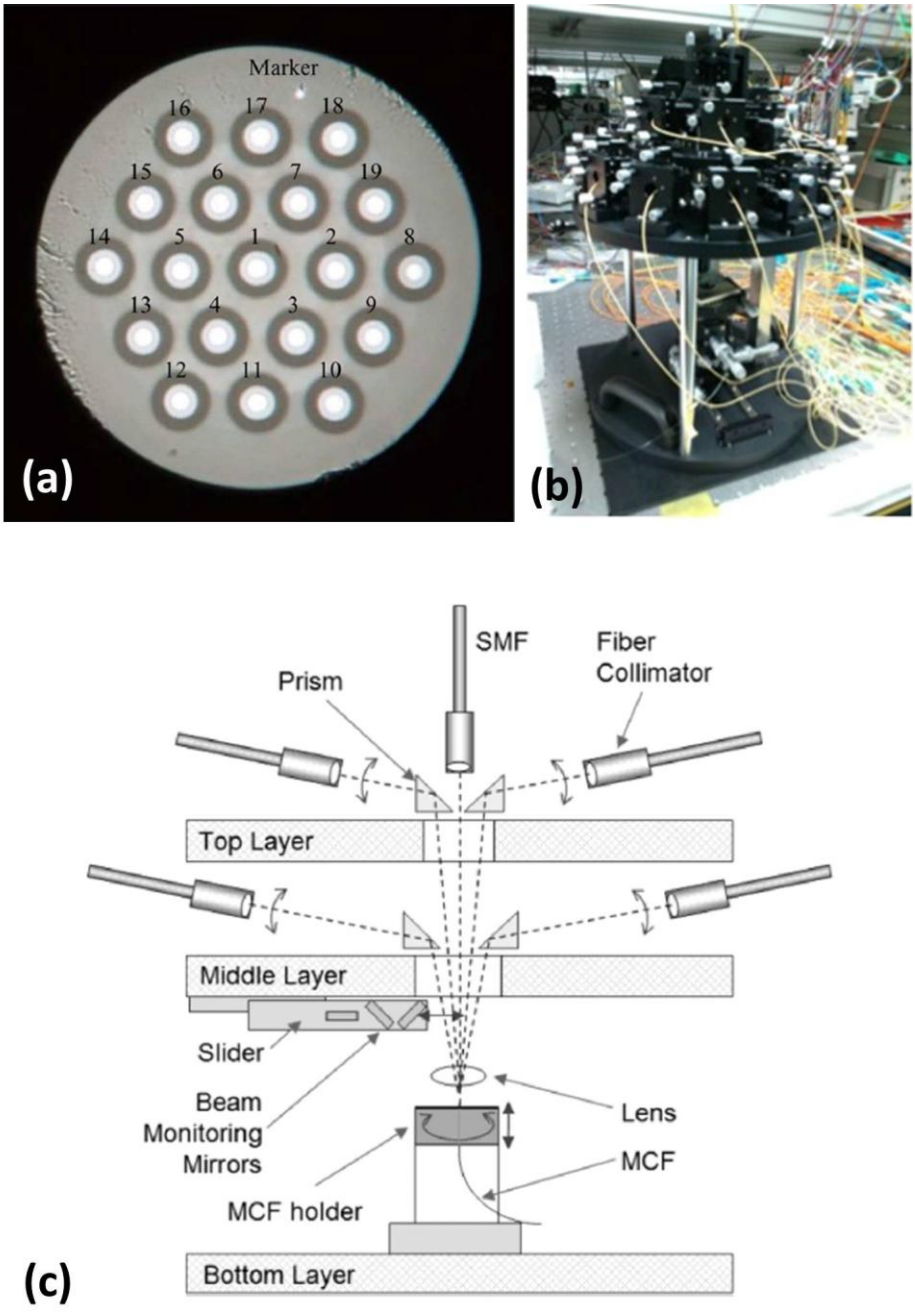

Figure 2.8. (a) Cross section of the 19 core MCF, (b) 19 channel free space coupling device and (c) schematic of the free space coupling device. Figure (a) and (c) has been taken from [42].

The coupling device uses two layers of prisms to couple light from 19 SMF's to the 19 cores of the MCF. This is a large device with height 43 cm and width 30 cm, however it was shown to demonstrate low insertion losses of 1.3 ± 0.3 dB across all 19 cores [41]. Due to the size of this device it wouldn't be suitable in practical

telecommunication applications, but the device offers flexibility over different MCF designs and core spacing allowing the same device to be reused for different fibres which other coupling techniques such as tapered fibre bundles or fan-out devices cannot offer.

For the 12 core TA-MCF shown in Figure 2.6 fan-in/ fan-out devices were designed to couple light into and out of the MCF [21]. The fan-in/ fan-out devices were made by stacking small diameter single mode fibres together, each with a diameter of 37 µm; the MCF is placed in a v-groove and is fusion spliced to the device. The measured insertion losses for the fan-in/ fan-out devices were 0.7 - 2.9 dB and 0.7 – 2.0 dB respectively, this includes the splice losses [21]. These high losses could be due to the mismatch of effective core area (A_{eff}); the A_{eff} of the MCF is 80.7 μm^2 at 1550 nm whereas the A_{eff} of the small diameter fibre used in the fan-in/ fan-out devices is 88 μm^2 [21].

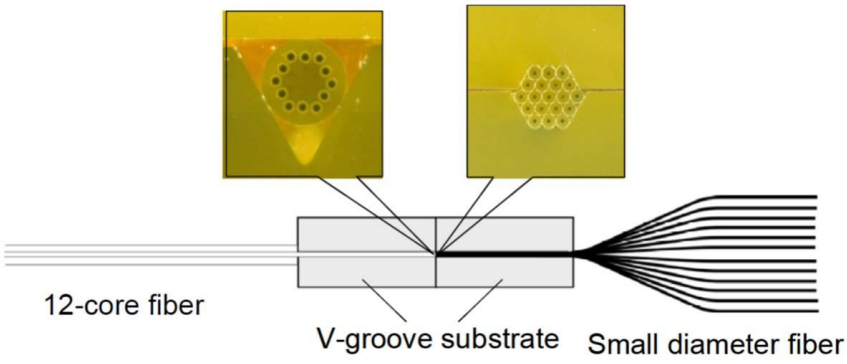

Figure 2.9. 12 core MCF fan-out device. This figure has been taken from [21].

Figure 2.9 shows a schematic of the fan-out device used to couple light into and out of the 12 core, 225 µm diameter MCF. It is made with stacks of small diameter fibres with the outer fibres used to couple light into the cores of the MCF. There is no fine alignment control over the positioning of the fibres relative to the cores of the MCF, the alignment relies on the cores of the MCF matching up with the stacking of the small diameter fibres. This may be the cause of the large variation of insertion loss for the

device. This device or fabrication method is also not scalable for use with fibres of different core arrangements.

Chiral Photonics sell optical interconnects using a tapered fibre bundle method [43]. Known as pitch reducing optical fibre array (PROFA), the device is made by tapering single core fibre together to match the core spacing of the MCF as shown in Figure 2.10. Insertion losses ranging from 0.7 – 1.05 dB per core of a single connector have been reported [43]. Similarly to the previous technique, this would be difficult to implement for MCF's that don't have hexagonal core arrangements because the fibres are stacked together before tapering and naturally align into a hexagonal arrangement.

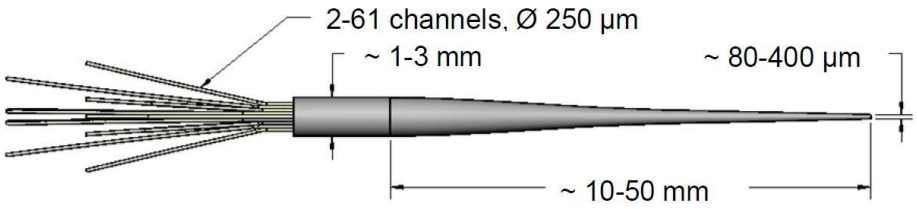

Figure 2.10. PROFA optical interconnect. This figure has been taken from [43].

Similar types of optical connectors have been demonstrated in optical network experiments for a variety of different core number MCF's [44].

Fan-out devices where there is more control over the position of the waveguides to couple light into each core of the MCF have been demonstrated [45, 46].

Watanabe et al., demonstrated a laminated polymer waveguide fan-out device with losses ranging from about 4 – 10 dB per core, due to fabrication error the position of some of the cores were offset and some of the spot sizes were mismatched leading to a higher loss for some of these cores [46]. The fan-out device was fabricated using film deposition and photolithography techniques; the core spacing in the lateral direction was controlled using an electron beam written photomask. In the vertical direction the core spacing was controlled using spin coating with viscosity control of the epoxy resin

cladding. The waveguides can only be written in two dimensions resulting in the input waveguides also being displaced vertically as shown in Figure 2.11.

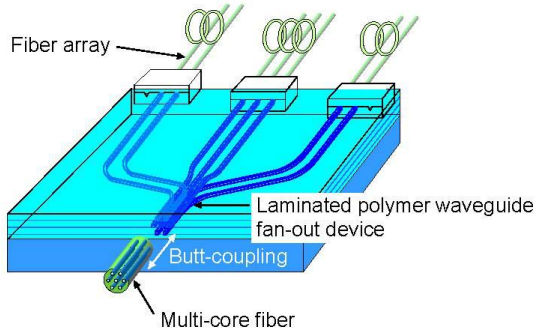

Figure 2.11. Laminated polymer waveguide fan-out device for a 7 core MCF. This figure has been taken from [46].

Three dimensional fan-out devices have been demonstrated using ultrafast laser inscription, enabling each core of an MCF to be addressed by a single mode fibre held in a v-groove array [45]. Femtosecond laser pulses modify the glass substrate by positively changing the refractive index to create waveguides. By focusing the femtosecond laser pulses into the dielectric material, optical energy is deposited in the focal region due to multi-photon absorption, tunnelling ionisation and avalanche ionisation processes [47]. The substrate can be moved in the x, y and z directions allowing three dimensional structures to be written. This can be used to create a fan-out device with waveguides with the same spacing and geometry as the MCF and the other side of the fan-out is designed to have waveguides in a one dimensional plane to match a v-groove array as shown in Figure 2.12.

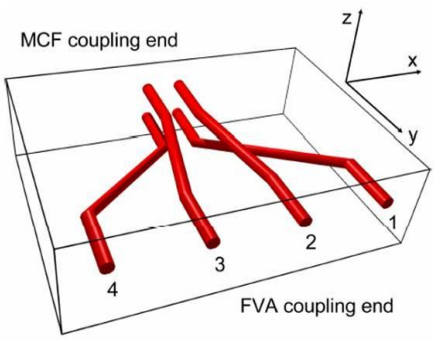

Figure 2.12. Three dimensional ULI fan-out device for a 4 core MCF. This figure has been taken from [45].

The fan-out device demonstrated by Thomson et al., [45], had a insertion loss of 5 dB at 1550 nm which is too high for practical applications however they noted that much lower insertion losses are possible to achieve with further optimisation. Since this work was carried out in 2007, this technology has been commercialised by Optoscribe who are a spin-out company from the same group led by Professor Ajoy Kar. Optoscribe now sell custom made fan-out devices using the ULI inscription method offering devices with insertion loss < 1 dB, typically 0.7 dB per channel with crosstalk of < -50 dB [48].

2.7. Fibre laser applications

Fibre lasers are advantageous due to their compactness, good beam quality, efficiency and reliability. MCF's have further advantages over single core fibre lasers due to their power scaling capabilities [23]. Power scaling in short single core fibre lasers is restricted by their small effective core size due to nonlinear effects and the doping concentration of active ions. The use of MCF's allows the increase of the effective core size whilst still maintaining single mode operation. Crosstalk between the cores can be exploited to allow single mode output to be produced with a large fundamental mode size, due to light travelling along the cores being coupled together by evanescent waves. This coupling produces supermodes in which the fundamental supermode locks all cores in the same phase. Zhang et al., demonstrated a compact phase locked 7 core Nd-doped phosphate MCF laser of about 8 cm in length [23]. The supermode produced had

a mode field diameter 5 times larger than the fundamental mode showing that MCF lasers could be useful for compact high power single frequency lasers. Work by Kurkov et al., demonstrated a similar mechanism of mode coupling inside a MCF [49]. They showed that there was strong coupling between the cores even for core separations of about 28 μm, that were very sensitive to bending of the fibre; power conversion of up to 70 % from core to core was demonstrated.

MCF's with uncoupled core geometries have also been considered for fibre laser applications. These have been motivated by the desire for integration with MCF's used in telecommunication and for sensing. For sensing applications, narrow linewidths are often desirable, recently a seven core MCF distributed feedback lasers (DFB's) with linewidths of less than 300 kHz at 1550 nm was demonstrated [50]. This is higher than the linewidth of SMF DFB lasers [51]; however it is still narrow enough for sensing applications. The fibre gratings were inscribed in each core using one exposure of radiation at 244 nm in order to ensure uniform radiation of all seven cores the MCF was orientated with respect to the writing beam, the beam was made larger than the fibre with a transverse dimension of 370 μm and fibre twist was also removed before exposure for the 8 cm long grating. The curved surface of the MCF acts as a lens refracting the writing beam inside the MCF. This acts as an advantage as the back cores are no longer blocked by the front cores as shown in Figure 2.13.

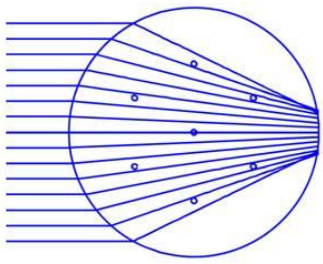

Figure 2.13. Ray tracing of the writing beam showing the cores at the back are not obstructed by the cores at the front. This figure has been taken from [50].

Although the authors Westbrook et al., tried to compensate for the multiple cores positioning to allow for uniform irradiation from the writing beam, the back two cores produced the weakest lasers, this is due to nonuniformities and possible over exposure

or defects in the fibre that caused the phase shift to drift from the desired π phase change [50]. As a result one of the cores lased with a power 100 times less than the other cores resulting in only six out of the seven cores lasing with useable power of over 0.1 mW's. However, this work shows with improvement DFB lasers can be made in MCF's, producing compact sources for MCF sensing applications that use interferometric or Radio Frequency (RF) interrogation. The work on fabricating precise gratings in MCF's could be useful for the development of astrophotonic atmospheric filters [50].

MCF with different rare earth dopants in each core have been fabricated [24]. By using different dopants, emission can be produced across different spectral regions from a common pump giving the prospect of multi band lasers. Work carried out so far on such fibre lasers showed amplified spontaneous emission (ASE) in the visible, near infrared and mid infrared spectral regions from a Tm^{3+}-Ho^{3+}-Yb^{3+}, Er^{3+}-Ce^{3+} and Tm^{3+}-Yb^{3+} doped tellurite glass fibre when pumped with a 980 nm diode laser. The results presented show ASE. However with improvements to the MCF design and dopant concentration potential amplification and lasing at 1550 nm, 1800 nm and 2050 nm could be achieved along with a visible laser in the blue, green and red spectral regions if the upconversion luminescence can be optimised.

2.8. Multicore fibre sensors

Another application where MCF has been found to be advantageous is their use as a fibre sensor; for completeness a general overview of some of the research into MCF sensors is detailed here. Optical fibre strain gauges are advantageous over electrical strain gauges as they are immune to electrical interference and are safe in hazardous environments. MCF sensors have been demonstrated in a variety of sensor types such as temperature, bend and shape. MCF sensors have increased stability over fibre bundle sensors as each core undergoes the same environmental changes such as vibration and temperature changes due to their shared cladding. Fibre Bragg gratings (FBG's) written into the cores of fibres can provide accurate measurements from changes in the reflected wavelength due to temperature or strain, they have established use as strain gauges for structural monitoring in aerospace, civil and marine applications [52]. The first

demonstration of using FBG's in an MCF for bend measurements was by Gander et al., when they reported single axis bend measurements [53]. Here they used FBG's written into two of the cores of a four core fibre; they were able to measure curvature with the FBG's acting as strain gauges. The fibre was wrapped around circular arcs of known curvature whilst the cores containing the FBG's were kept in the same plane of bending. The difference in the reflected Bragg wavelength between the two adjacent FBG's provides a measurement for curvature that is independent of both axial strain and temperature. Grating strain sensitivity in good agreement to single core FBG sensors was calculated as 0.997 pm.$\mu\varepsilon^{-1}$. ε is the unit for strain, 1 $\mu\varepsilon$ corresponds to the strain experienced by a 1 m length of fibre when it is stretched by 1 μm [54]. Bend measurements were calculated from FBG wavelengths with a residual wavelength error of ±7 pm, giving an associated curvature error of 0.14 m^{-1}. In 2003, further work by members of the same group showed that FBG's written into MCF's can provide two-axis curvature measurements [25]. FBG's were written into three cores of a four core MCF, by measuring the reflected spectra's from the Bragg gratings and using inverse matrix transformations they were able to determine curvature measurements for bending in the transverse and longitudinal axes simultaneously. Their sensor can measure both the magnitude and plane of the curvature with an associated curvature error of 0.047 m^{-1} calculated from the rms of the measured wavelength difference of 1.6 pm. This error is due primarily to the errors associated with determining the wavelength shift of the FBG's and is an improvement on their previous result reported in [53]. The same group then went on to improve the sensitivity of their two dimensional bend sensor by writing pairs FBG's in each core of the four core MCF [55]. The pairs of FBG's in each core form Fabry-Perot interferometers and use tandem interferometry to address each sensor. They demonstrated a 30 times enhancement of the sensor responsivity of previously reported FBG based sensors with a curvature resolution of 0.012 $km^{-1}.Hz^{-1/2}$.

The above FBG sensors are limited in applications such as shape monitoring as they can only measure bending and not torsion. A specialised MCF with three twisted outer cores and a straight inner core has been fabricated to measure both bend and twist using the FBG technique as shown in Figure 2.14 [56]. The central core is kept straight in this fibre as its reflected Bragg wavelength is used to distinguish between twist induced strain and changes in wavelength due to axial tension or temperature. The twisted cores

are fabricated using a helical bias during the fibre draw. Using this fibre curvature sensitivity below 0.005 m^{-1} was demonstrated with twist coefficients varying from 4.8 – 8.0 nε.(degree-meter)$^{-1}$ for the different cores. The twist accuracy was limited to 25 degrees.m^{-1} primarily due to imperfections in the cores and the switching optics used, however improvements could be made using extended cavities or tilted FBG's as currently this level of accuracy is too low for use in many practical applications [56].

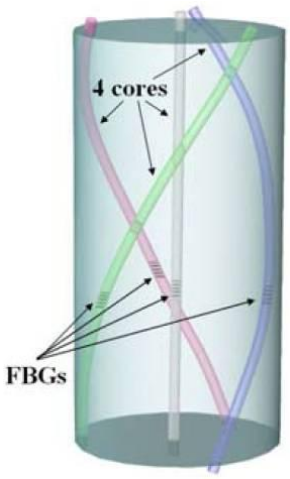

Figure 2.14. Bend and Twist FBG sensor MCF. This figure has been taken from [56] ©2008 IEEE.

MCF's with FBG's inscribed in the cores have also been used to provide background-free Raman sensing [57]. Raman sensing is used in biophotonics as a non-invasive, in situ analysis technique of living organisms with one of the main biomedical applications being the discrimination of malignant and benign cells [58, 59]. The use of an MCF probe will enable its use in *in vivo* applications that are currently limited due to the small size. FBG's are used as notch filters in the collection path of the probe, filtering of the probes are a necessary requirement due to Raman scattering inside fibres [57]. The probe is a fibre bundle consisting of six, nineteen core MCF's used for collection around a central MMF used for excitation as shown in Figure 2.15.

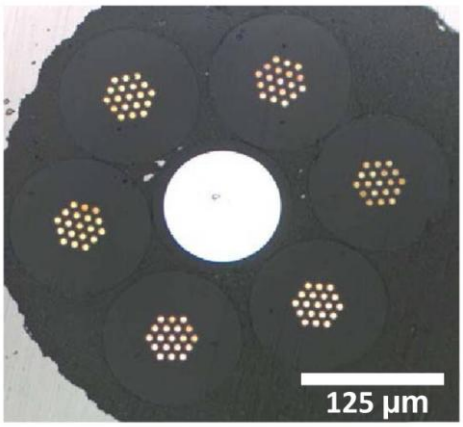

Figure 2.15. MCF probe used for background free Raman sensing, consisting of a fibre bundle with 6×19 core MCF used for signal collection surrounding a central MMF for delivery of the excitation light. This figure has been taken from [57].

FBG's are inscribed in each of the cores of MCF's, the length of the gratings and inscription time is adjusted to allow the probe to be used over a 20 K temperature range for use from room to body temperature. Unlike the previous mentioned uses of FBG's this application requires the FBG to work in transmission instead of reflection mode. The FBG's are used as filters to reduce the amount of the Rayleigh scattered light re-entering the fibre that can increase the fibre Raman background. In this probe the FBG had a filter efficiency -30 dB, meaning only 0.1% of the scattered light re-enters the fibre. The optimal distance between the probe and the sample was found to be 0.6 – 0.9 mm, acquisition times of 30 seconds were also required to take the experimental data however this can be reduced to 10 seconds or less to make them suitable for clinical applications by using MCF's with higher core numbers to increase the collection efficiency [57].

MCF's have also been used in optical profilometry [60]. Interference from a four core MCF was projected onto an object's surface, the reflected fringe pattern containing information on the objects surface was captured using a CCD camera and analysed using a two dimensional Fourier transform profilometry. This technique has applications in quality control, industrial automation equipment and in robotics for vision. A MCF is advantageous in this experiment as it permits a compact device, the MCF also provides a more stable fringe pattern compared to other fringe projection

systems. Objects were profiled with an rms error of 0.4 mm which was 11.3 % of the objects depth, this is quite high an error but can be improved with a smaller fringe spacing and higher number of fringes. Increasing the core separation of the MCF would increase the fringe spacing, as would decreasing the wavelength; in this paper the authors used a fringe spacing of 40.6 μm and a wavelength of 632.8 nm. Further work was carried out using the same fibre [61], this time only two cores of the MCF were used to produce the interference pattern and a phase step interferometry method was used to analyse the reflected fringe pattern. The phase step method was used as it is less computationally intensive compared to the previously used Fourier transform profilometry method. The authors claim an increased accuracy when measuring objects of high spacial variations than the previously reported technique. However an rms value of 0.7 mm for a different object was reported and the authors also used a longer wavelength of 798 nm that could result in decreased resolution. These rms values are currently too large for accurate profilometry experiments, however the authors state that the resolution can be improved using a greater number of fringes. Recently, the same fibre has also been used as a two dimensional force and longitudinal twist sensor [62]. This time 1550 nm light was coupled into all four cores of the MCF; the fibre was either bent or was twisted and its fringe pattern was compared to the straight fibres fringe pattern to give the phase of the fibre deformation.

MCF's with large numbers of cores (5000 – 50000 depending on the desired diameter and flexibility of the device) have seen promise for use in medical endoscopy as an alternative to coherent fibre bundles for providing ultrahigh resolution endoscopy [63]. MCF endoscopes will remove the need for bulky optics on the end of the probe allowing the development of miniaturised endoscopes that will be able to explore very small channels of the body such as coronary arteries, using medical techniques that are minimally invasive. Optical crosstalk due to coupling between parallel cores in the MCF limits the quality of the endoscopes. Research carried out on designing MCF's to reduce the crosstalk influence has shown the crosstalk is reduced if core diameter size is not constant and the inter-core spacing is increased. However, increasing the core spacing will result in a lower number of cores, limiting the resolution of the endoscope. Therefore for a typical core diameter size variation of 10% an inter-core spacing equivalent to 1.2 times the core diameter will result in the quality requirements for a V

parameter greater than 8. MCF's can also be used for holographic interferometry endoscopy, combining holographic interferometry with endoscopy enhances the imaging allowing measurements with submicron accuracy or viewing objects partially hidden or with small access apertures [64].

2.9. Summary

Multicore fibres have proven useful in a variety of applications from data communication, fibre lasers and sensing due to their compact nature and stability of their cores due to the shared cladding. The shared cladding of MCF's are advantageous over fibre bundles due to each core undergoing the same environmental changes such as temperature or vibrations this has shown to be important in improving the sensitivity in sensing applications [25, 53, 55, 56], or by attributing to crosstalk allowing its exploitation in phase locked fibre lasers [23, 49]. The shared cladding is beneficial in applications that rely on interference where MCF's have been shown to provide a more stable fringe pattern [60]. The applications of MCF's detailed here is not an exhaustive list, MCF's are currently being explored for use in new areas such as biophotonics as their small size in comparison to free space optical systems will be advantageous when dealing with the manipulation and studies into biological cells as the work detailed in this thesis will show. Integration with the use of fan-out devices has also improved to show MCF's are suitable in a wide range of future application. The work detailed here in the various applications can be applied to the results detailed in this thesis. The use of an MCF with cores spaced more than 50 μm apart will reduce the crosstalk between the cores, combined with the added advantage of the shared cladding will provide a stable fringe pattern that will allow for the creation of interference fringes with high visibility. The development of optical interconnects, primarily used in data communication applications can be used to create a fully integrated multicore fibre device for use in optical trapping experiments.

Chapter 3. Multiple Particles Optical Trapping

3.1. Introduction

The ability to trap and manipulate particles and cells using beams of light has enhanced the study of biology for cell sorting, examining individual cells and cell bonds. The non-invasive technique of using light beams at wavelengths where the cells do not absorb allows live cells and cellular process to be examined. Optical trapping is the manipulation of microscopic particles using the radiation force of laser beams. This phenomenon is due to the light's momentum. The energy and momentum of the photon can be related to its wavelength using the following equations:

$$E = mc^2 = \frac{hc}{\lambda} = pc \tag{3.1}$$

where E is the energy, m is the mass, c is the speed of light, h is Plank's constant, λ is the wavelength of light and p is the momentum. For a photon with a wavelength of 1047 nm the momentum will be 6.329 x 10^{-28} N.s.

Laser light was first shown to have the ability to move particles in 1970 by Arthur Ashkin [65]. Transparent latex microspheres suspended in water were drawn into the beam axis of a TEM_{00} mode of an argon laser and accelerated along in the direction of the light. The particles were drawn into the beam by the transverse gradient force of the light and were accelerated by the scattering force of the light. Ashkin also observed the optical trapping of high index microspheres using two opposing light beams, particles drawn into the beams axis were accelerated along the beam to a stable equilibrium position between the foci of the opposing laser beams. The following year Ashkin et al., showed that particles could be levitated using a single laser beam [66]. A focused TEM_{00} mode beam was directed upwards, the radiation pressure was shown to support the microsphere against the downwards pull of gravity. In 1986, Askin et al, demonstrated a single focused laser beam that could stably trap particles in three dimensions [67] in a set up known as optical tweezers. Particles ranging in size from 25 nm to 10 μm were stably held. The trapping was due to a three dimensional intensity

gradient formed by the transverse and axial forces of the tightly focused laser beam. Optical tweezers have the ability to pick the particle up and move it around this has found numerous applications such as examining molecular bonds [68], measuring the force extension relationship for single molecules of DNA [69] or measuring the forces exerted by individual proteins [70]. Over the past decade the optical manipulation group at the University of St Andrews led by Professor Kishan Dholakia have pioneered new methods for optical trapping and manipulation such as trapping in turbulent media and the use of vortexes and non-diffractive beams of light. The types of optical tweezers described above are single particle traps; the manipulation of multiple particles is possible using a variety of techniques such as rapid laser scanning [71], the use of diffractive optics to create arrays of optical tweezers [31], using computer generated holograms to produce multiple beams [30] or by using interferometry techniques [32]. Previous work involving interferometric optical trapping has been carried out using free space optics, combining this technique with MCF's will allow us to exploit the advantages of non-coupled cores with a shared cladding for improved stability in the fringe patterns and will also allow for the creation of a compact optical trapping and manipulation device.

3.2. Interactions between light and dielectric particles

When light beams interact with dielectric particles there is an exchange of forces that leads to optical trapping. There are two regimes that are associated with understanding the forces involved in optical trapping, the Mie regime and the Rayleigh regime. The Mie regime is based on the ray optics analysis of particles and is used to describe interactions where the particle diameter is large in comparison to the wavelength of light. The Rayleigh regime is based on the electric field of the light interaction with particles whose diameter is small in comparison to the wavelength of the light as shown in Figure 3.1. Only particles that can be described using the Mie regime are dealt with in this thesis as these are the same size as biological cells, typically a few microns.

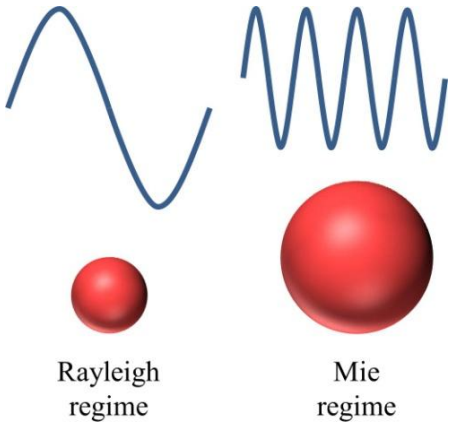

Figure 3.1. The Rayleigh and Mie regimes showing the particle size relative to the wavelength of light.

3.2.1. The ray optics approach

A ray optics approach is used to calculate the forces acting on a dielectric particle in the Mie regime. The effects of a laser beam on a transparent, non-absorbing sphere can be modelled using ray optics with rays weighted according to their intensity. Photons of light have momentum defined by $p = h/\lambda$, where h is Plank's constant and λ is the wavelength of the light. When light hits an object it changes direction on reflection or refraction, at the same time due to conservation of momentum the change of momentum of the light will cause an equal but opposite momentum change on the object. This force exerted on the object is in the order of piconewtons, large enough to move micron sized objects. For example, to lift a 2 μm polystyrene microsphere then a force greater than 0.043 pN is needed to overcome gravity. This can be calculated using the following equation,

$$F = mg = V\rho g = \frac{4}{3}\pi r^3 \rho g \qquad (3.2)$$

where g is acceleration due to gravity, V is volume of the microsphere, ρ is the density of the microsphere and r is the radius of the microsphere. The density of the polystyrene microsphere is 1.05 $g.cm^{-3}$ [72].

If a transparent dielectric Mie particle of higher refractive index than its surroundings is located within a gradient of light such as a Gaussian beam, the refraction of rays of different intensities result in a change of total momentum in the light exiting the particle as shown in Figure 3.2. The ray from the outer portion of the beam gives less force to the particle than the central ray. This causes a reaction force on the particle that draws it into the centre of the beam into the area of highest intensity where an equilibrium position is reached with the rays of light interacting with the particle are balanced resulting in no overall change in momentum of the beam.

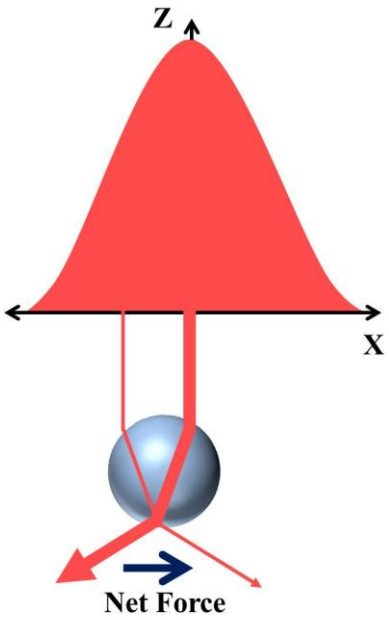

Figure 3.2. The rays of the Gaussian beam are refracted as they pass through a dielectric particle. The intensity gradient results in the bead being drawn to the centre of the beam by the transverse force.

3.2.2. Optical tweezing

The transverse force described above allows particles to be trapped effectively in two dimensions. To be able to pick particles up and move them around the particle must be trapped in three dimensions. To create a three dimensional trap an axial gradient force is required in the z (vertical) direction. This can be achieved by tightly focusing a Gaussian laser beam using a high numerical aperture (NA) lens typically > 1.2NA. Off-

axis rays hit the particle at a large angle with respect to normal and are refracted downwards resulting in a momentum change in the direction of the beam propagation. This results in an axial force in the opposite direction pushing the particle upwards as shown in Figure 3.3. The equilibrium position is reached when the axial force balances with the scattering force of the laser and force due to gravity that acts to push the particle downwards.

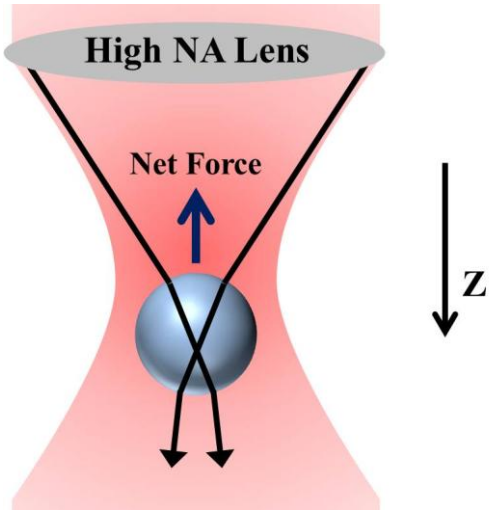

Figure 3.3. The off-axis rays of the focused Gaussian beam are refracted downwards as they pass through a dielectric particle, resulting in an opposing axial gradient force pushing the particle upwards.

To achieve a stable three dimensional trap where the gradient force is greater than the scattering force, a high NA objective lens with an NA > 1.2 is required. This creates steep gradients due to the angle at which the off-axis rays hit the particle. The NA of a lens is determined by the refractive index of the medium after the lens, *n*, by the equation NA= $n\sin\theta$. Most high NA lenses are oil immersion lenses that require a drop of index matching fluid between the lens and the sample slide. This is therefore a limiting factor of optical tweezers for their uses in *in-vivo* applications. The manipulation of optically tweezed particles normally occurs with a stationary beam whilst the sample slide is displaced in relation to the trap.

3.2.3. Trapping force

The trapping force is due to the change in momentum exerted on the object by the incident laser beam. This can be described through equation

$$F = \frac{\Delta p}{\Delta t} \tag{3.3}$$

where Δp is the change of momentum and Δt is the change in time. The change in momentum per second is equal to the force, F acting on a particle. This can be described as the force on a particle hit by N photons as the following equation.

$$F = \frac{NEn}{c\Delta t} \tag{3.4}$$

where E is the energy of each photon, n is the refractive index of the surrounding medium and c is the speed of light. This can be related to the power of the laser beam, P, through the equation

$$F = \frac{Pn}{c} \tag{3.5}$$

Not all of the light beam's momentum is transferred to the particle therefore the trapping efficiency of any optical trap can be described in terms of a dimensionless parameter Q.

$$F = \frac{nQP}{c} \tag{3.6}$$

Q is the percentage of the light beam momentum transferred to the particle, typical values of Q for optical traps using small dielectric particles are in the range of 0.03 - 0.1 [73]. If the power of the optical trap is 2 mW and the Q value is 3 % a trapping force of F = 0.266 pN will be applied to the microsphere held in a water medium. This force is greater than required to trap a 2 μm polystyrene microsphere that was found to be 0.043 pN from equation (3.2).

3.2.4. Water absorption

The wavelength of light used for the optical trapping of biological particles has to be selected to minimise water absorption. Increased water absorption induces a greater temperature rise due to the localised optical power of the traps. When trapping biological cells, temperature increases should be kept to a minimum so that the health and operation of the cells are not disturbed or influenced by the optical traps. Figure 3.4 shows that the water absorption is low over the wavelength range of 600 – 1100 nm, this range of wavelengths are commonly used for the optical trapping of biological particles. This provides minimal temperature rises in comparison to longer wavelengths such as 1550 nm as demonstrated in Section 6.6. The selection of wavelength for optical trapping must also take into account, the power required and the availability of suitable optical components. Since single mode operation is required for optical trapping, the cut of wavelength of the fibre must be lower than the wavelength used for trapping, therefore for the experiments demonstrated in this thesis a wavelength of 1047 nm was used to trap biological particles. This wavelength allows for low water absorption, low temperature increases and also single mode operation of the MCF.

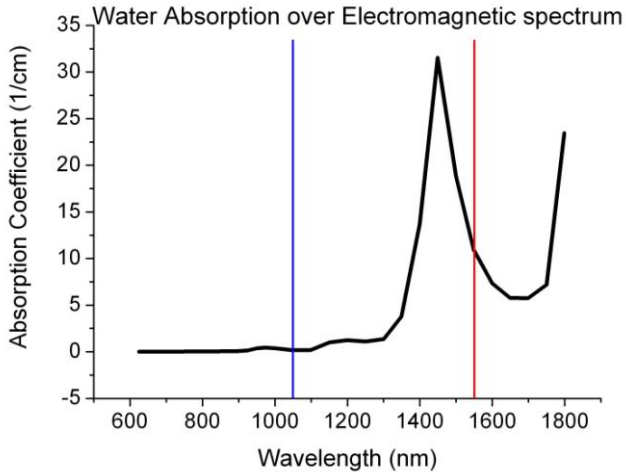

Figure 3.4. Graph showing the water absorption at various trapping wavelengths, the blue line indicated low water absorption at 1047 nm and the red line indicates the higher water absorption of 1550 nm. The data from this graph is from reference [74].

3.3. Multiple particle optical traps

Optical tweezers as described above are only suitable to trap single particles. Trapping multiple particles allows further biological processes to be examined such as cell to cell interactions when held in close proximity, biofilm formations and also the study of crystalline structures. For multiple particle optical traps there are a variety of methods such as the rapid scanning of a signal laser beam to multiple sites that trap multiple particles through time sharing of the single laser beam, using computer generated holograms to produce multiple beams such as the use of diffractive optics to create multiple static laser traps or spatial light modulators to create reprogrammable traps that can manipulate and move particles in real time and using interferometry techniques to create periodic arrays of traps suitable for the manipulate of multiple particles.

3.3.1. Laser scanning for multiple particle manipulation

Multiple particles can be trapped simultaneously by the rapid scanning of a single laser beam. The optical trap dwells briefly on each particle before moving onto the next particle. The repetition time that the trap revisits each particle is set higher than the diffusion rate so that the particle hasn't drifted from the trap position. The diffusion coefficient *D* for the particle can be calculated from Einstein's relation as follows [73].

$$D = \frac{k_B T}{\beta} \tag{3.7}$$

where k_B is Boltzmann constant, T is the absolute temperature and β is Stokes drag constant that can be calculated as $\beta = 6\pi r\eta$, where *r* is the radius of the particle and η is the viscosity of the surrounding medium. The diffusion coefficient can be used to calculate the rms diffusion distance *d* for a given time *t*.

$$d = (2Dt)^{1/2} \tag{3.8}$$

Trapping multiple particles with a rapid scanning laser was first demonstrated in 1991 by Sasaki et al., using two galvanometer mirrors that were operated by a driver

controlled by a microcomputer. The system allowed patterns to be written and the scan speed to be adjusted [75]. The repetition rate of the beam scanning is set higher than the time scale of the Brownian motion of the particle in order that the particles remain trapped. The thermal motion of the particle also depends on the viscosity of the surrounding medium and the size of the particle. The repetition rate needed for the particle to remain in the trap can be calculated using equations (3.7) and (3.8). If a 1 µm diameter particle is allowed to diffuse a length of 100 nm in the time that a scanning beam repeats over its position, a repetition rate of greater than 97 Hz is need for a particle held in a medium of water or a repetition rate of greater than 5.44 Hz is needed when the particle is in an ethylene glycol medium. With this technique 1 µm polystyrene latex microspheres were arranged into various patterns including the micrometre symbol as shown in Figure 3.5 (a), a laser scanning repetition rate of 13 Hz was used to produce this pattern at a laser power of 145 mW. A laser power of ~1.5 mW per particle is required for the manipulation of small particles [75]. The manipulation of 0.5 µm titanium dioxide particles were also demonstrated at a laser power of 145 mW for a repetition rate of 24 Hz as shown in Figure 3.5 (b). Both particles were trapped at room temperature in an ethylene glycol medium.

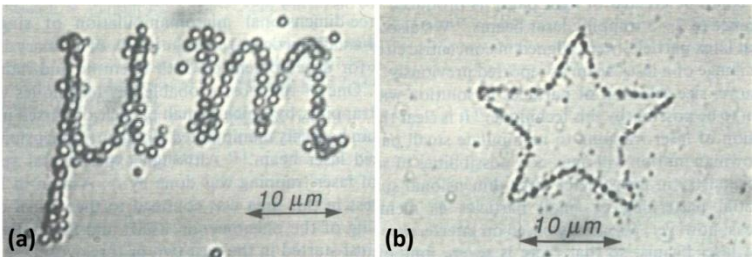

Figure 3.5. (a) Micromanipulation of 1 µm polystyrene latex microspheres in an ethylene glycol suspension by rapid laser scanning of the trapping beam and (b) 0.5 µm titanium dioxide microspheres in an ethylene glycol suspension. This figure has been taken from [75].

The same group went on to improve this technique to allow particles to be moved at a constant velocity along the produced pattern [71]. By adjusting the scan speed and laser power the flow velocity of the particles could be controlled in a plane for multiple particles arranged in a pattern. Using a scanning repetition rate of 12 Hz with a 1064

nm Nd:YAG laser operating at 290 mW the authors demonstrated micromanipulation of over 50 2 µm polystyrene latex microspheres held in an ethylene glycol suspension by arranging them into the Chinese character for light as shown in Figure 3.6. The flow velocity of the microspheres depends on the driving force of the laser, the frictional forces between the microspheres and the plate they are held on, and also the viscosity of the surrounding medium. Ethylene glycol has a viscosity of 16.06 mPas compared to water that has a viscosity of 0.893 mPas at 25°C and therefore the particle flow is slower in this suspension [76].

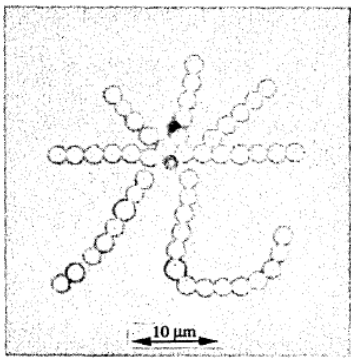

Figure 3.6. Micromanipulation of 2 µm microspheres in an ethylene glycol suspension by rapid laser scanning of the trapping beam. This figure has been taken from [71].

The independent manipulation of two particles can be demonstrated through the introduction of another laser beam that doesn't interfere with the first beam, this method has been used to bring multiple particles together to create structures [77]. The beams were produced using a linearly polarised continuous wave (cw) Nd:YAG laser that was passed through a quarter wave-plate to convert to circular polarisation before being split into two with a polarising beam splitter (PBS1) so that one was horizontally polarised whereas the other was vertically polarised. The beams then passed through sets of galvano mirrors (GM1 and GM2) before being recombined with a second polarising beam splitter (PBS2) as shown in Figure 3.7. The sets of galvano mirrors allow each beam to be manipulated independently.

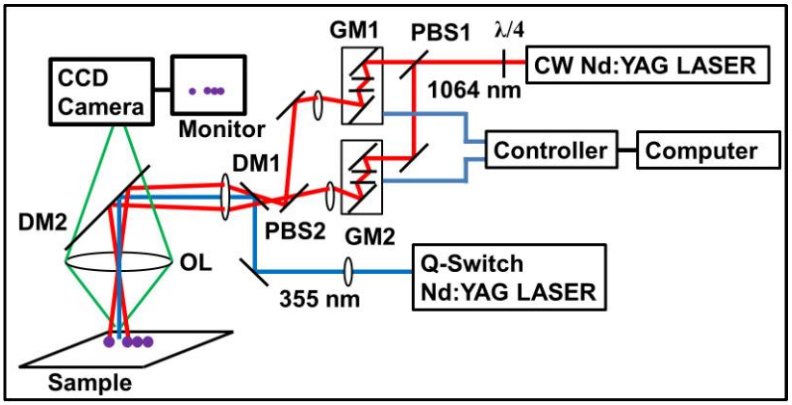

Figure 3.7. Experimental set-up of the multibeam rapid laser trapping and particle fixation experiment [77]. Where OL – objective lens, DM – dichroic mirror, PBS – polarising beam splitter, GM – galvano mirrors and λ/4 – quarter wave-plate.

This technique was used to create structures of particles fixed with chemical fixation [77]. The beams were used to trap particles that were brought together in an ethylene solution of acrylic acid, N,N'-Methylenebis (acrylamide) and a radical photoinitiator. A 355 nm Q-switched Nd:YAG laser was used to irradiate the particles for several seconds resulting in adhesion of the particles. This method was used to create chains of structures, as shown in Figure 3.8.

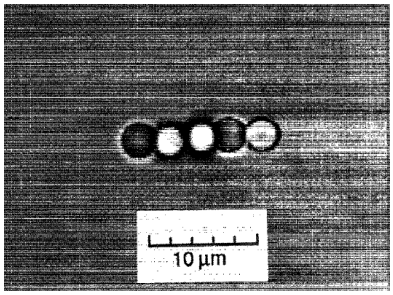

Figure 3.8. 3µm polystyrene latex particles photochemically fixed together after micromanipulation using a dual beam rapid laser scanning technique. This figure has been taken from [77].

Galvano mirrors such as those used in the above experiments have a relatively slow scanning frequency with a maximum of 300 µs i.e. 3.33 kHz, requiring either trapping of a small number of particles or for the particles to be suspended in a viscous solution

to limit the particle drift. Piezoelectric motors can operate at frequencies of a few kHz allowing multiple particles to be trapped in lower viscous fluids such as water suitable for manipulating live cells [78]. However, results showed that increasing the repetition frequency reduced the maximum extension of the piezo, therefore reducing the maximum separation of the trapped particles by up to 50% at a frequency of 1.3 kHz [78]. Reducing the maximum separation of trapped particles reduces the size of particle arrays possible, therefore reducing the number of particles that can be trapped in the arrays. Higher repetition frequencies of hundreds of kHz can be achieved using acousto-optic deflectors [79, 80]. Acousto-optic deflectors are more precise than scanning mirrors as scanning mirrors overshoot the desired position and can resonate at high repetition frequencies. However scanning mirrors have a wider scanning range and higher transmission efficiencies than acousto-optic deflectors [73]. The higher scanning frequency also allows more particles to be trapped, such as the 400 optical traps demonstrated using 1.4 µm fluorescein tagged silica microspheres in an ethanol solution at a repetition frequency of 96 Hz with a laser power of 1 W measured at the back focal plane of the trapping objective as shown in Figure 3.9 [80].

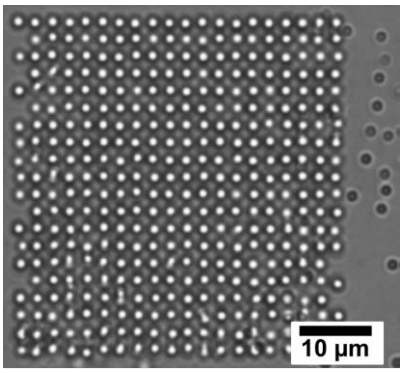

Figure 3.9. 1.4 µm fluorescein tagged microspheres trapped in ~ 400 individual optical traps created using an acousto-optic deflector using the rapid laser scanning technique. This figure has been taken from [80].

3.3.2. Holographic optical traps for multiple particle manipulation

Holographic techniques can be used to generate multiple particle trapping arrays. These traps can either be static when produced using a diffractive optical element or can be

used to move particles around to form different trapping arrangements when produced by a spatial light modulator (SLM) driven by a computer.

3.3.2.1. The use of diffractive optical elements for multiple particle manipulation

Diffractive optical elements can split a single laser beam into any desired array or pattern of beams to create multiple optical traps. To create arrays of optical tweezers the DOE is placed in front of the collimated laser and the array is then transferred to the back aperture of an objective lens by an imaging system. If the DOE has imperfections a telescope can be used with a spatial filter placed in the inner focal plane to remove these rays. The DOE's used for holographic optical trapping are phase-only holograms, as optical trapping is dependent on the beams intensity and not on its phase, the DOE is used to modulate only the phase of the input beam to achieve the desired trapping configurations [81].

The DOE's were fabricated using photolithographic techniques. This process includes creating a photomask from the phase profile hologram; each square of the hologram is designed to match the collimated laser beam diameter. The photomask is then used to create an etch mask on the surface of a fused silica substrate, photoresist is placed on the surface of a silica substrate that has been protected with a layer of chromium. The photomask is placed on top of the photoresist and the sample is exposed to ultraviolet (UV) radiation, the photomask is then removed and the photoresist and chromium layer at the exposed regions is removed. The sample is then etched again using reactive ion etching, the unprotected silica regions are etched at a rate of 0.5 $nm.s^{-1}$ [81]. The reactive ions don't etch through the layer of chromium. Finally the remaining chromium layer is removed to reveal a fused silica surface with an encoded phase profile. DOE's manufactured using lithographic techniques deviate from the desired design due to two main fabrication defects. The first is error in the phase modulation due to a mismatch between the wavelength and the etch depth. This limits the efficiency of light in the desired order to around 80 % [81]. The second error is random noise and phase fluctuations caused by the surface roughness as a result of the etching procedure. This reduces the efficiency by another 10 %, to achieve an overall efficiency of the DOE to around 70 % [81].

The first optical tweezers array generated using a DOE was demonstrated by Dufresne and Grier in 1998 [31]. They produced a 4 x 4 square array of optical tweezers using a 100 mW frequency doubled Nd:YAG laser operating at 532 nm, a commercially available DOE and a microscope objective with a high NA of 1.4 to create the tweezers. A 16 beam tweezers array with a 70 x 70 μm^2 field of view was formed and used to trap 0.5 µm silica microspheres suspended in deionised water, as shown in Figure 3.10.

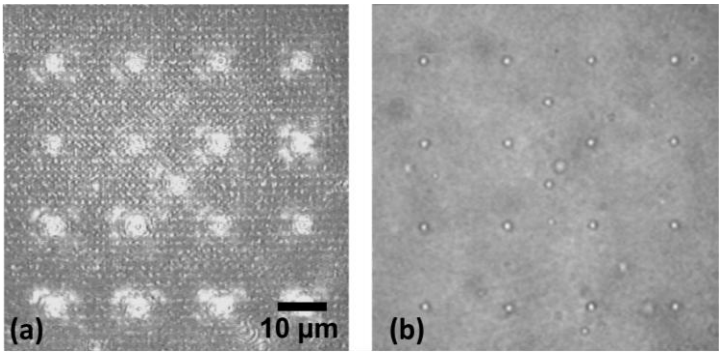

Figure 3.10. (a) 0.5 µm silica microspheres trapped in 16 individual optical traps created using diffractive optical element and (b) the particle array 0.033 s after the laser was turned off. This figure has been taken from [31].

In Figure 3.10 (b), two additionally trapped particles can be seen, these are from peaks in the diffraction pattern due to imperfections and are weaker than the primary optical traps. Suggested applications for these traps include assembling composite structures, studying the dynamic relaxation of artificially structured colloidal crystals and inducing order in colloidal monolayers [31]. This paper was followed up in 2001 with descriptions of how to design and create DOE's for holographic optical trapping [81]. To create the phase-only DOE's an adaptive-additive algorithm was used, eight iterations were typically required to reach an acceptable error tolerance. These allow any pattern of tweezers arrays to be created, the spacing between the tweezers can be scaled by tiling the hologram encoding as shown in Figure 3.11. Repeating the hologram like this allows the spacing between the tweezers to be scaled proportionally to the number of tilings along each dimension without reducing the resolution due to the periodic nature of the fast Fourier transforms used to calculate the holograms.

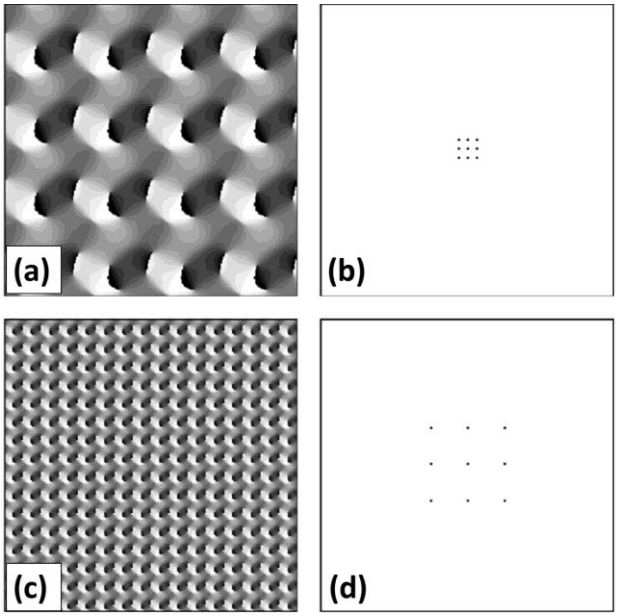

Figure 3.11. Tiling for a 3 x 3 array of tweezers to scale the spacing between the tweezers. (a) The input phase hologram with 4 copies of the tiled section, (b) the resultant output for (a), (c) the input phase hologram with 16 copies of the tiled section and (d) the resultant output for (c). This figure has been taken from [81].

When large trapping arrays are formed by DOE's, most of the particles tend to occupy the outer regions of the pattern which blocks access to the inner traps. This problem has been overcome with the use of a retractable knife edge in the conjugate output plane formed in the telescope region of the set up [82]. Blocking individual beams in the conjugate output plane eliminates them in the output plane, therefore the edge of a retractable knife can block out rows of the trapping pattern exposing all the traps to the particles to achieve a fully filled array of traps. The DOE's created to produce holographic optical tweezers are for specific static trap arrangements. Spatial light modulators such as phase-only liquid crystals can be used in place of a DOE to produce holographic optical tweezers with the ability to program different trap configurations for real time reconfiguration and optimisation.

3.3.2.2. Computer generated holograms using spatial light modulators for multiple particle manipulation

DOE's have been shown to be useful in creating arrays of multiple particle traps, however they have limitations due to only being able to create static traps with defects unable to be corrected. Originally used for image processing in overhead projectors, SLM's have shown use in creating multiple beams for optical trapping. Phase-only SLM's can be used in place of DOE's to create programmable holographic optical traps that can be altered in real time to create different optical trapping arrangements. Phase-only liquid crystal SLM's are commonly used to generate holograms suitable for optical trapping and manipulation. The SLM's create phase shifts in each pixel by varying the optical path length. In liquid crystal SLM's, this is achieved through controlled orientation of the molecules [83]. A liquid crystal SLM was first used in holographic optical trapping to convert the Gaussian beam into a doughnut-shaped beam for use in two dimensional trapping of both high index and low index particles [30]. Three holograms used to produce doughnut-shaped beams were superimposed to create three independent traps; the doughnut beam unlike Gaussian beams can trap both high index and low index particles, high index particles such as polystyrene microspheres can be trapped in the high intensity region of the doughnut beam whereas low index particles can be trapped in the centre of the doughnut. The three doughnut beams were used to trap three polystyrene microspheres, the microsphere can be independently manipulated. One of the particles was moved about 60 μm using ten consecutive hologram calculations whilst the other two particles were kept stationary. This work was improved on to trap multiple particles in three dimensions [84]. The liquid crystal SLM used allowed a phase shift of 1.6π radians when illuminated with 488 nm light. One SLM was used to trap seven 1 μm silica microspheres in a V-shape pattern as shown in Figure 3.12, each particle was able to be moved independently by changing the hologram programed in the SLM. In the same paper, trapping and manipulation of the particles in three dimensions were demonstrated for the first time using a single beam optical trap without moving parts. This was achieved by adding a lens term to the phase hologram, two 1 μm silica microspheres were trapped and one was moved out of the observation plane before being moved to the other side of the stationary particle and

back into the observation plane, the movement was carried out through changes to the hologram [84].

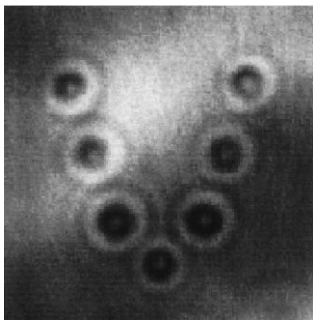

Figure 3.12. Seven 1 μm silica microspheres trapped in a V-shape using a liquid crystal SLM to produce holographic optical trapping. This figure has been taken from [84].

The progress in the field of holographic optical traps was delayed due to the lack of appropriate phase algorithms to address the SLM's. Using a Gerchberg and Saxton algorithm and a 480 x 480 pixel array liquid crystal SLM with up to 2π phase shift when illuminated with 532 nm light, twenty six 0.99 μm silica microspheres were trapped and manipulated into multiple configurations as shown in Figure 3.13 [85]. The particles were moved into each configuration in 2 μm steps with a translation speed of 10 $\mu m.s^{-1}$ at a trapping power of 10 mW per trap.

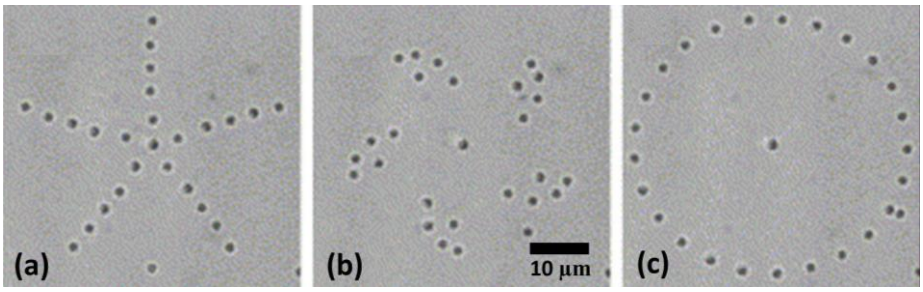

Figure 3.13. Twenty six 0.99 μm silica microspheres transformed into a variety of different configurations using holographic optical tweezers. (a) The original configuration, (b) after 16 steps the pattern is changed and (c) after a further 22 steps the final configuration is achieved. This figure has been taken from [85].

SLM's can be used to create a variety of different optical traps, aside from the conventional Gaussian beam traps, optical vortices, axial line traps, optical bottles and optical rotators can be created from different input phase algorithms [85]. These allow different particles to be trapped; optical vortexes can be used to trap particles such as low index particles.

Holographic optical traps that can manipulate multiple particles simultaneously in three dimensions have applications in creating micron-sized crystal structures that can be used in photonic crystal construction or for the seeding of biological growth [86, 87]. Crystal structures were first constructed using holographic tweezers created using a liquid crystal SLM with a phase hologram programed onto it that acts as a grating and a Fresnel lens to allow three dimensional manipulations [86]. With this technique three dimensional crystal structures were created that have the ability to be made permanent by setting them in gel. However as the individual microspheres that made up the crystal structures were held in close proximity, assembling the structures can be problematic as some of the traps are embedded inside. This resulted in multiple attempts being needed to assemble the complete structures. To improve on this technique, the programmable advantage of SLM's was exploited to use a sequence of holograms that assembles the structures from an initial simple trap arrangement that was then moved to form the desired more complex crystal structures, without any missing microspheres in the centre of the crystal structure [87]. This technique allows the real time arrangements of crystal structures to be created with the ability to control which particle goes into each position combining different sized microspheres into the crystal structures. This technique will reduce the need for multiple attempts needed to assemble the structure when only a single three dimensional holographic trap is used. SLM's have been shown to be useful in creating a variety of different multiple optical trapping arrangements with the advantage of being programmable allowing for defects to be fixed and arrangements to be altered in real time. However if simpler traps such as two dimensional arrays of particles are desired, SLM's are an expensive technique to use as they require a computer with prior knowledge of coding and algorithms to be used. A DOE can be used to produce static two dimensional arrays of particles at a less expensive cost than SLM's, however they only have an efficiency of 70 % [81], resulting in defects such as extra traps or missing traps. Traps can be formed using the interference of multiple

laser beams to produce static two dimensional periodic arrays of particles without defects and are less expensive than using SLM's.

3.3.3. Interferometric optical trapping for multiple particle manipulation

The superposition of two or more coherent light beams produces interference patterns. The intensity profile of the beam interactions gives rise to gradient forces that can be used to optically trap particles. The first demonstration of interferometric optical trapping was carried out in 1990 by Burns et al. They generated optical standing wave patterns in water to create and study periodic crystalline arrays of micrometre size [88]. A 10W, 514.5 nm Argon ion laser was split into up to five beams in this experiment using beam splitters and steering optics. The intensities, polarisations, focal properties and mutual phases of the beams were precisely controlled before being brought to a common focus on a sample cell made of two fused silica plates separated by 200 μm and containing a suspension of 3.4 μm polystyrene microspheres in water. Interference patterns were created using two beams, three equiangular beams, three non-equiangular beams or five equiangular beams. The intensity maxima act as periodic arrays of transverse optical traps in which microspheres can be trapped in; each variation of input beams creates a different crystalline array. Once the microspheres were trapped in the periodic arrays diffraction patterns were taken that corresponded to those expected of the two dimensional crystal structures [88].

The first demonstration of optical trapping and micromanipulation of microscopic objects using interference fringes was in 1997 by Chiou et al., [32]. Light from a 514.5 nm Argon ion laser source was divided into two beams before being recombined and focused through a 20 cm focal length focusing lens to form a set of interferences fringes at the back focal plane of a x20, 0.4NA microscope objective as shown in Figure 3.14. The microscope objective projects a smaller image of the fringes onto its front focal plane where the sample of 2.8 μm latex microspheres was positioned. Before the beams were recombined one of the beams was reflected by a mirror mounted on a motorised translation stage. When the mirror is translated, the fringes are shifted this allows particles trapped in the fringes to be manipulated. The fringes can be swept at speeds of 5 – 10 $\mu m.s^{-1}$, where particles trapped in the maxima of the fringes can be

moved along with the fringe bounded by the potential barriers at either side of the fringe. The fringes can also be used for the alignment and manipulation of rod-shaped particles [32]. In the same paper, the authors showed how the similar intensity patterns can be created with a single laser beam illuminating a Ronchi grating placed at the back focal plane of the microscope objective, the image is then projected into the sample plane. The fringes can also be swept by rotating the grating producing a more compact system than previously [32].

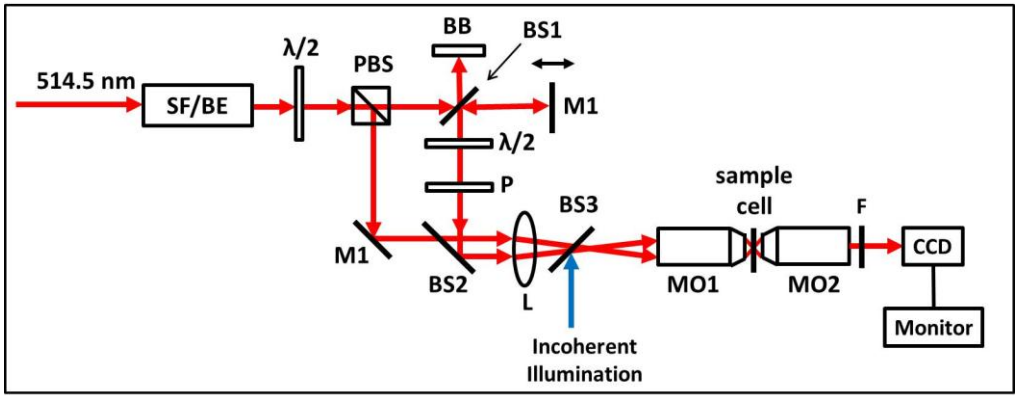

Figure 3.14. The experimental set up for the two beam interferometric optical traps demonstrated by Chiou et al., [32]. BB – beam block, BS – beam splitter, SF/BE – spatial filter/ beam expander, MO – microscope objective, M – mirror, L – lens and F – filter.

In 2003, Rubinov et al., examined theoretically the interaction of an ensemble of different sized particles in a dual beam interference field [89]. The results showed that the spatial separation of particles of different dimensions varies with the intensity of the light field. At a power density of 3 $W.cm^{-2}$, the 10 µm microspheres are all in the maxima positions of the interference fringes whereas the 2 µm microspheres are evenly spread over the interference pattern. At a power density of 0.5 $W.cm^{-2}$, some of the 10 µm microspheres can still be located in the intensity minima positions. This shows that a mixture of particles can be sorted by size by varying the intensity of the trapping beams [89]. Non-absorbing particles can also be sorted with respect to their polarisability, as particles with a refractive index lower than their surroundings such as air bubbles primarily gather in the minima positions of the interference fringes whereas

particles with a higher refractive index than their surroundings such as polymer microspheres primarily gather in the maxima positions. This was also shown to depend on the intensity of the trapping beams. The results showed that at a power density of 5 $W.cm^{-2}$, air bubbles and polymer microspheres both with 6 µm diameters were completely spatially separated across the interference fringes, than at a lower power density of 0.5 $W.cm^{-2}$, where a minority of either particle at any position across the interference pattern rather, than in the maxima and minima respectively. At a power density of 5 $W.cm^{-2}$ all the air bubbles were in the minima and all the polymer microspheres were in the maxima positions [89]. In the same paper, the authors experimentally demonstrated one dimensional interferometric optical trapping using dual beam interference from a 40 mW, 632.8 nm Helium Neon laser. The single mode laser beam was split into two using two 20° Fresnel biprisms as shown in Figure 3.15.

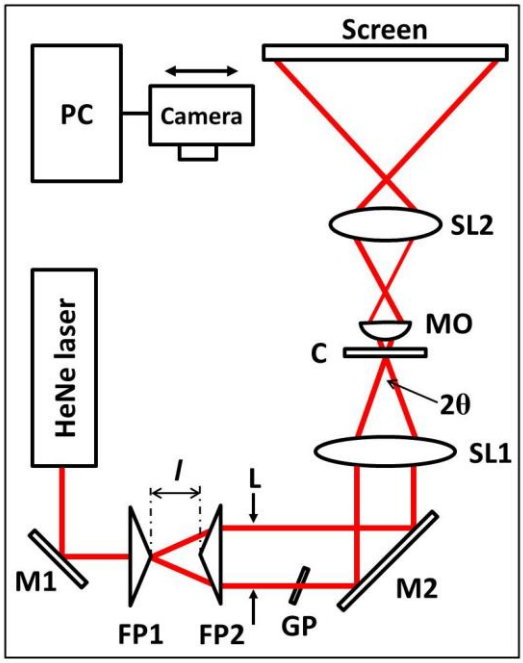

Figure 3.15. The experimental set up for interferometric optical trapping demonstrated by Rubinov et al., [89]. Here FP– Fresnel prism, GP – glass plate, SL – spherical lens, M – mirror, MO – microscope objective and C – cell.

The two beams were then brought together using a spherical lens to produce linear interference fringes whose period, Λ, can be described by the following equation [89].

$$\Lambda = \frac{\lambda}{2sin\theta} \tag{3.9}$$

where θ is half of the angle between the interacting beams that can be defined by the following equation.

$$\theta = tan^{-1}\left(\frac{L}{2f_1}\right) \tag{3.10}$$

where L is the distance the beams after exiting the Fresnel biprisms and f_1 is the focal length of the spherical lens. As L depends on the separation distance of the Fresnel biprisms l, the period of the fringes can be changed by increasing or decreasing the separation, over a range of 0.5 – 50 µm was achievable. For the experiment, interference fringes with a period of Λ = 8.2 µm were used to trap 5.8 µm polystyrene microspheres as shown in Figure 3.16.

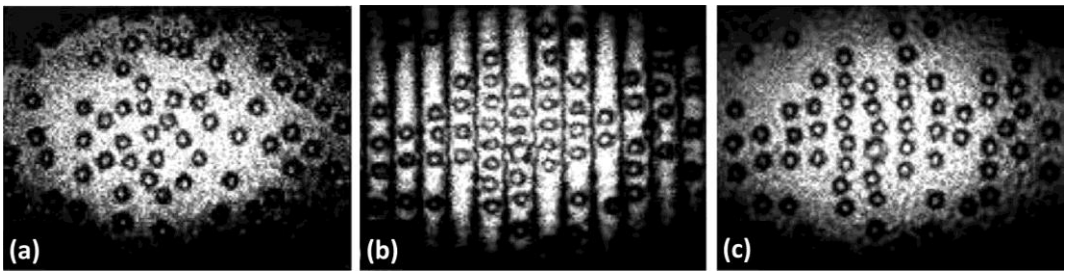

Figure 3.16. 5.8 µm polystyrene microspheres, (a) before, (b) during and (c) immediately after trapping using interferometric optical trapping. This figure has been taken from [89].

Figure 3.16 shows the microspheres optically trapped in one dimension along the fringes, where the particles are trapped by the edges of the interference fringes. The "before-and-after" images were taken by removing the interference fringes, this was achieved by blocking one of the beams. In Figure 3.16 (c), the microspheres are shown to still be in ordered lines however they soon disperse after a few seconds due to Brownian motion. It was noted that interferometric trapping occurred at powers as low as 2 mW [89]. This magnitude of power needed for interferometric optical trapping is

achievable using a MCF device. This shows that the objective of this thesis is feasible using interferometric trapping techniques.

Particles trapped in linear interference fringes can be trapped in the axial direction by adding a counter propagating beam that doesn't interfere with the previous two beams used to produce the interference fringes. Casaburi et al., created interference fringes with light from a 514 nm Argon ion laser source to trap 1 µm polystyrene microspheres in fringes with a period of 1.5 µm as shown in Figure 3.17 [90]. They then introduced a third beam to balance the radiation pressure of the previous two beams allowing axial trapping of the microspheres. The microspheres shown in Figure 3.17 were pushed against the coverslip to trap in the axial direction, when the third beam was introduced the microsphere can be moved away from the coverslip and held in the middle of the sample cell. In practice, this method is impractical for three dimensional trapping in comparison to other multiple particle trapping techniques such as holographic traps as it requires beams to be focused on the sample from both sides of the sample cell.

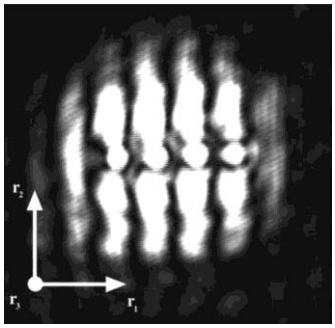

Figure 3.17. 1 µm polystyrene microspheres trapped in the centre of 1.5 µm interference fringes. This figure has been taken from [90].

The first demonstration of using interferometric optical trapping to create three dimensionally trapped arrays of particles was achieved by using a SLM to create the multiple beams [91]. SLM's were used to create multiple beams which were then interfered to produce fringes suitable for three dimensional optical trapping. It was shown that axial trapping can be achieved by increasing the number of beams. Schonbrun et al., demonstrated three dimensional trapping using eighteen beams with three different sets of radial wave vectors; the six inner hexagonal layer have the same

radial wave vector, $k_r(1)$, the six corner beams of the outer layer have a radial wave vector, $k_r(2) = 2k_r(1)$ and the six beams in the mid points in the outer layer have a radial wave vector $k_r(3) = \sqrt{3}k_r(1)$. Trapping is achieved in the axial direction when all the plane wave components are in phase. This can be described by the Talbot effect and can be described by the following equation [91].

$$z_{Talbot} = \frac{2\pi}{\Delta k_z(1,3) - \Delta k_z(1,2)} \tag{3.11}$$

where z_{Talbot} is the Talbot distance, the distance over which the plane wave components are in phase. The interference patterns of the eighteen beams produce periodic patterns in three dimensions; the plane wave configuration that forms the lattice structures are shown in Figure 3.18.

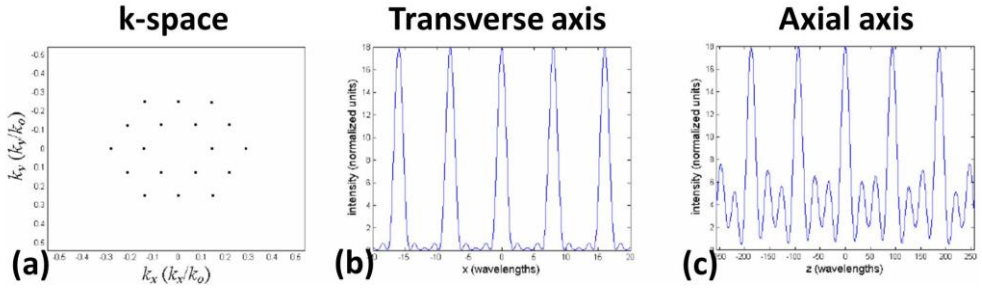

Figure 3.18. The eighteen plane wave configuration used to form the 3D optical lattice. (a) The eighteen waves in k-space, (b) the intensity peaks in the transverse direction with a period of 8λ, and (c) the intensity peaks in the axial direction with a period of 94λ. This figure has been taken from [91].

The authors demonstrated that arrays of particles can be trapped and translated in three dimensions for the first time using interferometric optical trapping [91]. However any particles trapped in a particular plane blocked the light patterns in the subsequent layers, therefore the particles could only be trapped in single layers but could be translated to different axial planes. SLM's have also been used to create three dimensional arrays of particles using umbrella like beam geometries [92]. The geometry allows for particles to be trapped in three dimensions in multiple layers, as shown in Figure 3.19.

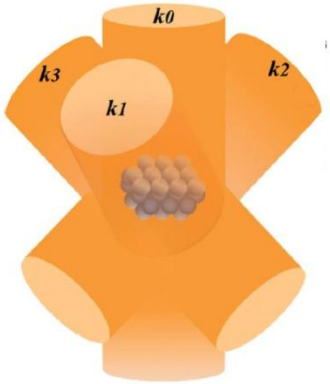

Figure 3.19. Schematic of multi-layered three dimensional trapped particles created using interference patterns formed using a SLM. This figure has been taken from [92].

Interferometric optical trapping can also be combined with single particle manipulation to create two dimensional patterns without defects or arrays with specified defect sites [93]. Mu et al., used light from a 514.5 nm, Argon ion laser, split into four beams, to create a two dimensional lattice. The x and y axes of the lattice were created from two sets of interfering beams. There was no mutual interference between the beams resulting from the path difference between the sets exceeding the coherence length of the laser. A helper beam generated using a 647.1 nm, Krypton-ion laser, which does not interfere with the interference pattern, was used to trap and move the particles around that were assembled in the interference pattern as shown in Figure 3.20. The interference pattern has a period of 3 μm that was used to trap 3 μm microspheres in the high intensity regions of the lattice pattern; the helper beam has a focused spot size of 3 μm; the same size as the microspheres.

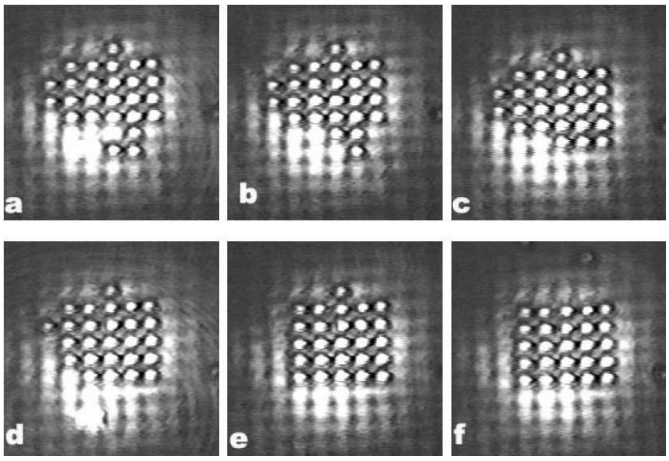

Figure 3.20. (a)-(e) The 3 µm microspheres were moved to the traps in the lattice pattern by the helper beam to complete the defect free lattice as shown in (f). This figure has been taken from [93].

The 3 µm microspheres shown in Figure 3.20, are trapped in two dimensions in the lattice pattern in a sample cell composed of two coverslips separated by a 80 µm spacer made of scotch tape.

Three dimensional arrays of particles can be created using interferometric optical trapping without the need for counter propagating beams or SLM's. Slama-Eliau and Raithel created three dimensional optical crystals using four optical beams [94]. A 1064 nm, Nd:YAG laser source was split into two parallel beams of orthogonal polarisation using a birefringent calcite crystal, the beams were then split into four by a polarising beam splitter that steers two of the beams upwards and two of the beams remain in a lower horizontal plane. The two sets of beams were then focused through two identical x100, 1.25NA objectives that were confocally aligned to have a common axis creating a highly symmetric optical lattice in the confocal plane. The set-up was used to trap 490 nm diameter polystyrene spheres in a three dimensional crystalline structure held in a sample cell made from two coverslips separated by a 100 µm paraffin film. The path lengths and intensities of all the beams were carefully controlled helped by the high level of symmetry in the system. Various half wave-plates were also used to control the polarisation and intensity of the beams, as shown in Figure 3.21.

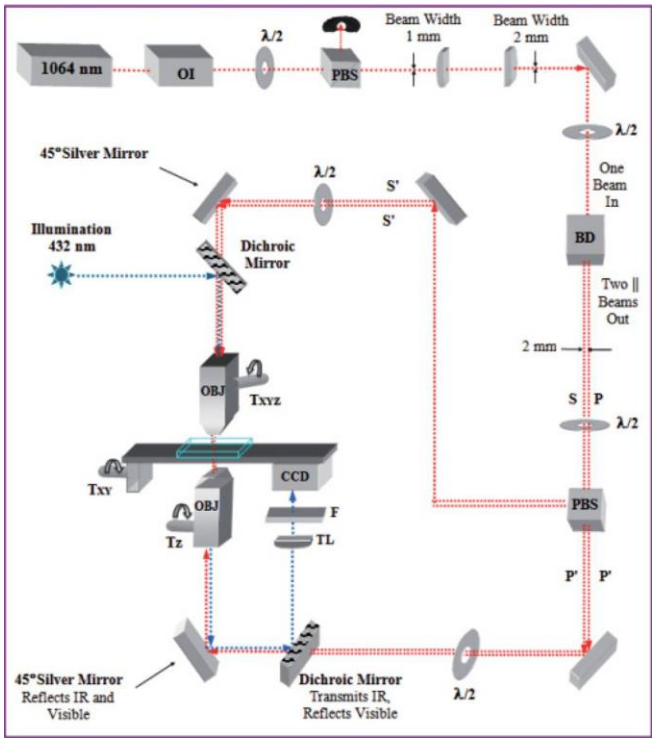

Figure 3.21. Experimental set up for creating three dimensional arrays of particles. This figure has been taken from [94]. Where OI – optical isolator, BD – beam displacer, OBJ – objective, T_z, T_{xy}, T_{xyz} – translation stages and TL – tube lens.

3.4. Summary

The work described in this chapter shows that free space optics result in a complex design that would be unsuitable for use in non-optics based laboratories. The work however gives an indication of the optical powers needed to form trapping regions that are achievable using fibre based systems. Fibre based systems will result in a compact "turn-key" device that will not rely on optical alignment, which will be suitable for use in biological laboratories.

There are various methods for multiple particle trapping and manipulation such as the laser scanning method, holographic optical trapping techniques and interferometric optical trapping. All these methods use free space optics to create the multiple traps resulting in large complex systems. The laser scanning method and the computer-controlled holographic trapping method are capable of producing any arbitrary trapping

arrangement desired; however a computer is required to control the SLM or deflectors that create the trapping arrays. When two-dimensional periodic arrays are the desired trapping arrangement the laser scanning technique and holographic trapping techniques often have impurities caused by beams not diffracted by the DOE, impurities in the liquid crystal pixels or the shutter used in laser scanning not completely closing when moving to the different trap positions. However the interferometric optical trapping technique will always produce periodic trapping regions, provided the trapping beams are in phase with each other allowing the interference fringes to be formed. To keep the beams in a constant phase relationship, the path lengths must be carefully controlled; this can be quite difficult when various beams are needed due to the mechanics of directing the beams using free space optics. If a multicore fibre is used all of the path lengths will be the same length and with the added benefits of a shared cladding stable fringe patterns can be produced [60]. The use of a multicore fibre for interferometric optical trapping will reduce the number of free space optical components needed, creating a more compact trapping system. In interferometric optical trapping, a focusing lens is used to create the interference fringes at the back focal plane of an objective that normally projects a further size reduced interference pattern into the sample plane. This is mainly due to the separation distance of the beams to keep them parallel before entering the lens. Using a multicore fibre will ensure the beams will be kept parallel at a close distance, the use of a lensed multicore fibre will remove the need for both lenses allowing the fibre to be focused directly onto the sample plane. The close separation distance of the beams also result in interference fringes with micron sized periods suitable for optical trapping of microspheres and biological cells such as *Escherichia coli (E. coli).*

Chapter 4. Dual Core Interferometric Optical Trapping

4.1. Introduction

The use of fibre optics in optical trapping as an alternative to free space optics provides greater flexibility, simplicity and a reduction in cost as they do not require expensive high numerical aperture lenses or confocal microscopes that are used for both trapping and imaging. Single fibre optical traps provide even greater flexibility allowing for the creation of compact devices. In this chapter, the functionalisation of the lensed MCF will be discussed and the results for using the fibre for interferometric optical trapping with one dimensional fringes will be presented. The uses of a single fibre probe for multiple particle trapping and manipulation through interferometric optical trapping techniques enhances the stability of the fringes and will provide all the advantages of using fibre optics such as creating a more compact system than current free space alternatives.

4.2. Fibre optics in optical trapping

The first demonstration of optical trapping using fibres was in 1993 when Constable et al., demonstrated three dimensional optical trapping, created with two counter-propagation single mode fibres [95]. The fibres were used to trap and manipulate 0.1 – 10 μm polystyrene microspheres as well as yeast cells with a fibre separation of 20 – 280 μm. The frequency difference between the lasers ensured that no interference effects occur, resulting in the trapping force being only dependant on the sum of the forces from the separated fibres. The transverse gradient component of the force that keeps the particle in the centre of the beam is treated the same as for optical trapping in free space configurations as described in Figure 3.2. The scattering force acts along the axis of propagation and in the case of opposing fibres at the position where the forces from either fibre balance, stable trapping occurs as shown in Figure 4.1.

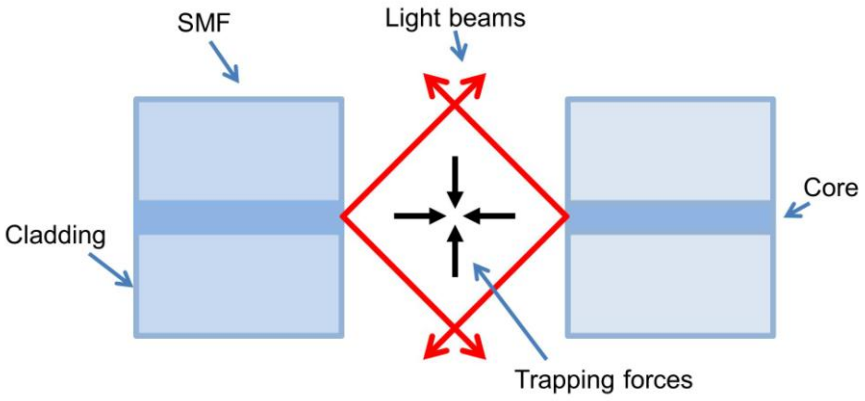

Figure 4.1. A stable trap occurs in the central position between two opposing SMF, where the red arrows represent the light beams and the black arrows represent the direction of the trapping forces.

To improve the stability of the trap, the fibres can be tapered and lensed to increase the beam divergence angle [96], as shown in Figure 4.2 (a). When the power from both lasers is equal there are two stable trapping positions at the foci of each lensed fibre as shown in Figure 4.2 (b), varying the power independently in each laser creates stable traps at a position between the fibres where the scattering forces balance. The lensing of the fibres creates an optical trap with stronger transverse optical confinement than cleaved fibres.

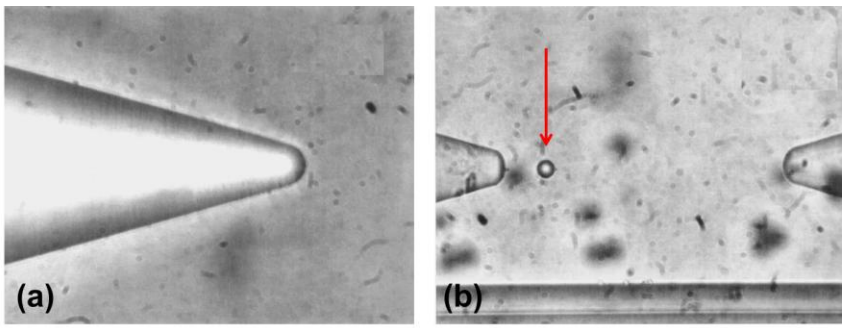

Figure 4.2. (a) Image of one of the tapered fibres used in the dual fibre trap, with a 10 µm radius hemispherical microlens fabricated at the end and (b) the dual fibre trap with a 10 µm polystyrene microsphere at the stable trapping position situated at the focus of the left tapered fibre indicated by the red arrow. This figure has been taken from [96].

The first demonstration of optical trapping with a single fibre was in 1997, Taguchi et al., polished a SMF to create a tapered spherical end suitable for trapping in two dimensions [97], as shown in Figure 4.3 (a). The lensing of the fibre creates a focal point approximately 20 µm from the fibre end that was used to trap single yeast cells or 10 µm polystyrene microspheres as shown in Figure 4.3 (b).

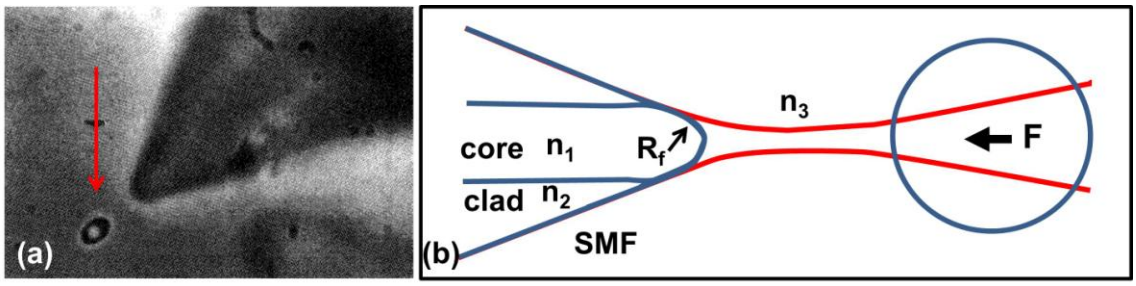

Figure 4.3. (a) Image of polished tapered SMF optically trapping a yeast cell at its focus and (b) a schematic diagram of a microsphere trapped by the focused beam emitted from a single polished tapered fibre. Figure (a) has been taken from [97].

In 2001, this paper was followed up with another showing that the polished fibre created stronger transverse optical confinement than a cleaved fibre [98]. With the polished fibre transverse optical trapping and manipulation of a particle on a surface was demonstrated. A similar lensed probe was used to manipulate nine yeast cells to form the letter "T" on the bottom of the sample chamber [99]. This was achieved by mounting the fibre tip on a needle attached to a multidimensional micromanipulator that could transcribe out the "T" shape. The yeast cells were only trapped one at a time and would move from trapped position due to Brownian motion when the probe was moved to a different trapping position. The first demonstration of three dimensional optical trapping using a single optical fibre was in 2003 [100]. Taylor and Hnatovsky demonstrated three dimensional optical trapping of a 2 µm borosilicate microsphere using a selectively chemically etched, tapered, hollow tipped metalized fibre probe. The probe was made by chemically etching a high germanium dioxide doped, 0.3NA single mode fibre in hydrofluoric acid to reduce the fibre diameter from 125 µm to a conical structure with a diameter of approximately 20 µm. The etching of the fibre also produces a hollow region in the centre of the conical structure with a height of 3 µm and depth of 1 µm as shown in Figure 4.4. The probe was then covered with a 100 µm thick

layer of aluminium, before focused ion beam technology was used to remove the layer of metal from the end face of the probe, exposing an annular silica region whilst leaving the hole still metal coated [100].

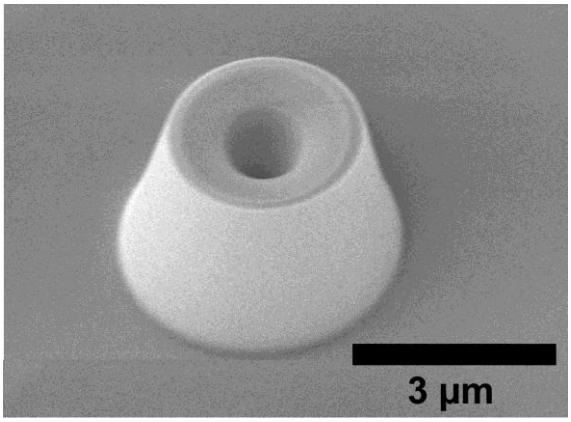

Figure 4.4. A scanning electron microscope image of the selectively chemically etched, tapered, hollow tipped fibre probe before the end was metalised. This figure has been taken from [100].

Optical trapping of the microsphere in the transverse direction was due to the annular light distribution emitted from the fibre. Trapping in the axial direction was thought to be due to the electrostatic forces produced from surface charging effects as a result of the metalised centre of the fibre, which balances with the scattering forces on the glass microsphere. Recently, chemical etching was used to create a tapered graded index multimode fibre probe suitable for optically trapping particles at a distance approximately 5.4 µm from the end of the fibre [101]. The graded index multimode fibre was shown to provide a transverse gradient trapping force about four times higher than a SMF with the same shaped end and was used to trap both 916 nm polystyrene microspheres and 5 µm yeast cells with a 980 nm diode laser. This is because the graded index MMF has a higher intensity peak and a greater convergence than the SMF. The trapping performance of the tapered SMF is more strongly influenced by the asymmetry and roughness of the taper at the core region than the graded index fibre that has a larger core.

Fibre bundles and multicore fibres have also been used to trap particles. In 2004, multiple particle trapping was demonstrated using three different imaging fibre bundles [102]. Each fibre in the imaging fibre bundle is capable of optically trapping a single particle if each fibre ends with a lensing element. Tam et al., created three different fibre probes for trapping multiple particles these were: (1) a step index fibre bundle with wells chemically etched into them before a ball lens was inserted into the well at the end of each fibre, (2) a step index fibre bundle with a convex lens structure chemically etched at the end of each fibre, and (3) a graded index fibre bundle where each fibre self focuses [102]. Fibres with 3 μm diameter cores were used in the fibre bundles that were positioned 25 μm from the bottom surface of a sample chamber, 3 or 4.5 μm silica microspheres were trapped in two dimensions against the bottom of the sample chamber, the number of particles trapped depended on the number of fibres illuminated in the fibre bundle. Using the graded index fibre bundle, thousands of 3 μm silica microspheres were trapped, and it was noted that the particles trapped at the sides prevented other microspheres from entering the centre traps, to overcome this, the solution of microspheres and de-ionized water was flowed in alternating directions to move particles to all areas of the optical traps. Fibre bundles have also been used to trap particles in three dimensions [27, 28]. In 2007, Liberale et al., created a fibre probe that utilises total internal reflection at the interface between the fibre and the surrounding medium to create focusing with a high NA [27]. Focused-ion-beam milling was used to shape the end of a four core fibre bundle at an angle of approximately $\theta = 70°$ at each core; this causes the light carried in the cores to experience total internal reflection at the fibre/medium interface. The light is refracted through the fibre cladding before converging at a point approximately 40 μm along the probe axis causing a focusing effect as shown in Figure 4.5.

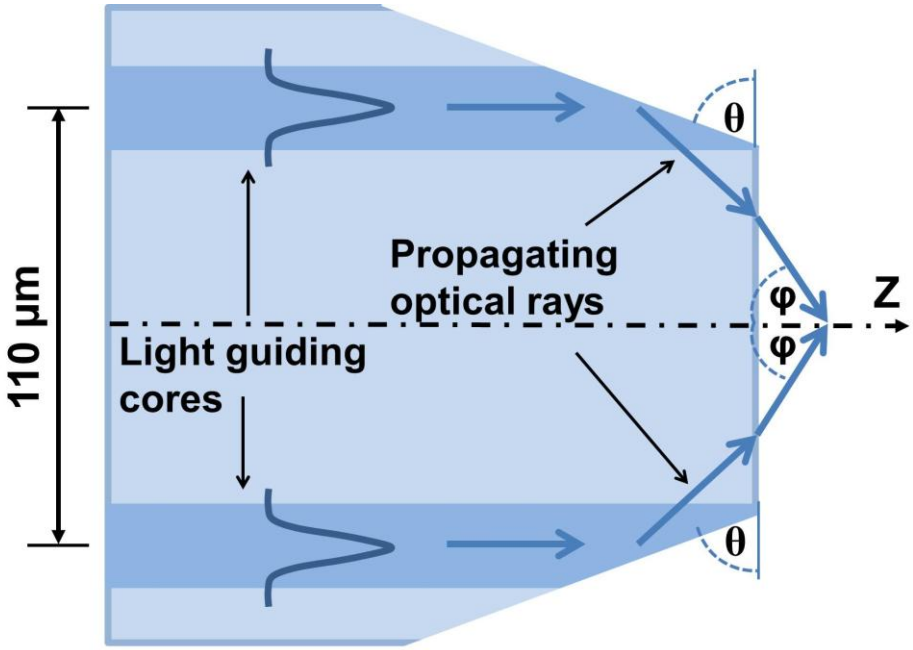

Figure 4.5. Cross section of the shaped fibre bundle depicting how total internal reflection at the fibre/medium interface results in a focusing effect suitable for three dimensional optical trapping [27].

The modified fibre bundle with an equivalent NA of approximately 0.93 was used to trap a 10 µm polystyrene microsphere in three dimensions allowing the particle to be lifted and translated throughout the sample chamber [27]. In 2013, Liberale et al., reported an improvement on their fibre bundle tweezers probes created by fabricating microprism reflectors on the end of each fibre by the two photon lithography technique as shown in Figure 4.6 (a) [28]. The microprism reflectors also create three-dimensional traps by utilising total internal reflection at the interface of the microprisms with the surrounding medium, the beams are then transmitted through the other side of the microprism and come to a crossing point 46 µm from the end of the fibre producing an optical trapping region as shown in Figure 4.6 (b). In a comparison to their fibre bundle probe described in reference [27], the two photon lithography fabrication method makes fabrication of devices easier and can produce probes with a longer trapping distance than the focused ion beam milling method. The focused-ion-beam milling method is also more expensive, time consuming and does not allow for the creation of complex structures. Although the two-photon lithography technique is less complex than the focused-ion-beam milling as it is more controllable, it still relies on precise

alignment of each microprism and low surface roughness of below 100 nm to reduce scattering and allow for total internal reflection.

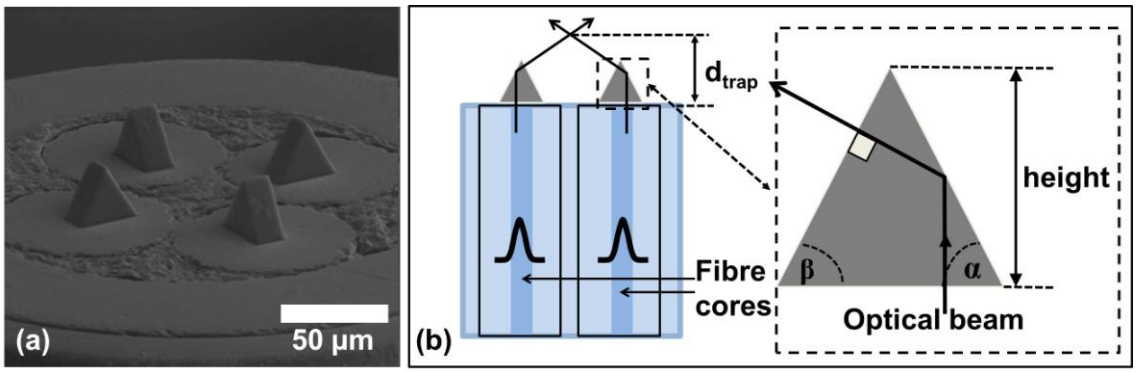

Figure 4.6. (a)The microprisms are fabricated over each core in the fibre bundle and (b) schematic showing how the traps are produced by total internal reflection at the outer surface of the microprisms. This figure (a) has been taken from [28].

The microprisms were made from a polymerised resin with a refractive index of 1.56; when the probe is placed in water, a minimum angle of $\alpha = 58.5°$ is required to have total internal reflection. Therefore the microprisms were created with an angle of $\alpha = 60°$, this produces a probe with an effective NA = 1.15 [28]. The probe was used to trap single polystyrene microspheres with diameters of 7, 10 and 15 µm as well as red blood cells and tumour cells in three dimensions with an output power of 5 mW from each prism. The authors also demonstrated how the probe can be integrated into a microfluidic device to aid in the Raman and fluorescence spectroscopy of single cells.

Multicore fibre has also been used for single fibre optical trapping [103, 104]. In 2008, Yuan et al., tapered a dual core MCF with a core to core separation of 62.5 µm down to a half-spherical lens with a radius of 2.5 µm, that acts as a high NA microlens [103]. The fibre was used to trap single yeast cells with a diameter of about 5.5 – 6.5 µm at the tip of the probe in three dimensions. Manipulation of the cell was accomplished by creating a Mach-Zehnder interferometer inside the probe by splicing an SMF fibre onto the dual core fibre before tapering to form a coupling zone at the splice point and a further tapered region between the splice point and the probe tip to form the second

coupling zone as shown in Figure 4.7. Bending of the fibre at the interferometer section varies the intensity in each core, allowing orientation control of the trapped cell.

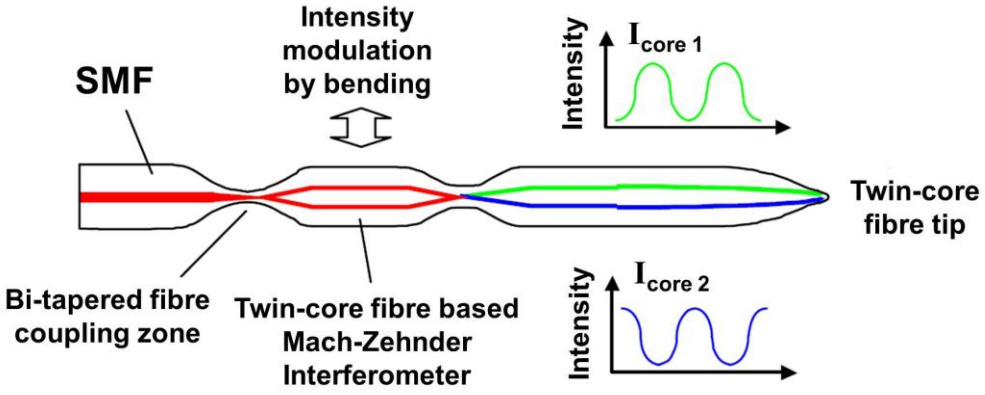

Figure 4.7. Schematic of the dual core fibre tweezers with an integrated Mach-Zehnder interferometer for orientation control of trapped cells. This figure has been taken from [103].

Particles trapped with the above dual-core fibre tweezers touched the probes tip. In 2012 the same group created non-contact MCF tweezers [104]. Zhang et al., created MCF trapping probes using either a two core MCF or a fibre with an annular core; however they state similar probes can be created with any MCF with an annular core distribution. The probes were created by grinding and polishing the fibre while the fibre was rotated, the front point was also polished back as shown in Figure 4.8. To allow for trapping in the axial direction the angle where the beams intercept should be around β = 90°. With the dual-core fibre, multiple yeast cells were trapped in three dimensions approximately 20 µm from the end of the fibre. The annular core fibre was used to trap a single 45 µm dielectric microsphere close to the end of the fibre, as shown in Figure 4.8 (b).

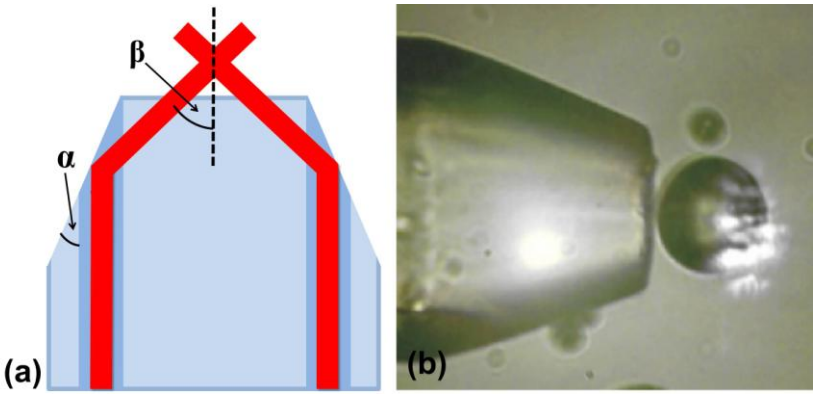

Figure 4.8. (a) Schematic of the polished MCF showing the light from the cores undergoes total internal reflection before coming together to form an optical trap close to the end of the fibre and (b) a 45 µm dielectric microsphere is trapped in three dimensions using the annular core fibre. Figure (b) has been taken from [104].

The fibre probe demonstrated in Figure 4.8 (b), although described as non-contact shows the trap is positioned close to the end of the fibre. All single fibre or fibre bundle traps require the end of the fibre to be modified effectively increasing the NA to induce a trapping region. The methods demonstrated such as fibre polishing, focused ion beam milling and two photon lithography are time consuming methods that require a high degree of precision. Modifying fibres through chemical etching requires hydrofluoric acid which is extremely hazardous and requires specialist equipment and training to use. In the experiments described in this thesis, we modified the MCF by lensing with a fusion splicer. This method has many advantages over the other techniques mentioned above; such as a reduction in time, less fabrication costs, high repeatability and does not require the use of chemicals such as hydrofluoric acid.

4.3. Gemini multicore fibre

The use of an MCF for trapping multiple particles through interferometric optical trapping will enhance the stability of the fringes compared to using fibre bundles or free space optics and will also create a more compact system compared to free space alternatives. Throughout the experiments reported in this thesis, a four core MCF was used as shown in Figure 4.9 (a). The MCF is a commercially available fibre supplied by Fibertronix AB and is known as Gemini fibre. Fibertronix AB is a spin out company

from Acreo a Swedish information and communication technology research institute. The MCF is fabricated by drawing four standard telecommunication fibre preforms together to form a single fibre as shown in Figure 4.9 (b) [105]. The cores have a 7 µm diameter and are arranged in a square with an inter-core spacing of 80 µm and a diagonal core spacing of 113 µm. The MCF has a width of 165 µm in the square directions and a width of 200 µm diagonally. The MCF is surrounded by a circular acrylate coating with a diameter of approximately 315 µm. The fibre is similar to the standard telecoms fibre SMF-28; it is made of silica with germanium doped cores and designed for single mode operation and low loss at 1550 nm. Two versions of the Gemini fibre were used in the experiments demonstrated in this thesis; the major difference between them was the cut off wavelength. The first version was used in the work reported in this chapter and had a cut off wavelength of 1300 nm. The second version of the fibre was used in the work reported in Chapters 5 and 6 and had a cut off wavelength of 1 µm.

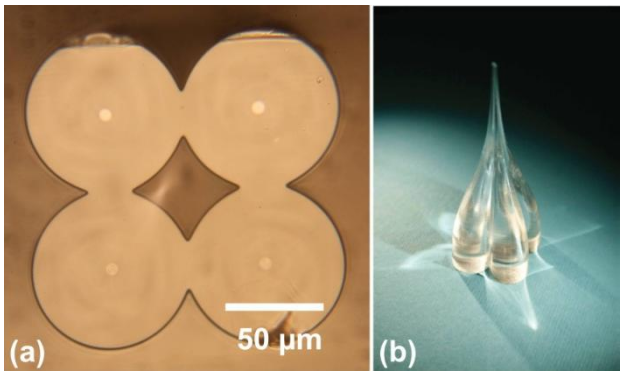

Figure 4.9. (a) End face image of the four core Gemini MCF and (b) the preform of the Gemini MCF. Figure (b) has been taken from [105].

4.4. Functionalising the MCF

To be able to use a single multicore optical fibre for optical trapping i.e. to functionalise the fibre, the output end needs to be modified to focus the beams to a common point. This can be accomplished through a variety of methods such as focused ion beam milling, laser processing, two photon lithography, polishing, chemical etching and lensing. We chose to functionalise our fibre through fibre lensing with a fusion splicer

as it is rapid, unproblematic, utilizes readily available equipment already present in most fibre laboratories and so is cost effective and is an extremely reliable and repeatable system. The MCF was cleaved with a fibre scribe and then placed in a Sumitomo T-36 fusion splicer. With the fusion splicer on manual settings the fibre was aligned to the splice point and a 14 second arc was performed. This shapes the end of the fibre as shown in Figure 4.10. A 14 second arc was chosen to lens the MCF as that was the highest preprogramed arc time and the second highest preprogramed arc time of 4 seconds did not produce a fully lensed fibre end, it only slightly curved the edges of the fibre and does not alter the surface in front of the cores, whereas a 14 second arc modifies the whole end facet as shown in Figure 4.10. The position of the MCF relative to the electrodes, over the translation range available, was shown to have no visible effect on the curvature of the resultant lens. If higher power was able to be delivered to the electrodes, ball lenses could be produced on the end of the MCF, this could possibly result in greater confinement in both the transverse and axial directions.

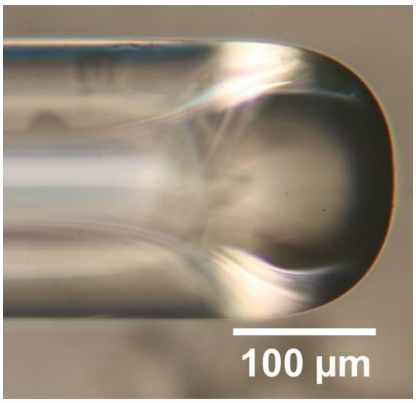

Figure 4.10. The modified end of the MCF after lensing for 14 seconds in a fusion splicer.

The shape and behaviour of the lensed fibre was shown to vary depending on the diameter size of the fibre and the material of the fibre, ball lenses could be formed on smaller fibres such as SMF-28 and also on softer glasses such as a MCF made from Tellurite as shown in Figure 4.11. The diameter of the MCF is larger compared to standard fibre such as the 125 µm diameter SMF-28 and is made of silica which is a

harder glass than Tellurite. The softening temperature of silica glass is 1600 °C [106], in comparison to Tellurite that has a softening temperature of 340 °C [107].

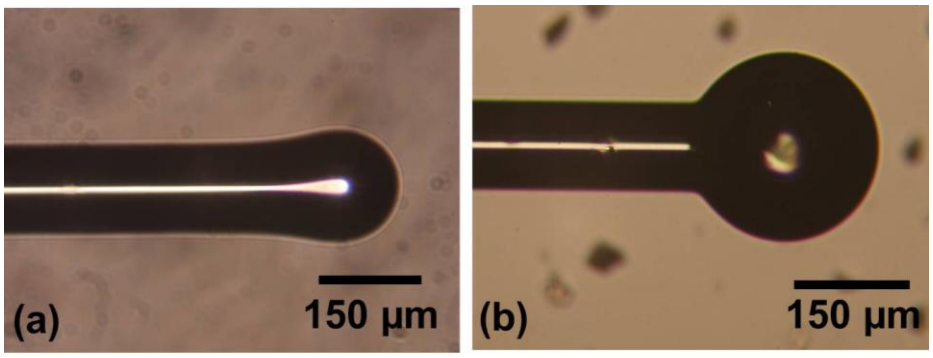

Figure 4.11. (a) A 14 second arc applied to a SMF-28 fibre produces a ball lens with a lower radius of curvature than the MCF and (b) a ball lensed is produced at the end of a 125 µm diameter tellurite fibre when a sputter of less than 1 second is applied.

Lensing the fibre in such a way was found to produce repeatable results using conventional equipment. Occasionally the lensing can cause the outputs from the cores not to come together at the same crossing point, but provided the MCF is cleaved straight and orthogonal to the fibre length, without any defects the lensing will result in a usable probe around 50 % of the time. The fusion splicer is an extremely reliable and repeatable system; therefore even if the lensing is inadequate, the lensing process can be repeated quickly compared to other lensing methods. This technique has proven advantageous over techniques such as focused ion beam milling, laser processing, two photon lithography, polishing and chemical etching such as a reduction in time, fabrication costs, and commercial viability. The use of fibre lensing is also a safe process compared to chemical etching as it does not use hazardous chemicals such as hydrofluoric acid. The lensing also anneals the end of the fibre resulting in a clean, smooth and scatter free surface.

4.5. Dual core coupling

The lensing properties of the MCF were assessed by coupling into two of the diagonal cores using a Nd:YLF laser source (Elforlight: model L 500-1047) operating at a

maximum power of 800 mW at 1047 nm. The diagonal cores were chosen as the outputs come together from opposite sides of the fibre resulting in an equal symmetry across the fibre. If adjacent cores were used, they would still produce fringes with a larger fringe spacing, however the force components across the fibre would not cancel out resulting in a residual force in the direction across the MCF away from the cores as shown in Figure 4.12. The intensity of the fringes using the diagonal cores will be highest in the centre of the fringe pattern decreasing further from the centre with a Gaussian like profile. However for the adjacent cores, the intensity will be greatest on the left side of the fringe pattern nearest the cores which will be undesirable for multiple particle trapping experiments.

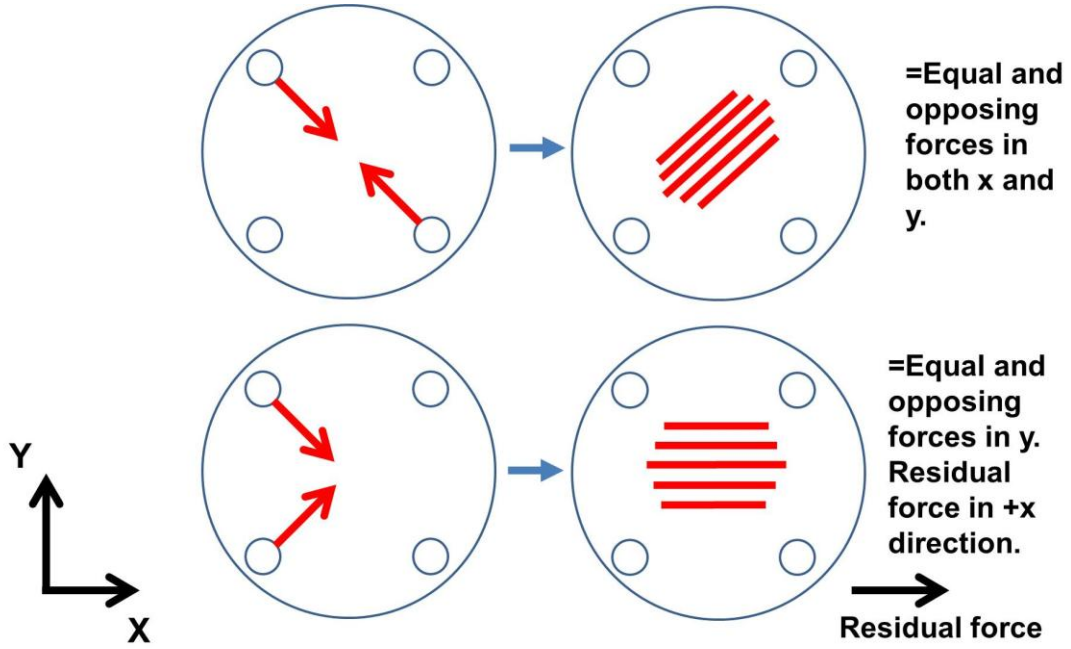

Figure 4.12. The difference between using the diagonal cores versus coupling into two adjacent cores.

A 50:50 Thorlabs polarising beam splitter was used to split the light into two, before being coupled into the diagonal cores of the MCF through a single x20, 0.54NA microscope objective using sets of mirrors as shown in Figure 4.13. Both beam paths were made to be the same length to ensure the wavefronts are coherent with one another and a half wave-plate was used to adjust the polarisation in one of the beams to improve the visibility of the fringes as the fibre is not polarising maintaining. Mirror sets M1,

M2, M5 and M3, M4 were used to ensure the two beams enter the microscope objective at an angle and offset optimum for even coupling into the two diagonal cores.

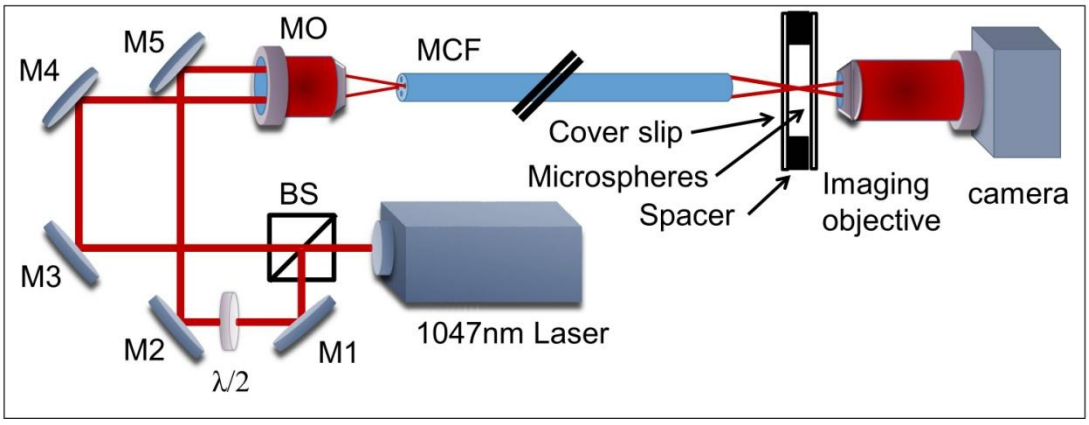

Figure 4.13. Experimental set up for dual core coupling of the MCF where M1-M5 are silver mirrors, MO – microscope objective, BS – beam splitter and λ/2 – half wave-plate.

The lensing of the fibre was shown to refract the output beams from the cores to a crossing point approximately 250 ± 25 µm from the end of the fibre when the fibre is in air. This increases to approximately 500 ± 25 µm from the end of the fibre when submerged in water as shown in Figure 4.14. This increase in distance to the crossing point is caused by the increase of refractive index from 1 in air to 1.33 in water; this decreases the angle at which the rays are refracted as can be described by Snell's Law, resulting in a crossing point further away from the fibre.

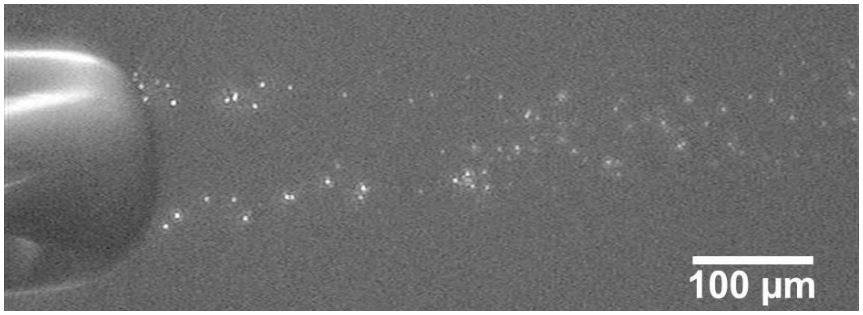

Figure 4.14. Side profile of the lensed MCF showing 1047 nm light scattered from 1.3 µm polystyrene microspheres in water.

At the crossing point high contrast interference fringes are produced, these were found to have a period of approximately 2 ± 0.3 μm in air which increases to 4.3 μm in water as shown in Figure 4.15. The uncertainty given was calculated by measuring the fringe spacing of ten lensed fibres and calculating the mean and range, the uncertainty is due to the repeatability of the lens. When two cores are used, the beams will always cross at some point even if the lens is too poor to produce a 4 core crossing point; however the crossing point might not be on the same axis as the centre of the fibre and at a different distance from the fibre than expected. There is also an error of approximately ± 0.1 μm from the difficulty in determining where the crossing point is, that itself has an uncertainty of ± 25 μm. The smallest fringe spacing is found at the position where all beams overlap, creating the narrowest beam size and the fringe spacing increases either side of this position. This error could be eliminated by using alignment software that finds the position of the beam waist or by measuring each fringe set over a range of distances to find the smallest fringe spacing. The fringe spacing was measured from an average of at least eight fringes and approximated to be the same for each fringe over the whole image. The spacing is calibrated by imaging a graticule with the same optical system as used to image the fringes. The graticule gave a calibration of 0.170 μm.pixel^{-1} for a x40, 0.55NA aspheric objective lens from Newfocus (model number 5722) with a 1/3 inch CCD colour camera from Dedicated Micros (model number DM/ICE-CM3H). There will be a small error in the calibration of the graticule and the resolution of the camera but as the fringes were measured over hundreds of pixels these errors will be negligible in comparison to the errors caused by the uncertainty due to the repeatability of the lensing process and the position of the crossing point. The error from the calibration will be of the order of 0.01μm.

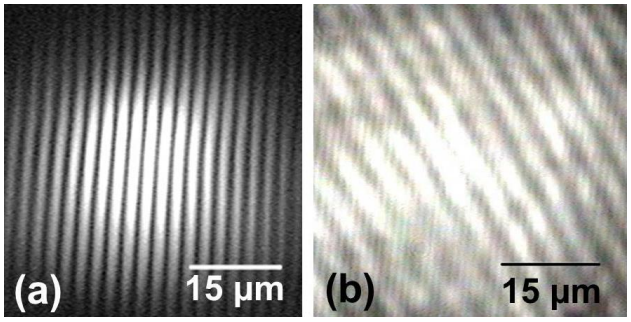

Figure 4.15. Interference fringes produced at the crossing point of the lensed MCF when two of the diagonal cores are coupled into using 1047 nm light. (a) When the MCF is in air and (b) when the MCF is in water.

The interference fringes produced intensity gradients across the crossing point as shown in Figure 4.16. This pattern is similar to fringe patterns produced using free space optics that have been used for micro-particle trapping and manipulation [32].

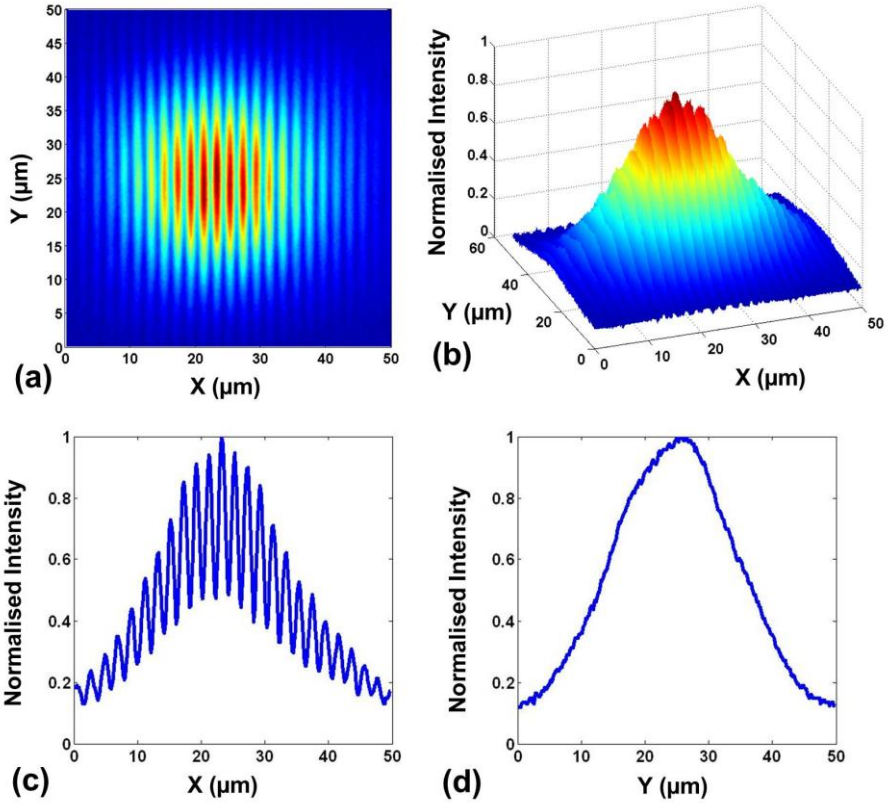

Figure 4.16. Interference fringes produced at the crossing point of the lensed MCF when two of the diagonal cores are coupled into, when the MCF is in air. (a) Two

dimensional intensity plot of the fringe pattern, (b) three dimensional normalised intensity plot of interference pattern, (c) the cross section through the centre of the normalised interference pattern in the x direction and (d) the cross section through the centre of the normalised interference pattern in the y direction.

The intensity plots in Figure 4.16 (c) and (d) were taken by plotting a cross section in both x and y directions respectively, through the maximum intensity point in Figure 4.16 (a) and (d). The plots show that the highest intensity is found in the centre of the middle fringe and falls to a minimum both along the fringe axis and perpendicular to the fringe axis with Gaussian like profiles. Figure 4.16 was produced by importing an image of the fringes at the crossing point into MATLAB and calibrated using a graticule that gave a calibration of 0.158 μm.pixel^{-1} for images taken using a x30, 0.40NA aspheric objective lens from Newfocus (model number 5723) and a Thorlabs, high resolution USB CCD camera (model number DCU224C). The data from the image was normalised then plotted in two and three dimensional graphs. The highest intensity peak was then found and cross sections were taken along both the x and y directions of the fringe pattern.

4.6. Simulations for dual core interference

The lensed fibre was modelled using beam propagation software (BeamPROP, RSoft Design Group Inc.). BeamPROP is a design tool that is based on the beam propagation method for the design and simulation of integrated and fibre optic waveguide devices and circuits. The purpose of the simulations is to understand the lensing properties of the MCF. This will allow us to compare the experimental results to the simulated results. It is difficult to fully understand what happens to the cores of the MCF during the lensing process. The structure of each core may deform and taper or expand, the refractive index of the core or cladding glass itself may be modified and the shape of the air void structure in the centre of the fibre will be altered. The structure of the model was therefore estimated from images of the lensed MCF like that shown in Figure 4.10. The model was approximated by using a spherical lens with a radius of curvature of 82.5 μm followed by a straight section with a thickness of 5.6 μm and a diameter of 165 μm, this produced an outer surface that matched the dimensions of the lensed fibre

shown in Figure 4.10. The lens was on top of a straight section of fibre with a core diameter of 7 μm and fibre diameter of 165 μm. The cores of the fibre stopped before the spherical lens as shown in Figure 4.17 (a) and (b). This was due to the capability of the software as it models the propagation of the beam in sequence through the system and only simple lenses can be drawn, to get the desired lens, the cores had to stop at the back of the spherical plano-convex lens. Tapered fibre ends were modelled; however they did not produce sensible results and could not be combined with the curved lens without causing scattering points in the software. However as can be seen from Figure 4.17 (c) and (d) the mode field diameter increase only slightly inside the lens by approximately 1.5 ± 0.5 μm, with the largest divergence occurring at the curved end of the lens. The refractive index of the lensed section is approximated to be the same as the cladding with a refractive index of 1.46, compared to the cores that have a refractive index of 1.47 from information provided by the supplier. However slight variations in refractive index were shown to have little effect on the results of the model. This approximation was made as the lens could only be created from a single element and as the output from the cores only diverges slightly inside the lens, the lens was given the same refractive index as the cladding. As can be seen from Figure 4.10, the lensing of the MCF distorts the cores so it looks like they taper, it is estimated that this effect causes the refractive index of the cores to reduce to be the same as the surrounding cladding, however this could not be confirmed experimentally. The outputs when light is coupled into two of the diagonal cores was modelled for when the fibres were in a medium of air and water as shown in Figure 4.17 (c) and (d) as a comparison to the experimental results.

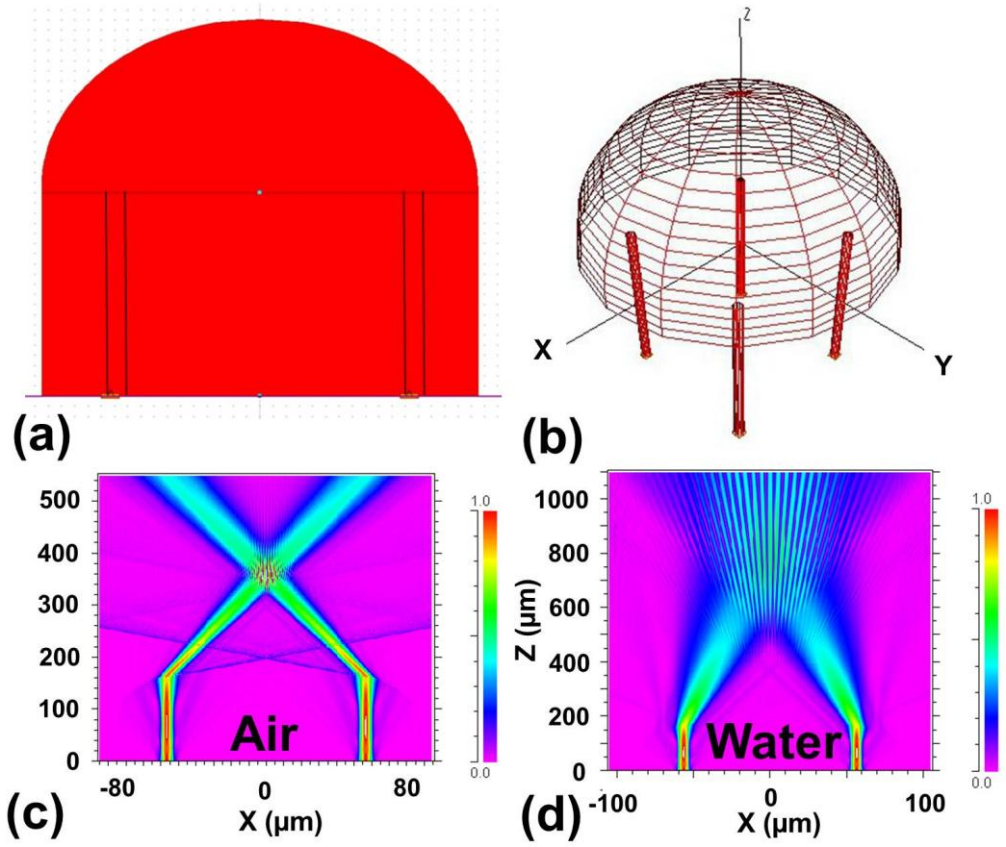

Figure 4.17. (a) BeamPROP model of the lensed MCF, (b) a three dimensional model of the lensed MCF, (c) the simulated output of the lensed MCF in air, and (d) the simulated output of the lensed MCF in water.

As expected from the experimental results the models show that the output from the MCF was shown to vary depending on the refractive index of the surrounding medium. The model shows that the distance from the end of the fibre to the crossing point increases from a distance of 195 µm in air to 535 µm in water and the period of the fringes also increases from 1.22 µm in air to 3.35 µm in water, this was carried out by changing the refractive index difference of the components in the model to be relative to water instead of air. Although the model does not produce the same values for fringe spacing and distance between the fibre and the crossing point as those measured experimentally, it does show the same trend in the large increase of using the fibre in a medium of water compared to air. The reason they do not agree is due to radius of curvature of the lens being estimated as spherical from a microscope image such as that shown in Figure 4.10, when in fact the lens is not completely spherical as the model

suggests. The differences may be due to the difficulty in determining what happens to the cores during the lensing process, as can be seen in Figure 4.10, the cores appear to taper slightly but the spherical surface of the lens distorts the image of the fibre making it difficult to determine the structure of the cores.

An experiment was carried out to investigate the effect of lensing on the cores. The output surface of the fibre was imaged for different distances as the fibre was polished back. To ensure that the MCF is polished evenly across its facet, the MCF was glued and UV cured into a glass block that had a v-groove etched into it using the ultrafast laser inscription process and selected chemical etching in hydrofluoric acid. The glass block was polished back to the tip of the fibre where the first measurement was taken measuring the central positions of the outputs from the cores. The block was then polished back and measured until the output positions did not vary and were the same spacing as an unmodified MCF, this was at a distance of 94 μm from the end of the fibre. The positions of the outputs were shown to vary by approximately 5 μm, bending further towards the centre of the cores as shown in Figure 4.18. This is only a small change in position therefore it was concluded that the majority of the lensing property came from the curvature of the output surface of the modified fibre rather than the modification to the cores inside the fibre. This agrees with the results of the model that showed the beams only expanded slightly inside the lens yet the largest diffraction comes from the output surface of the lens. In Figure 4.18 (c), positions z = 94 μm corresponds to the end of the lensed MCF.

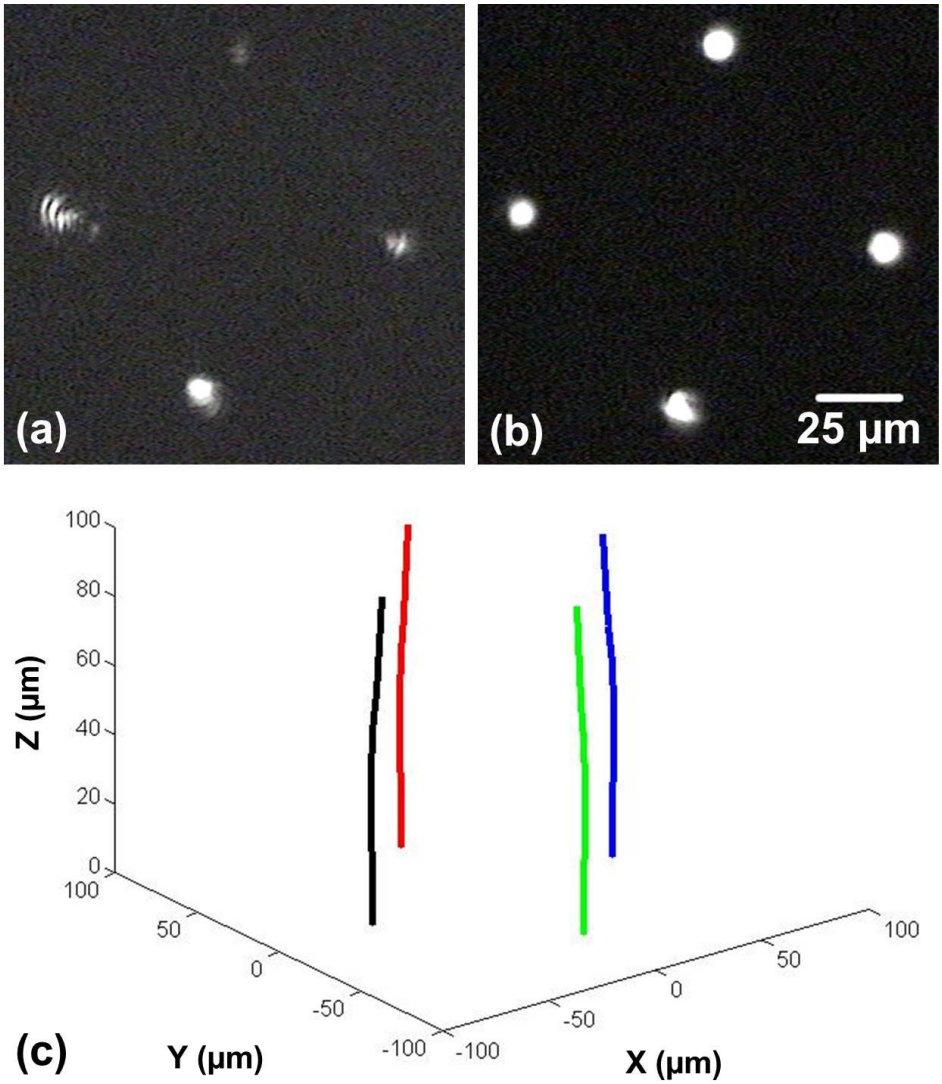

Figure 4.18. (a) Output of the cores at the end of the fibre at polishing position z = 94 µm, (b) the output of the cores at the end of the fibre at polishing position z = 0 µm has the same spacing as an unlensed MCF and (c) plot of how the positions of the cores vary due to the lensing of the fibre from data taken by polishing the fibre back over a length of 94 µm.

As the end surface of the MCF caused most of the lensing, the BeamPROP model was modified by increasing the radius of curvature of the lens until the results of the model correlated with the experimental results for fringe separation and the distance to the crossing point. The model was also modified to include a 100 µm thick cover slip and an 80 µm thick water sample to represent the sample chamber that contains the microspheres where the crossing point of the fringes is positioned as shown in Figure

4.19 (a). A spherical lens with radius of curvature of 130 µm and a diameter of 200 µm was placed on top of a straight fibre section with 7 µm diameter cores spaced 80 µm apart in a square with a shared cladding with a diameter of 200 µm. Increasing the radius of curvature was shown to increase the distance between the crossing point and the end of the fibre, as a result the fringe spacing also increases. A 100 µm cover slip with a refractive index of 1.45 was placed 90 µm from the end of the fibre and was followed by an 80 µm thick section of water with refractive index of 1.33 to represent the sample. The addition of the coverslip and water increases the distance to the crossing point and the fringe spacing as shown experimentally when the microspheres are added.

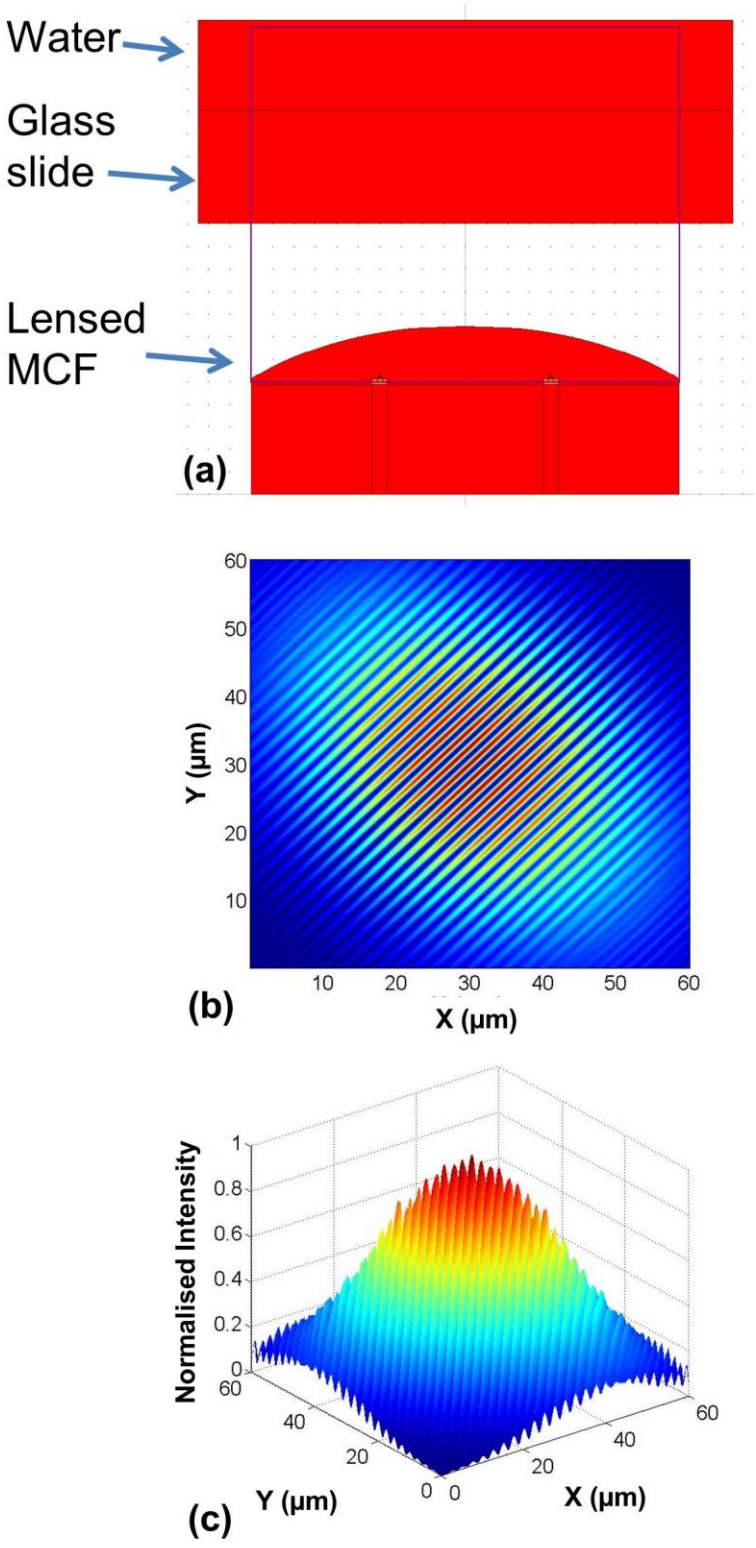

Figure 4.19. (a) BeamPROP model of the lensed MCF with sample chamber, (b) the simulated normalised intensity plot of the overlap region for two cores, and (c) the simulated normalised intensity plot of the interference fringes in three dimensions.

The BeamPROP model as shown in Figure 4.19 (a) produced an overlap region 220 µm from the tip of the MCF that produced fringes with a period of 1.77 µm as shown in Figure 4.19 (b) and (c). This is within the uncertainty of the experimental data of 2 ± 0.3 µm. The results from the models show that the lensing of the MCF can be accurately modelled using a spherical lens with a radius of curvature of 130 µm. This curvature did not match the curvature of the MCF determined from microscope images however the results produced from the model are within the uncertainty of the experimental data.

4.7. Optical trapping using linear interferences fringes

As demonstrated in the previous sections, the lensed MCF produces high contrast interference fringes with a fringe spacing of approximately 2 µm. Interference fringes created using free space optics have previously been used to optically trap multiple particles in the high intensity regions of the fringes [32, 90]. The use of an MCF to create interference fringes for multiple particle trapping will improve the stability of the fringes due to the shared cladding and create a more compact system. A solution of microspheres were held between two 100 µm thick cover slips and kept in place using an 80 µm thick vinyl spacer between the cover slips. The lensed MCF was positioned in air outside the cover slips with an imaging system at the other side of the sample chamber as depicted in Figure 4.20.

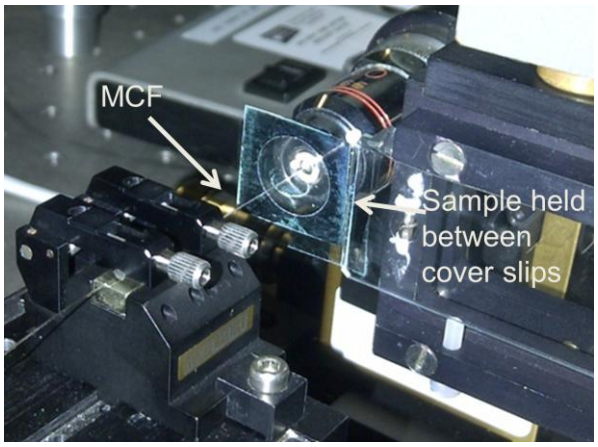

Figure 4.20. The sample chamber is made of two cover slips separated by a vinyl spacer; it is held perpendicularly to the fibre and imaged through from the other side.

Whilst imaging the crossing point, the sample chamber was held perpendicular and inserted between the fibre and imaging objective, the sample chamber was then moved toward the fibre until the microspheres were focused in the same plane as the crossing point. Having the fibre in air increases the intensity of the fringes as the beams diverge less than when they are in water so the size of the interference pattern and the fringe spacing is smaller, this can be seen from Figure 4.15. The interference fringes produce transverse gradients through the same method as the optical traps described in Section 3.2.1, in which microspheres can be trapped in the high intensity regions of the fringes. The movement of the microspheres is restricted along the fringes by the force pulling them into the centre of the fringe, but mainly confined to the centre of the fringe where the highest intensity can be found. The lensed MCF was used to trap polystyrene microspheres (Polysciences: Polybead® Microspheres) with diameters of size 1.3 µm, 2 µm and 3µm as shown in Figure 4.21. The particles are pushed to the back of the sample chamber trapping them against the surface of the cover slip. As can be seen from Figure 4.21 (b), the 1.3 µm microspheres were often difficult to image due to their small size but they can be seen to align along the fringes. The 3 µm microspheres were larger than the period of the fringe, resulting in them overlapping and making them harder to distinguish as shown in Figure 4.21 (d). We therefore chose to use 2 µm diameter microspheres in our further experiments, as these were around the same size as the fringe spacing and didn't overlap, as shown in Figure 4.21 (c).

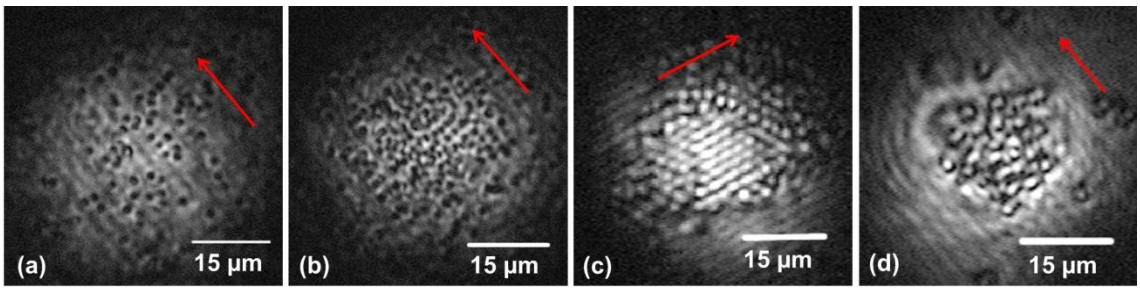

Figure 4.21. Polystyrene microspheres trapped along the interference fringes produced from the lensed multicore fibre when coupling into two of the diagonal cores. (a) 1.3 µm microspheres trapped in the high intensity region of the fringe pattern, (b) the 1.3 µm microspheres are often difficult to image when in high concentration, (c) 2 µm microspheres are around the same width as the fringe spacing, and (d) 3 µm

microspheres are bigger than the fringe spacing. The red line indicates the direction of the fringes.

To assess whether the alignment of the particles was due to the interference fringes or whether it was due to the overall intensity, one of the beams were blocked with a beam dump to remove the fringes. The microspheres were shown to spread out in all directions, but when the fringes are reintroduced the microspheres become ordered and align along the fringes again as shown in Figure 4.22. In Figure 4.22, the time when the fringes are reintroduced is indicated as t = 0 seconds. In this experiment, carried out to produce the images depicted in Figure 4.19, the combined power exiting the fibre from the two cores was 30 mW when a power of 250 mW was measured after the microscope objective at the input of the fibre. This high loss is due to the difficulty in coupling into the two cores through a common objective lens, due to the large core separation of 113 μm the lens has to be offset to allow even coupling into each of the cores, the use of an optical interconnect such as those described in Section 2.6 can improve on these losses. Care was taken to ensure even coupling into each core, to improve the visibility of the fringes, by measuring the power coupled into each fringe independently by blocking each beam in turn and optimising the coupling until the power in each core is equal.

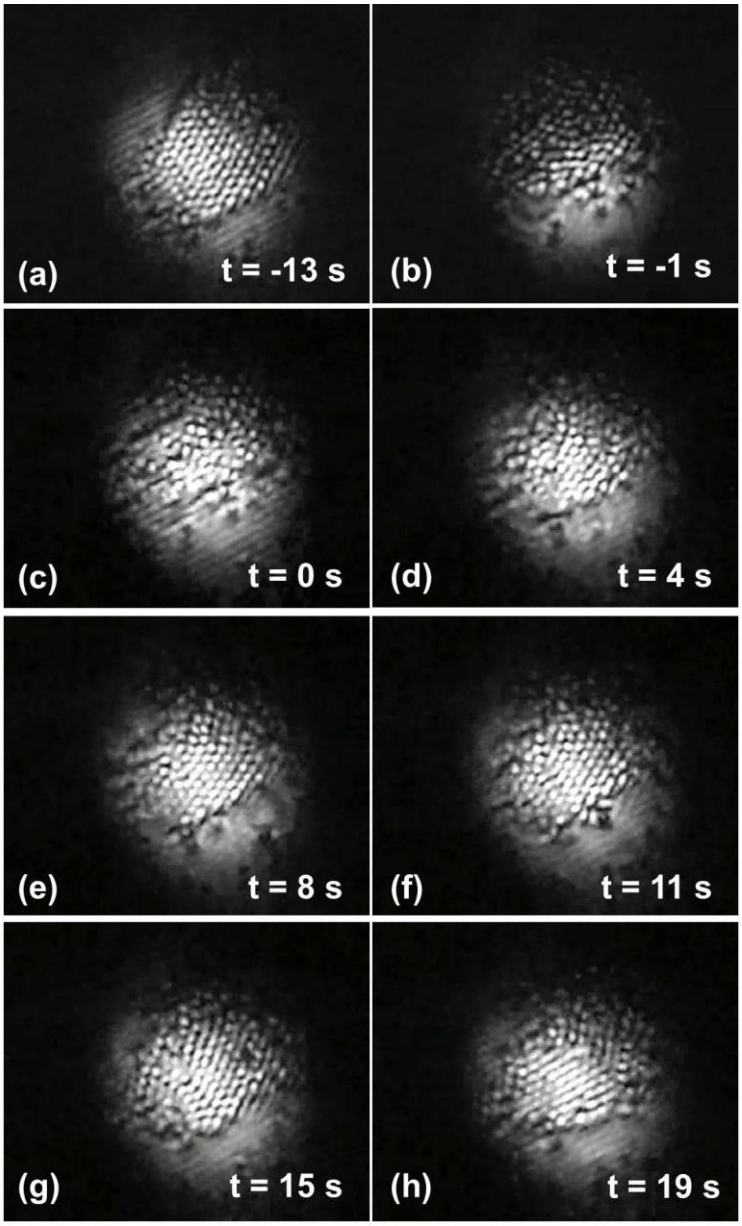

Figure 4.22. Single frame excerpts from a video recording of 2µm polystyrene microspheres trapped along the interference fringes. (a) The microspheres are trapped along the interference fringes created when both beams are present, (b) the fringes are destroyed when one of the beams are blocked, the microspheres become disordered and are free to move, (c)-(g) the fringes are reintroduced at time t = 0 seconds and the particles start to align along the fringes, they are confined to the centre of the beam rather quickly within a few seconds but take longer to align along the fringes and (h) 19 seconds after the fringes are reintroduced the particles align along the interference fringes.

4.8. Conclusions

One dimensional interferometric optical trapping has been demonstrated using the dual core output from a single lensed multicore fibre. Lensing the MCF with a conventional fusion splicer is a robust way of functionalising the end of a fibre for use in optical trapping that does not result in additional costs through expensive equipment or fabrication costs as it utilises equipment commonly found in most fibre optical laboratories which is appealing. In comparison to other methods previously used for fibre optical trapping, such as ion beam milling, two photon lithography, fibre polishing and chemical etching, this method produces repeatable results with high quality, scatter free surfaces and offers a large reduction in fabrication time and costs.

The lensing of the fibre produces a crossing point in the far field from the output of two diagonal cores where high contrast interference fringes are formed. The longitudinal position of this point and the period of the fringes were shown to vary greatly depending on the surrounding medium. In air, the crossing point was approximately 250 μm from the end of the fibre with a fringe spacing of approximately 2 ± 0.3 μm. When the fibre was immersed in water, the distance of the crossing point from the fibre increases to approximately 500 μm with a fringe spacing of 4.3 μm. The fringe spacing and the distance from the fibre to the crossing point for the model based on the shape of the lensed MCF was shown to increase, in water, as compared to air, just as the experimental data shows; however there was a discrepancy in both with regards to results suggested by the modelled and experimental results. The modelled results gave a fringe spacing of 1.22 μm at a distance of 195 μm from the fibre in air that increased to a fringe spacing of 3.35 μm in water at a distance of 535 μm from the end of the fibre when placed in water. The fringe spacing increases when the fibre is placed in water, in comparison to air; however these modelled results are not within an acceptable error range of the experimental values of 0.3 μm for the fringe spacing and 25 μm for the distance to the crossing point. This may be due to not being able to determine the exact structure of the fibre and how the cores are affected by the lensing, although an experiment to find out the central position of the cores showed that each core was tapered by approximately 5 μm, this may aid in bringing the outputs to the same position in the far field. It is thought that the main lensing is due to the external shape

of the fibre at the output of the cores. A modified model created by increasing the radius of curvature of the lens until it agreed with experimental data yielded a period of 1.77 μm at a distance of 220 μm from the tip of the fibre. This new model was shown to simulate the lensed MCF more accurately than the first model based on the shape of the lensed MCF.

Light from the linear interference fringes were used to trap particles in the high intensity regions of the fringes. Polystyrene microspheres with diameters of 1.3 μm, 2 μm and 3 μm were trapped in the fringes. The 2 μm microspheres were chosen for further experiments as they were the closest to the size of the fringes so did not overlap each other and were large enough that they could be imaged clearly with the available optical imaging system. The trapping was shown to be due to the interference fringes, when the fringes were removed and the particles could move freely; but when the fringes returned the particles lined up along the fringes. Coupling into two diagonal cores produces strong trapping regions across the fringes but weak trapping along the fringes with the particles collecting in the centre of the fringes separated only across the fringes. This can be seen from the gradients of the edges of the intensity peaks. Separation of the particles is only achievable in the direction across the fringe. By using all four cores of the MCF, strong trapping confinement can be achieved in both transverse directions across the crossing point. Traps created using all four cores of the MCF will be able to separate particles in both the x and y directions allowing cell to cell interactions to be examined. To couple into all four cores of the MCF optical interconnects will need to be used such as those described in Section 2.6 or using a diffractive optical element. In the next section, results showing two dimensional trapping using all four cores, coupled using a diffractive optical element will be presented.

Chapter 5. Two Dimensional Optical Trapping Using a Lensed Multicore Fibre and a Diffractive Optical Element

5.1. Introduction

In the previous Chapter, optical trapping using dual core interference from a lensed MCF was demonstrated. The results showed that particles can be trapped in the high intensity regions of the fringes and can be separated across the fringes but gather together along the fringes in the central regions. Further confinement of the particles can be achieved using four core interference by coupling into all four cores of the lensed MCF. This will achieve two dimensional interferometric optical trapping and complete separation of the particles in both transverse directions across the interference pattern. In previous work, the laser beam was split into two and coupled into two diagonal cores of the MCF using a beam splitter, a microscope objective and steering mirrors with careful consideration taken to ensure both the path lengths were the same. To couple into four cores of the MCF the desire to create a compact system means a similar coupling set up cannot be used. Coupling four beams into each core of the MCF through the same microscope objective would present additional difficulties, reduce efficiency and uniformity. To couple light evenly into each core of an MCF, there are various optical interconnects, as previously described in Section 2.6, that overcome the difficulty of coupling, due to the close proximity of the cores and geometrical arrangements. Diffractive optical elements can split a single laser beam into any number of beams or arrangements allowing a custom DOE to be created for coupling light into an MCF. In this Chapter, two-dimensional interferometeric optical trapping is demonstrated using the lensed MCF described in the previous chapter with coupling achieved using a custom made DOE.

5.2. Diffractive optical element fabrication

Light was launched into the four cores of the MCF using a DOE created by our collaborators Dr Andrew Waddie and Professor Mohammad Taghizadeh from the Diffractive Optics research group at Heriot-Watt University. The DOE used split one

beam of light evenly into four beams was a phase only hologram. These types of holograms can be designed using either a closed-form solution to the Fraunhofer diffraction integral for a small number of fan-out orders such as are required here or by using a modified Gerchberg-Saxton phase retrieval algorithm for a large number of fan-out orders [108]. The DOE's can be created to produce arbitrary distributions of diffraction orders to match any fibre core geometry by adapting the hologram used to create the DOE. Large fan-out geometries can be created with high efficiencies (> 90 %) and with a low level of non-uniformity between the fan-out orders of < 1 %. The DOE design was formed from a two dimensional array of pixels that are dependent on the required number of fan-out orders. An array of 2Nx2M pixels is required for MxN fan-out orders. Between the pixels, there is a relative phase delay chosen from a basis set of available phase steps to $1/2^m$ multiples of 2π where m=1, 2, 3… (i.e. 0.5, 0.25, 0.125…). The fabrication of the DOE is achieved by repeated applications of binary amplitude masks with successive deeper features with high spatial frequencies using a photolithographic/ reactive ion etching process. The number of photolithographic/etching stages required is dependent on the number of phase levels in the design and can be calculated as $\log_2 X$, where X is the number of phase levels. High uniformity of < 0.1 % between the output beams was required to ensure even coupling to each core of the MCF therefore only two phase levels were used to create the DOE as shown in Figure 5.1 (a), resulting in a diffraction efficiency of approximately 65 %. The efficiency could be improved by increasing the number of phase levels; however the uniformity between the output beams would reduce due to misalignment of the levels and unavoidable etch errors. As the cores for our MCF are arranged in a square with no central core, the central zeroth order of the diffraction pattern needs to be extinguished. The intensities of the central order and the launch orders can be controlled by manipulating the DOE design and the overall etch depth of the structure [109]. Figure 5.1 (b) shows the simulated output from a 2x2 fan-out DOE used to couple to the MCF with a supressed zeroth order.

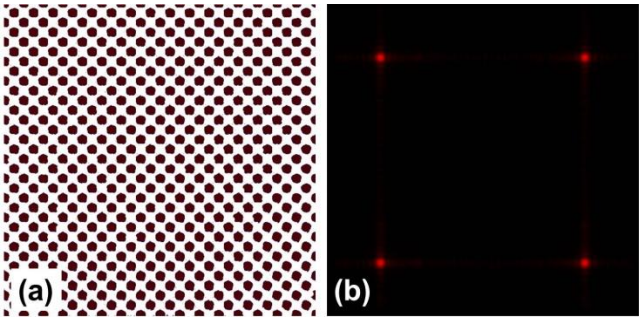

Figure 5.1. (a) Phase profile of a 2 level 2x2 fan-out element with lower intensity zeroth order. Black represents 0 relative phase delay and white represents π relative phase delay and (b) simulated output from the 2x2 fan-out DOE with supressed zeroth order.

5.3. Four core coupling characterisation

The DOE was custom-made to produce four even beams with the same spacing and arrangement as the MCF when it is placed at the back focal plane of a x10, 0.16NA aspheric objective lens from Newfocus (model number 5726) and illuminated with the same 1047 nm Elforlight laser source as used in Chapter 4. The position of the DOE from the back of the lens was varied until the output of the beams had the same spacing as the cores of the MCF. This was found to be at a distance of 16 mm from the back of the lens; however there was only a change of 5.7 μm in the spacing when the DOE was moved 40 mm behind the lens. These measurements were taken by imaging the focal point of the x10, 0.16NA aspheric objective lens and measuring the spacing of the diffracted beams. As stated in Section 5.2, the diffraction efficiency of the DOE was approximately 65 % due to the requirement of even coupling into each order to achieve high visibility fringes at the output of the MCF. The other diffraction orders also have the same spacing as the desired diffraction order as can be seen from Figure 5.2. Figure 5.2 also shows that the central zeroth diffraction order has been fully suppressed, as desired.

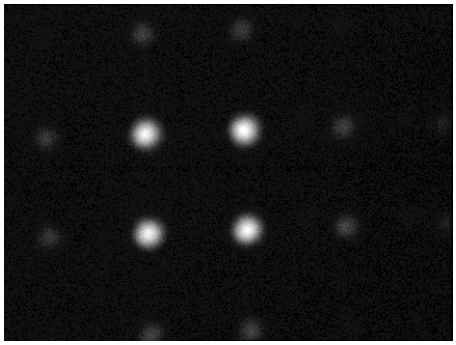

Figure 5.2. Higher diffraction orders from the DOE are evident. The desired diffraction order has a diffraction efficiency of approximately 65 %.

To couple light into the MCF, it was placed at the focal point of the x10, 0.16NA aspheric objective lens and rotated to match the same orientation as the DOE. Both the DOE and the MCF were on separate x, y and z translation stages to optimise the coupling into the four cores. The experimental set-up is illustrated in Figure 5.3. The use of the DOE guarantees that the path lengths are all the same ensuring an optimum mutual coherence. Mirrors M1 and M2 were used to optimise the coupling into the four cores by ensuring the beam arrives at the DOE, normal to its surface.

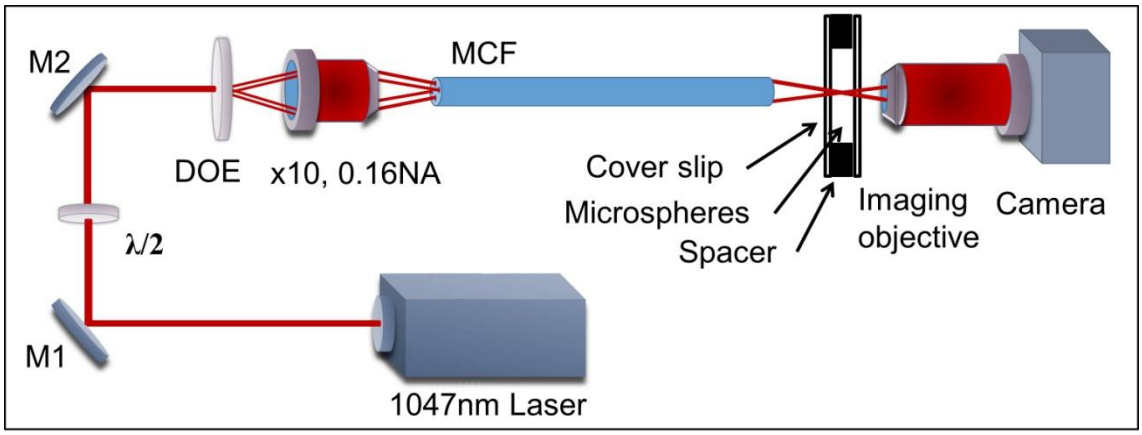

Figure 5.3. Experimental set up for four core coupling using a DOE where M1 and M2 are silver mirrors and λ/2 – half wave-plate.

The half wave-plate positioned in the input beam path to the DOE was used to improve the visibility and appearance of the fringes. The MCF was lensed as described in

Section 4.4, where the lensing causes the output from the four cores to refract and come to a crossing point approximately 250 µm from the end of the fibre. At the crossing point an interference lattice pattern is produced as shown in Figure 5.4 with a fringe spacing of 2.75 µm. The fringe spacing was calibrated by imaging a graticule with the same imaging system used to view the fringes. The graticule gave a calibration of 0.0549 µm.pixel^{-1} for a x100, 0.7NA Mitutoyo, infinity corrected, long working distance lens (model number #46-147) and a Thorlabs, high resolution USB CCD camera (model number DCU224C).

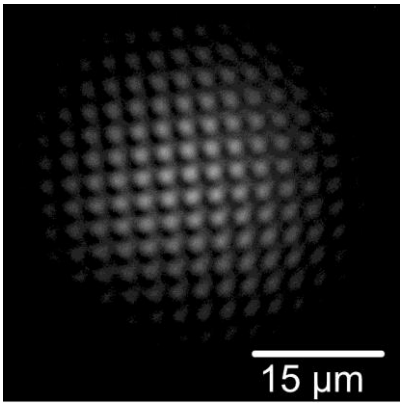

Figure 5.4. The output from the lensed MCF with all four cores illuminated produces a lattice interference pattern with a fringe spacing of 2.75 µm.

The interference fringes produced an array of intensity peaks across the crossing point as shown in Figure 5.5 (b). These are similar to those produced using free space optics [93].

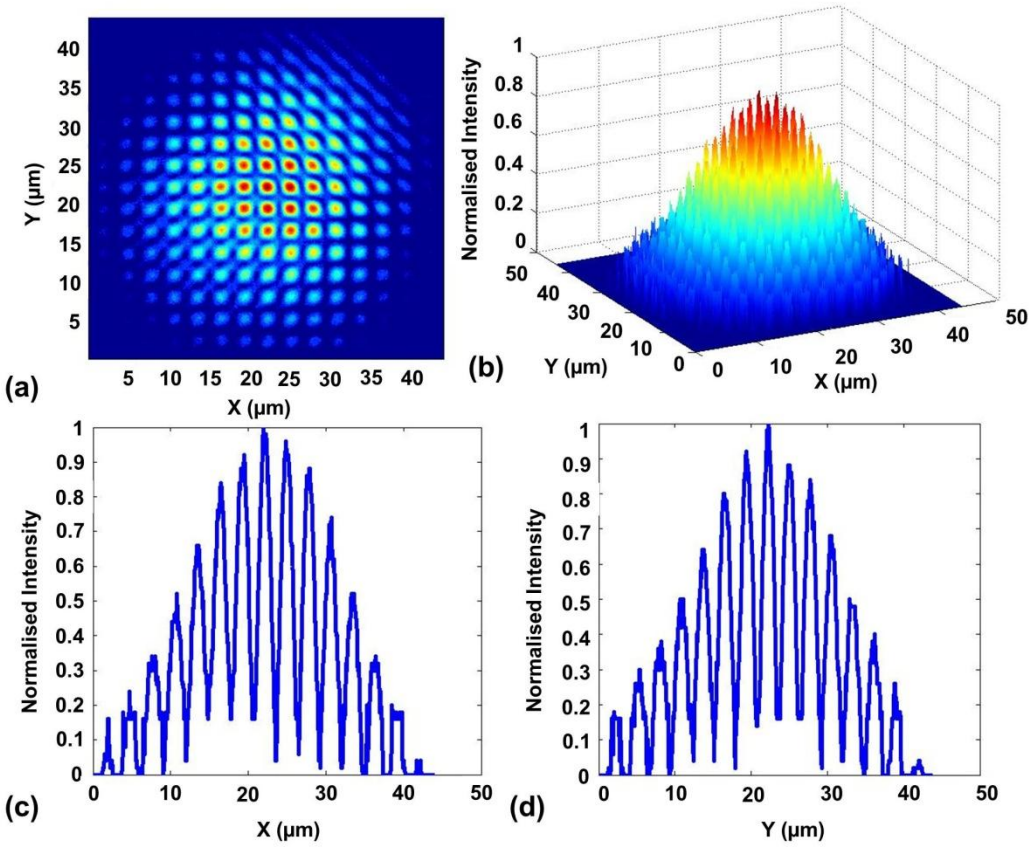

Figure 5.5. Interference fringes produced at the crossing point of the lensed MCF when light is coupled into all four cores using a diffractive optical element. (a) Two dimensional intensity plot of the fringe pattern, (b) three dimensional normalised intensity plot of interference pattern, (c) the cross section through the centre of the normalised interference pattern in the x direction and (d) the cross section through the centre of the normalised interference pattern in the y direction.

Figure 5.5 (c) and (d) shows the cross section intensity plot through the highest intensity point in Figure 5.5 (a) and (b). The use of the DOE ensures even coupling into each core. The addition of the half wave-plate improves the visibility of the fringes as shown in Figure 5.5 (c) and (d); the visibility of the fringes is greater than 80 % that produces intensity peaks suitable for optical trapping. Figure 5.5 (a) and (b) shows that even lensing across the end of the MCF was achieved, producing a crossing point where the cores overlap in the same plane producing high quality fringes. Figure 5.5 was generated by importing an image of the fringes into MATLAB and calibrated with the same calibration as Figure 5.4 of 0.0549 µm.pixel^{-1}. The data from the image was

normalised, then plotted in both two and three dimensional graphs. Using MATLAB the coordinates of the highest intensity peak were found and a cross section in both x and y through this point was taken to produce the graphs shown in Figure 5.5 (c) and (d).

The addition of the half wave-plate in the input beam to the DOE improved the visibility of the fringes but also allowed for the manipulation of the fringe pattern to produce different fringe patterns and different optical trapping arrangements. Rotation of the half wave-plate produces four distinct fringe patterns spaced 22.5° turn apart and repeated every 90° turn, as shown in Figure 5.6. A 22.5° turn of the half wave-plate corresponds to a 45° rotation of polarisation of the beam. For the images presented in Figure 5.6, the lattice fringe pattern shown in Figure 5.6 (a) was taken when the input polarisation to the DOE is at an angle 45° after horizontal; however if the fibre was moved the input polarisation angle required to produce the same fringe pattern was shown to vary.

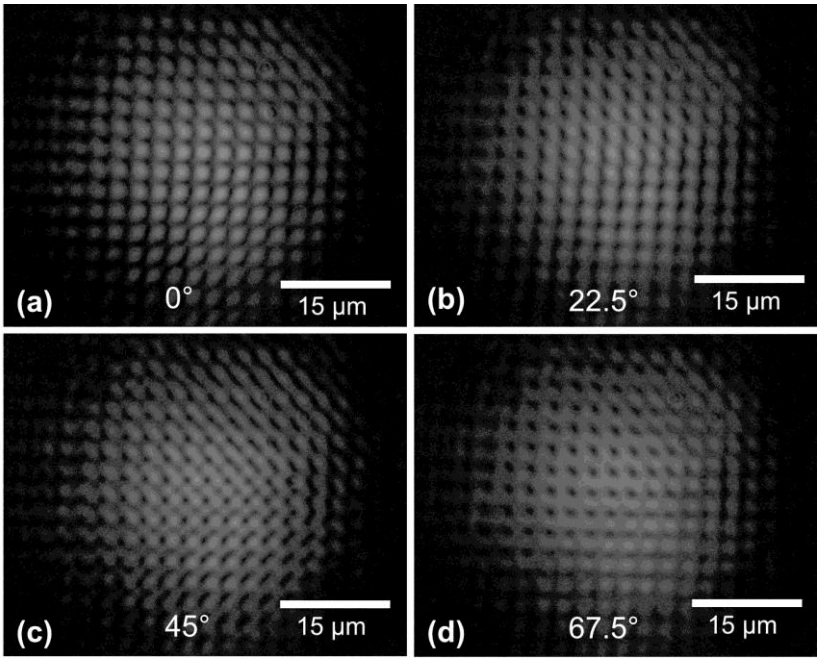

Figure 5.6. Rotation of the half wave-plate varies the output fringe pattern from the lensed MCF. (a) The high visibility lattice fringe pattern at 0° half wave-plate rotation, (b) the fringe pattern at 22.5° half wave-plate rotation resembles 1D fringe patterns with peaks joined along the vertical direction, (c) the fringe pattern at 45° half wave-

plate rotation appears to be almost the inverse of the high visibility lattice pattern and (d) the fringe pattern at 67.5° half wave-plate rotation appears to be a waffle like interference patter with peaks joined along the horizontal direction.

Moving the MCF was also shown to vary the output of the fringe pattern. To examine the effect the MCF has on the polarisation of the light exiting it, linearly polarised light was launched into the MCF and the output was imaged through a polariser. Rotation of the polariser did not completely extinguish the image, as would happen if the output of the MCF is linearly polarised; therefore the MCF gives an additional polarisation component to the output. This additional polarisation component may be caused by variations between the cores such as their refractive index, diameter or residual stress in the fibre. The output of each of the fringe patterns shown in Figure 5.6 was imaged through a polariser; the visibility of the lattice fringe pattern was shown to improve when only linear polarisation component contributing to the pattern is let through the polariser as shown in Figure 5.7 (a). For each image taken at 22.5° rotation intervals of the half wave-plate shown in Figure 5.6, an image was also taken through a polariser shown in Figure 5.7. Figure 5.7 (b) gives the appearance of vertical linear fringes and is the image shown in Figure 5.6 (b) when viewed through a polariser.

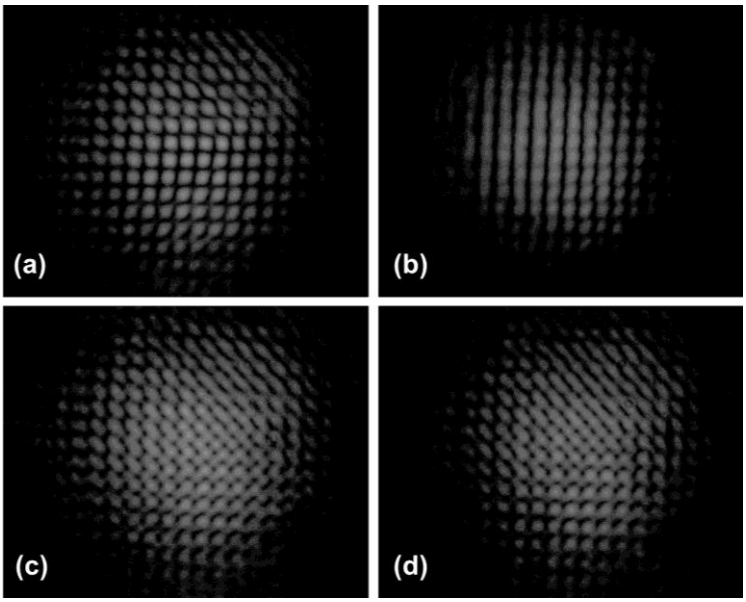

Figure 5.7. The images shown in Figure 5.6, taken at 22.5° half wave-plate rotation intervals, when viewed through a polariser, (a) when only the linear component of the

polarisation is viewed the visibility of the fringes is improved, (b) the fringe pattern of Figure 5.6 (b) resembles linear fringes when viewed through a polariser, (c) the visibility of the reversed lattice pattern is improved when viewed through the polariser and (d) when the waffle pattern is imaged through the polariser it appears similar to the image in (c) with the visibility of the fringes improved in the vertical direction.

The visibility of lattice fringe pattern at the output of the lensed MCF will not reach 100 % due to the addition of a polarisation component by the MCF. The visibility could be improved if the MCF was polarising maintaining or if a polariser could be placed after the lensed MCF before the crossing point but that would defeat the advantage of using a MCF for multiple particle trapping and manipulation. It would also be impractical due to the short working distance of the lensed MCF. The visibility of the lattice fringe pattern produced with the half wave-plate at its optimum position, as shown in Figures 5.4, 5.5 and 5.6 (a), is greater than 80 % which produces distinct optical gradients over each peak that will provide stable optical trapping of dielectric particles. Rotation of the half wave-plate will also allow the manipulation of trapped particles.

5.4. Simulations for four core interference

To examine the interactions of the beams at the output of the lensed MCF when all four cores are coupled into, the same BeamPROP model as used for the dual core interference and shown in Figure 4.19 (a) was used. The model has a lens with a radius of curvature of 130 µm and a diameter of 200 µm on top of a 150 µm long section of fibre with 7 µm diameter cores with a refractive index of 1.47, spaced in a square 80 µm apart and surrounded by a cladding with a diameter of 200 µm and refractive index of 1.46. The sample chamber was also included in the model by using a 100 µm thick glass section with a refractive index of 1.45, followed by an 80 µm thick water section with a refractive index of 1.33. In the model, the sample chamber was placed 90 µm after the end of the fibre. The results from the model, shown in Figure 5.8, gave a crossing point at a distance of 245 µm from the end of the fibre with a fringe spacing of 2.75 µm. These values agree with the experimental results of a crossing point at approximately 250 µm from the end of the fibre with a fringe spacing of 2.75 µm,

showing that this simple model accurately describes the effects of the lensing of the MCF even if the effects of the lensing procedure on the cores of the MCF is not fully known.

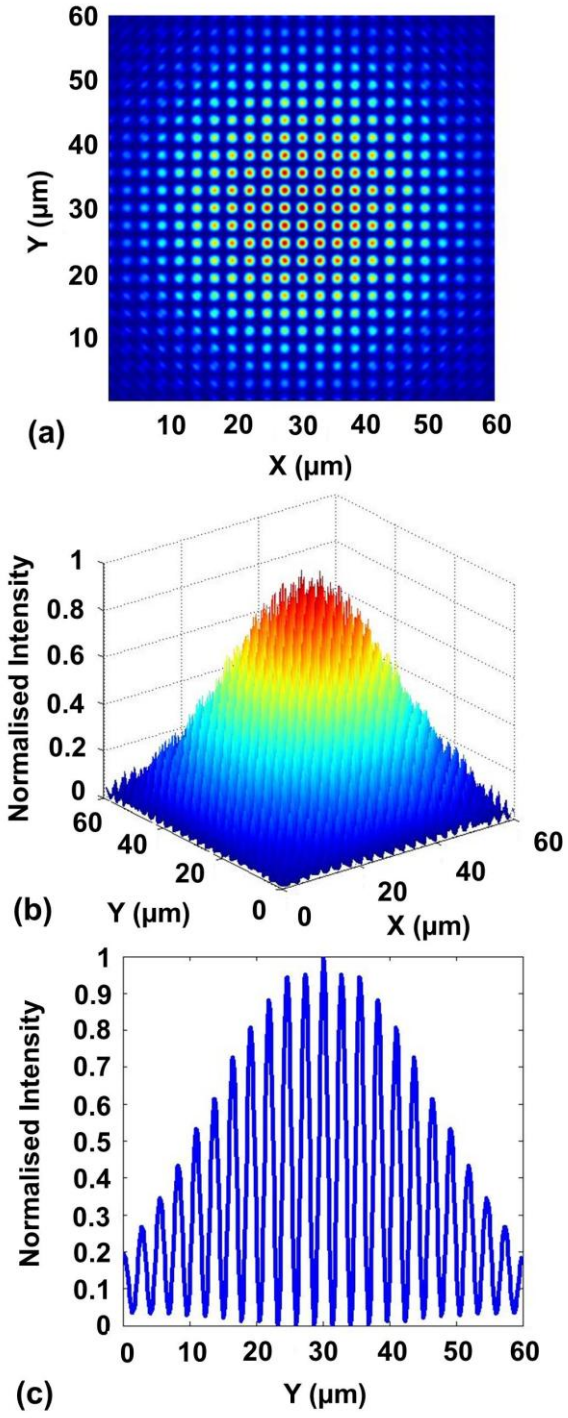

Figure 5.8. (a) The simulated normalised intensity plot of the overlap region for four cores, (b) the simulated normalised intensity plot of the interference fringes in three

dimensions and (c) a cross section along the y direction through the highest intensity point.

The simulated results as shown in Figure 5.8 agree with the experimental results in both the distance from the MCF to the crossing point and the fringe spacing. The cross section through the highest point of Figure 5.8 (a) and (b) is shown in Figure 5.8 (c), it shows that the visibility of the fringes is 100 %; this is because the model cannot accurately describe the polarisation effects demonstrated in the experiment. This shows that without the added polarisation component from the fibre, 100 % visibility could be achieved. Figure 5.8 (c) shows the cross section in the y direction, the same results is obtained along the x direction.

5.5. Optical trapping of polystyrene microspheres using two dimensional interferences fringes

The output of the lensed MCF when light is coupled into all four cores, produces high visibility interference peaks across a two dimensional lattice as shown in Figure 5.5 (b). Each of these intensity peaks can be used to optically trap single particles in both the x and y transverse directions across the interference pattern. Each of the peaks act like separate optical traps and can trap particles through the mechanism described in Section 3.2.1 where the movement of the particles are restricted by the force pulling them into the centre of the peak where the highest intensity is found. The lensed MCF was used to trap polystyrene microspheres with diameters of size 1.3 µm, 2 µm and 3µm (Polysciences: Polybead® Microspheres) as shown in Figure 5.9. The microspheres were held in a sample chamber created by sandwiching two 100 µm cover slips together separated by an 80 µm vinyl spacer, the same as previously described for dual core trapping in Chapter 4. As before the MCF was placed in air outside the cover slips with an imaging system on the other side of the sample chamber as shown in Figure 4.20. The crossing point was imaged and the sample chamber containing the microspheres was moved towards the MCF until the microspheres were focused in the same plane as the interference fringes.

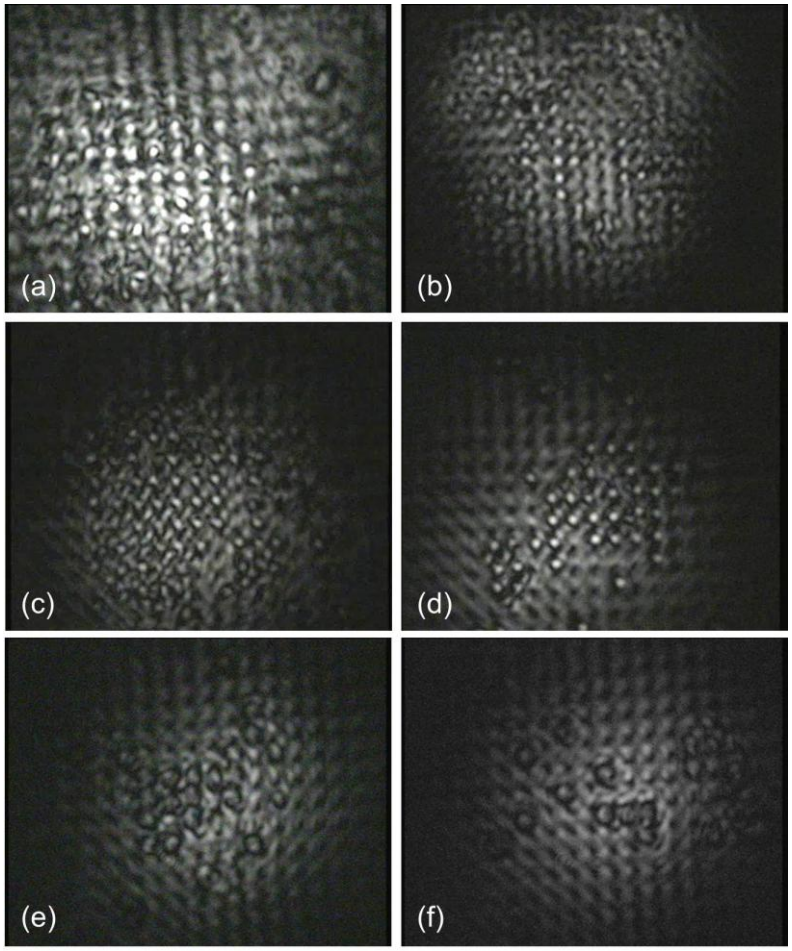

Figure 5.9. (a) + (b) 1.3 µm polystyrene microspheres trapped in two dimensions in the high intensity regions of the lattice fringe pattern, (c) + (d) 2 µm polystyrene microspheres trapped in two dimensions in the high intensity regions of the lattice fringe pattern and (e) + (f) 3 µm polystyrene microspheres trapped in two dimensions in the high intensity regions of the lattice fringe pattern.

As demonstrated in Figure 5.9, the lensed MCF is capable of trapping multiple particles of different sizes. The 1.3 µm microspheres shown in Figure 5.9 (a) and (b) were often difficult to image due to their small size but they could be seen to be trapped in the high intensity regions of the lattice pattern. Similarly the 3 µm microspheres are slightly bigger than the fringe spacing resulting in them overlapping each other in the trapping sites as shown in Figure 5.9 (e) and (f). Therefore the 2 µm microspheres were chosen for further experiments as they are smaller than the fringe spacing so can be spatially separated and are large enough that they can be imaged as shown in Figure 5.9 (c) and (d). The images in Figure 5.9 were taken using a x60, 0.65NA aspheric objective lens

from Newfocus (model number 5721) with a 1/3 inch CCD colour camera (from Dedicated Micros (model number DM/ICE-CM3H) that has 720 x 576 pixels. To improve the viewing of the microspheres a higher resolution USB CCD camera from Thorlabs (model number DCU224C) with 1280 x 1024 pixels was used to take the image shown in Figure 5.10.

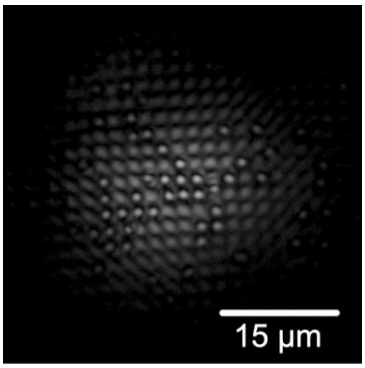

Figure 5.10. (a) 2 µm polystyrene microspheres trapped in the high intensity regions of the lattice fringe pattern taken with a higher resolution camera.

To test that the trapping was caused by the fringes and not by the total power in the beam the fibre was perturbed. This effectively "destroys" the fringes; as a result the particles are free to move, as soon as the fringes returned, the particles align back into the optical traps, as shown in Figure 5.11.

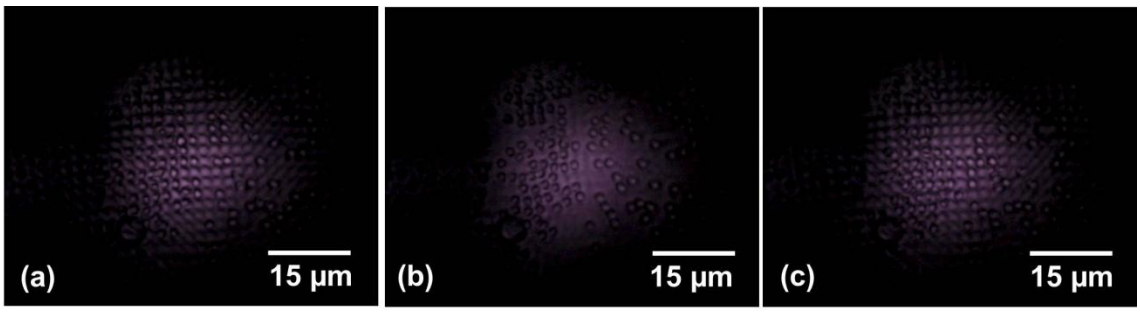

Figure 5.11. (a) 2 µm polystyrene microspheres trapped in the high intensity regions of the lattice fringe, (b) the fringes are destroyed by disturbing the fibre allowing the particles to move out of the traps and (c) as soon as the fringes reappear the particles are trapped.

When the fringes were destroyed, the particles were free to move around the crossing point as shown in Figure 5.11 (b), but once the fringes reappear they align back into the fringe pattern as shown in Figure 5.11 (c). This shows that the optical trapping is caused by the fringes and not the combined intensity of the beam spots alone. The total power out of the lensed MCF was 150 mW when the output from the laser is at 800 mW. Using a Matlab code, the intensity peaks were split into sections separating each peak. The power in each peak was then calculated by evaluating the percentage of power under each peak by integrating over its area. The power contained in the highest central peak was found to be 2.37 mW, although it was estimated that trapping was seen at powers as low as 0.38 mW as can be seen from Figures 5.10 and 5.11 (a) and (c) that particles are trapped in the outer fringe regions.

As previously demonstrated in Figure 5.6, rotation of the half wave-plate at the input to the DOE changes the appearance of the fringes. This can be used to manipulate the trapped microspheres. The fringe pattern used to trap particles in two dimensions is shown in Figure 5.6 (a) when the half wave-plate is at 0°, when the half wave-plate is rotated by 22.5 ° from this position, the appearance of the fringe pattern resembles linear fringes in the vertical direction similar to those demonstrated in Chapter 4 produced by dual core coupling. When the particles are trapped in the linear fringes, they are closer together as shown in Figure 5.12 (a), (b) and (c); when the half wave-plate is rotated anticlockwise by 22.5° the fringe pattern turn into the lattice fringe pattern separating the particles in both the x and y directions as shown in Figure 5.12 (d). This can be seen with the three particles shown above the red arrow in Figure 5.12 (c) in Figure 5.12 (d) when the lattice fringe pattern appears these particles are separated in approximately one second. In the image taken one second later shown in Figure 5.12 (e) another particle appears in the trapped lattice indicated by the red arrow, a further two seconds later another particle appears in a trap indicated by the red arrow as shown in Figure 5.12 (f). The images in Figure 5.12 were acquired from a video recording, the times between each image is indicated showing the time it takes for the particles to align.

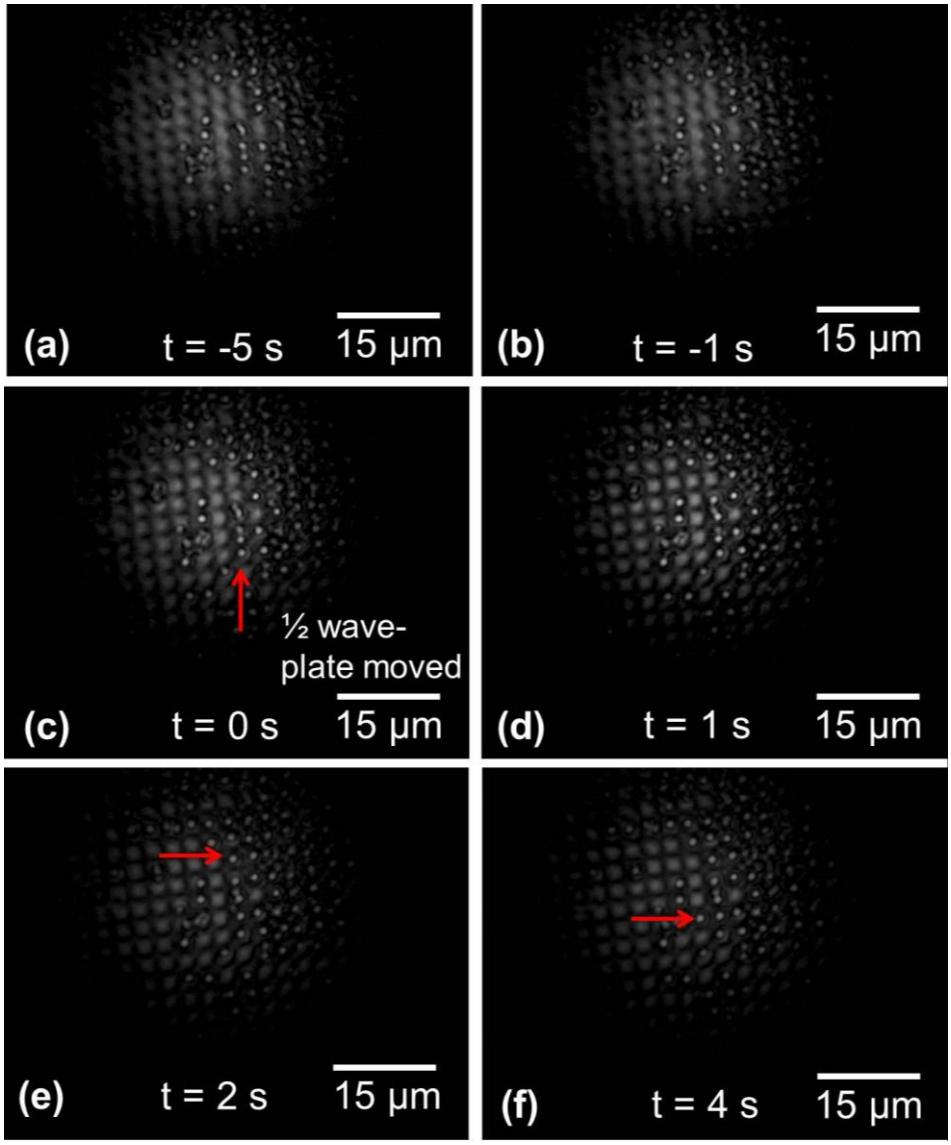

Figure 5.12. Manipulation of the 2 µm polystyrene microspheres by rotation of the half wave-plate. (a) + (b) Initially the half wave-plate is at a position that makes the fringes appear like one dimensional linear fringes, these trap the microspheres in the fringes but are only spatially separated along the x direction, (c) when the half wave-plate is rotated to a position where the fringes appear like an array of two dimensional traps the microspheres, (d) after approximately one second the particles are trapped and separated spatially in both the x and y direction, (e) two seconds after the half wave-plate is rotated the microspheres appear in the traps indicated by the red arrow and (f) a further two seconds later the microsphere indicated by the arrow appears in the optical trap.

These results show that by rotating the half wave-plate the position of the microspheres in one direction can be controlled as they are closer together in the vertical direction in Figure 5.12 (a) and (b) than in Figure 5.12 (e) and (f). This could be useful in controlling the separation of optically trapped cells or used in cell sorting by refractive index or size due to the polarisability of the particle as demonstrated in 2003 by MacDonald et al., using a three dimensional optical lattice [110]. To test that the lensed MCF is suitable for optically trapping biological particles, we used *Escherichia coli (E. coli)* due to its size of approximately 2 μm by 0.5 μm being close to the size of the fringes. This will indicate whether the MCF can produce traps that can trap cells that could aid in cell to cell interaction studies.

5.6. Optical trapping of *Escherichia coli* using two dimensional interferences fringes

Some *E. coli* bacteria strains are responsible diseases such as gastroenteritis, neonatal meningitis and food borne illnesses. Other strains are harmless and have been shown to be useful in biotechnology applications such as creating recombinant Deoxyribonucleic acid (DNA). The ability to trap and study *E. coli* will aid in the research of how the cells interact with one another. This will enable researchers to understand how some of the cells cause disease or to demonstrate how they can be useful to prevent disease and cure illnesses.

The optical trapping of *E. coli* not only demonstrates that the trapping system is suitable to trap biological particles, it demonstrates that the lensed MCF would be suitable for trapping multiple biological cells at close distances suitable for cell sensing applications such as examining cell-to-cell interactions. Biological particles such as *E. coli* cells are more difficult to optically trap as their refractive index of 1.38 [111], is closer to the refractive index of their surrounding medium of water compared to the polystyrene microspheres that have a refractive index of 1.59; both of these refractive indices are stated for the visible wavelength region. Due to their low refractive index and small size, it was not possible to image the *E. coli* cells using just the light created from the interference fringes. They could not be seen when the laser light interference pattern was present, therefore an infra-red (IR) filter was used to block the 1047 nm laser light

and the *E. coli* was side illuminated with a 460 nm light emitting diode (LED). Due to the small size of the cells, of approximately 2 µm by 0.5 µm, and the resolution of the camera, the orientation of the rod shaped bacterial cells is not distinguishable even when imaged using a x100, 0.7NA Mitutoyo, infinity corrected, long working distance lens (model number #46-147) and a Thorlabs, high resolution USB CCD camera (model number DCU224C) which gave a calibration of 0.0546 µm.pixel^{-1}. The side illumination by the 460 nm LED also caused shadows across the cells due to confocal imaging being impractical in the set up.

The *E. coli* cells were cultured and grown by my collaborator Dr Thomas Aspray from the School of Life Sciences at Heriot-Watt University. The cells were grown as one or two day batch cultures in liquid Luria-Bertani medium (tryptone, 10 g l-1; yeast extract 5 g l-1; NaCl 4 g l-1) at 37 °C. The cells were either used directly or diluted 1:1 with sterile 0.85 % sodium chloride (NaCl) and used in the same sample chambers as the microspheres. The particular strain of *E. coli* was chosen due to the fact that it contains the high copy number plasmid carrying the green fluorescent protein (GFP) gene, in the attempt to be able to see the green fluorescence by exciting the protein with the 460 nm LED; however the fluorescence was too weak to view when imaged through a 500 nm longpass filter from Thorlabs (model number FEL0500) that blocks the 460 nm LED light but allows the 509 nm emission from the GFP through. Therefore the *E. coli* was imaged by side illuminating it with the 460 nm LED. Optical trapping of multiple *E. coli* cells was realised using the lensed MCF as shown in Figure 5.13.

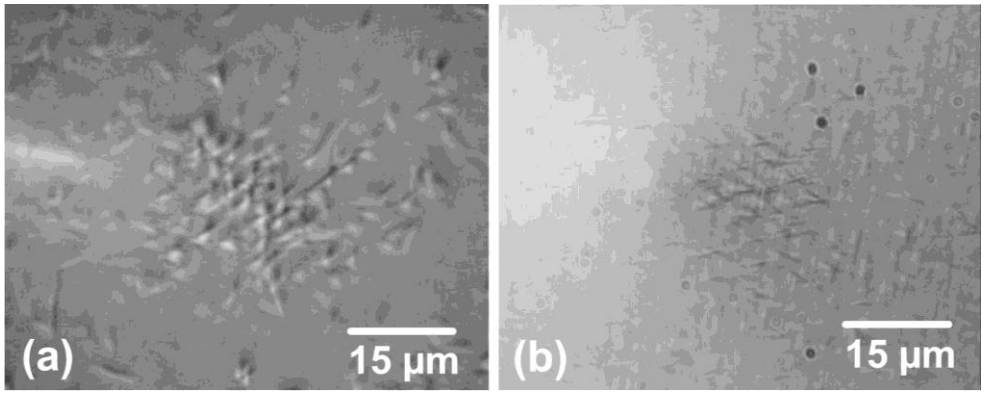

Figure 5.13. (a) E. coli bacterial cells trapped in the interference lattice produced at the interaction region of the lensed MCF when all four cores are coupled into and (b) the E. coli cells when the lensed MCF was rotated in comparison to the previous image.

The ability to optically trap multiple biological cells in such close proximity will allow the study of cell-to-cell interactions, such as the formation of biofilms and biological flocculation, as well as facilitating the research of quorum sensing and metabolic cooperation interactions. Cells interact with each other through sending signals as a response to changes in their surrounding environment such as temperature changes, pH and food availability. The ability to send and receive signals is essential to the survival of the cells as they can tell each other whether it is a suitable time to grow or divide; loss of these communications can result in uncontrollable cell growths and cancer. The ability to study these metabolic cooperation interactions on a cellular level by trapping the cells in close proximity could allow for theses interactions to be examined by changing their surrounding medium and measuring the cells' response when held at known distances apart. One of these interactions is termed quorum sensing where the cells' response is correlated to the density of cells in the population. If the cells at the top of a sample or on a surface are trapped the formation of biofilms could be examined. Biological flocculation is a process involved in sewage treatment in which particles are held together by weak bonds and these bonds could be studied using the multiple trapping device.

5.7. Conclusions

Two-dimensional interferometric optical trapping has been demonstrated using the four core output from a lensed MCF that had been coupled into using a custom-made diffractive optical element. The lensing of the MCF produces a crossing point in the far field from the output of the four cores; a high contrast lattice fringe pattern is formed. In air the crossing point is approximately 250 µm from the end of the fibre with a lattice spacing of approximately 2.75 µm. Across the lattice fringe pattern, intensity peaks are created that can be used to optically trap particles in equal spatially separated sites across the crossing point. The lensed MCF was demonstrated to optically trap polystyrene microspheres with diameters of size 1.3 µm, 2 µm and 3 µm in two dimensions across the crossing point. The intensity peaks created by the interference of the four beams act as individual optical traps with each trap suitable to trap one microsphere. The optical trapping of *E. coli* bacterial cells was also demonstrated using the lensed MCF. This shows that the MCF device is a versatile tool to study the properties of *E. coli*, enabling us to learn how they interact with each other as well as to develop their use in biotechnology to help fight diseases. The optical trapping of multiple biological cells in such close proximity could be useful in investigating cell to cell interactions such as quorum sensing, metabolic cooperation studies and the formation of biological flocculation and biofilms.

The use of a custom-made diffractive optical element provides a simple and effective way to couple light evenly into all four cores without the need for beam splitters, providing a compact system. A half wave-plate was used at the input of the DOE to improve the visibility of the fringes. Rotation of the half wave-plate also changes the appearance of the fringes to a variety of different trapping patterns. Manipulation of multiple 2 µm polystyrene microspheres was demonstrated by rotating the half wave-plate from a one-dimensional trapping linear fringe pattern to a two-dimensional trapping array of interference peaks. This could be useful in manipulating optically trapped cells and controlling their separation for use in cell to cell interaction studies or it could be useful in cell sorting applications where the motion of particles can be controlled along the high intensity regions. Due to the close proximity of the DOE to the MCF separate polarisation controls could not be used on each input to the four core

MCF; instead a half wave-plate was used at the single beam input to the DOE. The use of an optical interconnect such as a fan-out device will allow for polarisation controller to be used on the input to each core of the MCF allowing for further control of the fringe pattern and manipulation of the trapped particles. The use of a fan-out device will also create a more compact, robust device without any free space coupling components. In the next section work towards creating an optically integrated "turn-key" MCF device using ultrafast laser inscription will be presented. The creation of a turn-key device will be useful in biological laboratories where trapping set-ups using free space optics are difficult to implement due to their numerous components and need for highly trained optics personnel.

Chapter 6. Towards a Turn Key Optical Trapping Device Using a Lensed Multicore Fibre

6.1. Introduction

In the previous Chapter optical trapping using interference fringes from four cores of a lensed MCF was demonstrated with the cores coupled into using a diffractive optical element. The use of a DOE to couple light into the MCF provides even coupling into each core, achieving high visibility fringes at the output. Up to 150 mW of power was delivered to the output fringe pattern of the MCF when 800 mW is measured at the output of the laser. This high power, combined with the high visibility of the fringes allowed the trapping of multiple biological particles, as demonstrated by trapping *E. coli* bacterial cells [112]. The use of the DOE however requires the use of free space optics such as the objective lens positioned between the DOE and the MCF; it also requires moving alignment parts to achieve the optimum coupling into the cores that can drift over time when equipment settles or alignment is knocked. These requirements are not a deterrent for optical research-based facilities; however, if the device was to be used commercially or in non-optics laboratories such as biological laboratories, the end goal would be to create a probe that does not rely on any optical alignment and could be operated as a "turn-key" device. A fully integrated device can be created using optical interconnects such as tapered fibre bundles [43, 44], stacked small diameter SMF's [21] and fan-out devices created using laminated polymer waveguides [46] or by using ultrafast laser inscription [45]. Optical interconnects created using tapered fibre bundles and stacked small diameter SMF's are not scalable and are difficult to produce for MCF's with cores that are not arranged in hexagonal geometries such as the four cores MCF used throughout the experiments demonstrated in this thesis. They have also been shown to produce interconnects with insertion losses that are not uniform over each channel ranging from as much as 0.7 dB – 2. 9 dB [21] for the stacked SMF's or from 0.38 dB – 1.6 dB [44] for tapered fibre bundles with the inner cores experiencing less loss than the outer cores. Fan-out devices such as those described in Section 2.6, provide further control over the positioning of waveguides making them ideal for MCF's with nonstandard core geometries. The laminated polymer waveguides are fabricated using film deposition and photolithography techniques and as a result

waveguides can only be written in two dimensions so the input waveguides to the fan-out are also displaced vertically providing further integration difficulties. Using the ultrafast laser inscription method fan-out devices with three dimensional waveguides can be fabricated, customised to fit any arbitrary core geometries and with the input waveguides to the fan-out in a single plane designed to match the dimensions of a commercial fibre v-groove array to ease integration. The nonlinear optics research group at Heriot-Watt University, of which I am a part are active in the field of ultrafast laser inscription for creating devices such as compact waveguide lasers [113-116], microfluidic devices [117] and optical interconnects [45]. Optoscribe Ltd. are a spin out company from the group who have commercialised this technology for various optical components such as fan-out devices. To create a fully integrated MCF optical trapping device, a fan-out was fabricated using ultrafast laser inscription in collaboration with Dr Graeme Brown from Optoscribe Ltd. The specifications for the "turn-key" device are that the losses should be as low as possible; less than 6 dB of insertion loss would result in a device with enough power for trapping with the currently available laser. The waveguides and fibre must operate in the single mode LP_{01} as required for optical trapping.

6.2. Ultrafast laser inscription

Ultrafast laser inscription exploits the nonlinear properties of the inscribed material to induce a refractive index modification. The short pulse durations used in ULI produces high peak irradiances when focused into the sample. This has an effect on the nonlinear properties of the material. The nonlinear component of the materials refractive index, n_2, is influenced by the irradiance of the pulses which as a result has an effect on the refractive index of the material as described by the following equation.

$$n = n_0 + n_2 I \tag{6.1}$$

where n is the refractive index of the material, n_0 is the linear component of the refractive index and I is the irradiance of the laser pulses. In the case of ULI, n_2 is generally positive resulting in an increase in refractive index at the centre of the focused Gaussian beam where the irradiance is highest, as it propagates through the material.

This leads to a creation of a positive lens by the nonlinear phenomenon known as self-focusing, the beam eventually collapses to a point producing high enough irradiances that lead to laser induced breakdown effects and the formation of waveguides in the substrate.

6.2.1. Energy deposition in transparent dielectric material

Ultrafast laser inscription uses femtosecond laser pulses to modify transparent, dielectric material to produce a refractive index modification that creates waveguiding regions in the material. When the femtosecond pulses are focused into the transparent, dielectric material, optical energy is deposited into the focal region through laser induced breakdown processes that transform the transparent material into highly absorbing plasma induced by the intense laser pulse. This leads to energy deposition and material modification that result in the refractive index modification that creates waveguides. The wavelength of the incident ultrafast light is chosen to have a photon energy below the band-gap energy required to promote an electron from the valance band to the conduction band; therefore nonlinear mechanisms are required to achieve the material breakdown and energy deposition. These nonlinear mechanisms are the laser induced breakdown processes and rely on photo-ionisation and avalanche ionisation. The photo-ionisation effects involved in ULI are multi-photon ionisation and tunnelling ionisation. Multi-photon ionisation is when an electron simultaneously absorbs multiple photons to promote itself from the valance band to the conduction band this occurs under an intense electric field. Tunnelling ionisation occurs when an intense electric field is present that is comparable to the Coulomb potential experienced by the bound electron, allowing the electron to tunnel out of its bound state. The initial theoretical model developed to describe the photo-ionisation processes was established by Keldysh in 1964 [118]. The model formulated a parameter that can determine the dominant photo-ionisation mechanism. This is known as the Keldysh parameter, γ, and can be described by the following equation.

$$\gamma = \frac{\omega}{e}\sqrt{\frac{nmc\varepsilon_0 E_g}{I}} \tag{6.2}$$

where ω is the laser frequency, e is the electron charge, n is the refractive index, m is the mass of the electron, c is the speed of light, ε_0 is the permittivity of free space, E_g is the band-gap energy of the material and I is the irradiance of the laser. When $\gamma > 1.5$, the multi-photon ionisation is the dominant photo-ionisation mechanism and when $\gamma < 1.5$, the tunnelling ionisation is the dominant photo-ionisation mechanism. When $\gamma = 1.5$ an intermediate state occurs encompassing both the multi-photon ionisation and tunnelling ionisation mechanisms. Each mechanism is illustrated in Figure 6.1.

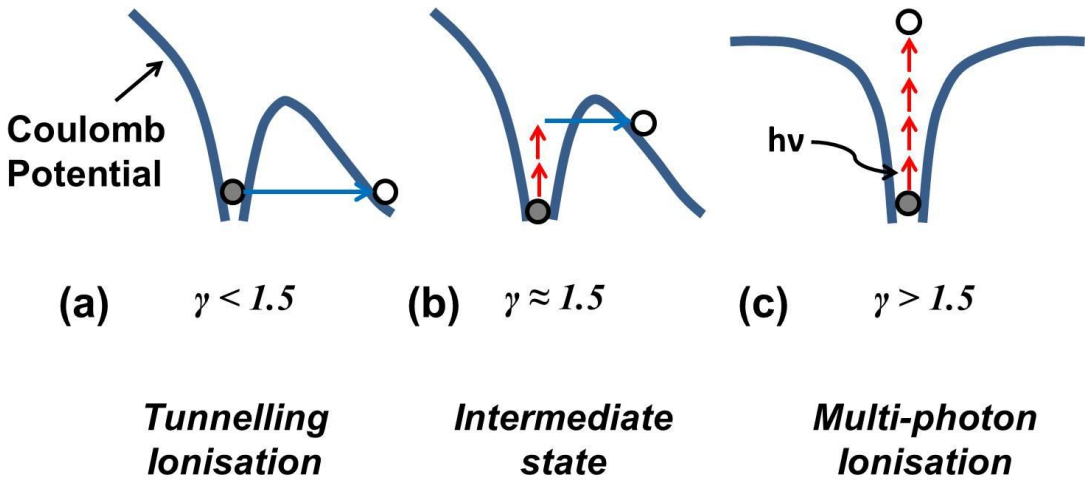

Figure 6.1. Illustrations representing the photo-ionisation mechanisms as described by the Keldysh parameter, (a) represents tunnelling ionisation when $\gamma < 1.5$, (b) represents the intermediate state when $\gamma = 1.5$, and (c) represents multi-photon ionisation when $\gamma > 1.5$. The blue lines represent the Coulomb potential, the solid black circles represent bound electrons and the hollow black circles represent free electrons. The red arrows represent the absorption of a photon and the blue arrows indicate tunnelling.

The other laser induced breakdown process involved in ULI is avalanche ionisation. This occurs after an electron has been released from its bound state through one of the photo-ionisation methods described above. The electron is then free to absorb energy from the laser pulse. Once its energy is greater than the Coulomb potential, the electron can free another electron from the valance band through impact ionisation. Whilst still under illumination from the laser pulses the free electrons can continue the absorption and impact ionisation process, releasing other electrons and creating an avalanche process increasing the population of the electrons in the conduction band exponentially.

6.2.2. Waveguide fabrication

Ultrafast laser inscription is a versatile technique that can create waveguides in a large range of material by optimising parameters such as inscription beam wavelength, pulse duration, pulse energy, pulse repetition frequency, polarisation of the inscription beam, the NA of the focusing objective, pulse front tilt and the translation speed of which the material is moved through the beam focus. There are also two main types of waveguide structures that can be created. Type I is when there is a smooth refractive index change in the material at the focus of the beam; this refractive index change can be either positive or negative. Type II is used in materials such as crystals, where Type I modification is difficult to achieve [119], the absorption of the lasers energy creates damage in the material which in turn causes stress inside the material. The refractive index of the material changes due to the strain and light can be confined between strain induced regions. The waveguides created for the fan-out device are Type I waveguides where the refractive index change is positive; this results in the modified region acting as the core with the unmodified bulk material acting as the cladding region. The positive change of refractive index is the most common waveguide produced by Type I, negative refractive index changes can be useful in material whose lasing properties are altered by the ULI process therefore a non-modified region is used as the core surrounded by a cladding region produced from the negative refractive index change due to ULI.

To create our waveguide we used a transverse geometry where the sample is translated perpendicularly to the beams propagation axis as shown in Figure 6.2. This geometry allows samples to be translated over large distances restricted by the moveable distance of the translation stages. The intensity distribution of the focal volume has a highly asymmetric cross section due to the confocal parameter of the lens as shown in Figure 6.2. The use of a high NA lens such as 1.0NA would reduce the asymmetry; however the depth of the inscription would reduce, which would limit the three dimensional writing capabilities required to create fan-out devices.

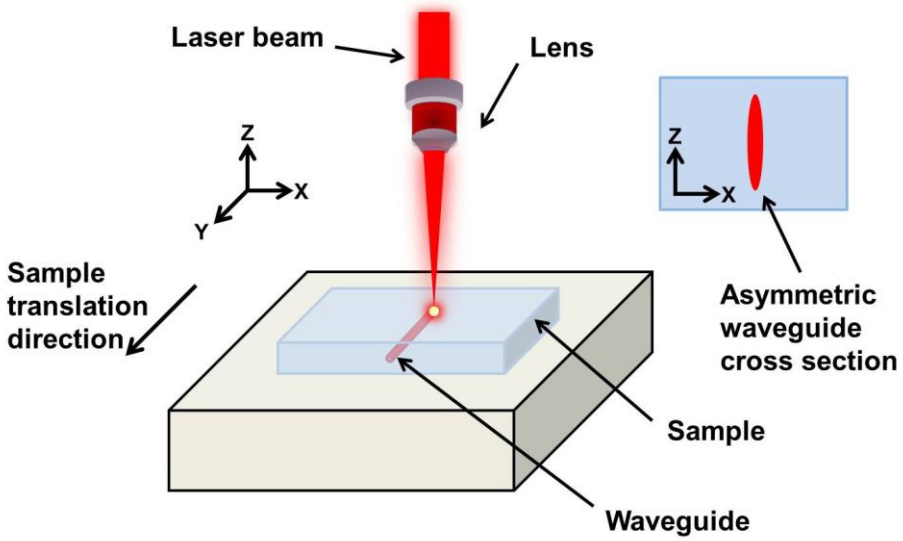

Figure 6.2. The transverse inscription geometry used in ULI to create the fan-outs. The low NA lens results in asymmetric waveguide cross sections as shown in the insert.

To compensate for the asymmetry of the waveguides, various techniques have been demonstrated such as the slit method [120], the cylindrical telescope method [121], using a deformable mirror [122], or the multiscan technique [123]. The multiscan technique was used to create the waveguides in the fan-out device. The multiscan technique uses multiple scans written one after another to build up a symmetric waveguide, as shown in Figure 6.3. The separation of these scans can be used as another fabrication parameter. The waveguide width is controlled by the number of scans and the width of their separation.

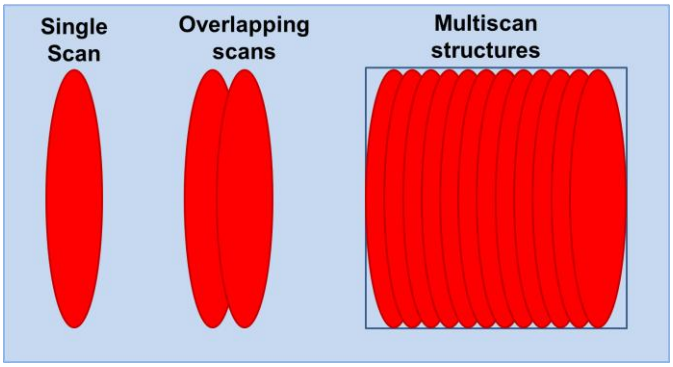

Figure 6.3. The multiscan technique can create symmetric cross sections by stacking single scan side by side.

6.2.3. IMRA® inscription laser

The inscription laser used to create the fan-out devices was an IMRA® μJewel D400 fibre master oscillator power amplifier (MOPA) system with a central wavelength of 1047 nm. The laser has an adjustable repetition rate from 100 kHz to 5 MHz and an adjustable compressor that can achieve pulse durations over this range of 350 – 460 fs. The set-up of the inscription laser system is shown in Figure 6.4. The beam is collimated through a symmetric telescope made of lenses L1-L4, and aligned using mirrors M1- M3 onto a half wave-plate, polarising beam splitter, beam tap and power meter that is used for power calibration of the system. The AOM can be used to modulate the inscription beam. The polarisation of the pulses is then controlled and rotated by the half wave-plate and the quarter wave-plate. A mechanical shutter is used to block the beam to control when the waveguides are written. The pulses are aligned to the back aperture of the focussing optics using mirrors M5-M8 and onto the sample that is mounted on three axis air bearing stages from Aerotech (model number ABL 1000). The back reflected beam spot from the sample is focused on a camera using mirror M9 and lens L5. The translation stage and the optics not attached to the optical table are attached to granite blocks to increase the stability of the laser system. The wave-plates and shutters used in the set-up are controlled using the computer to implement the desired writing parameters of power and polarisation.

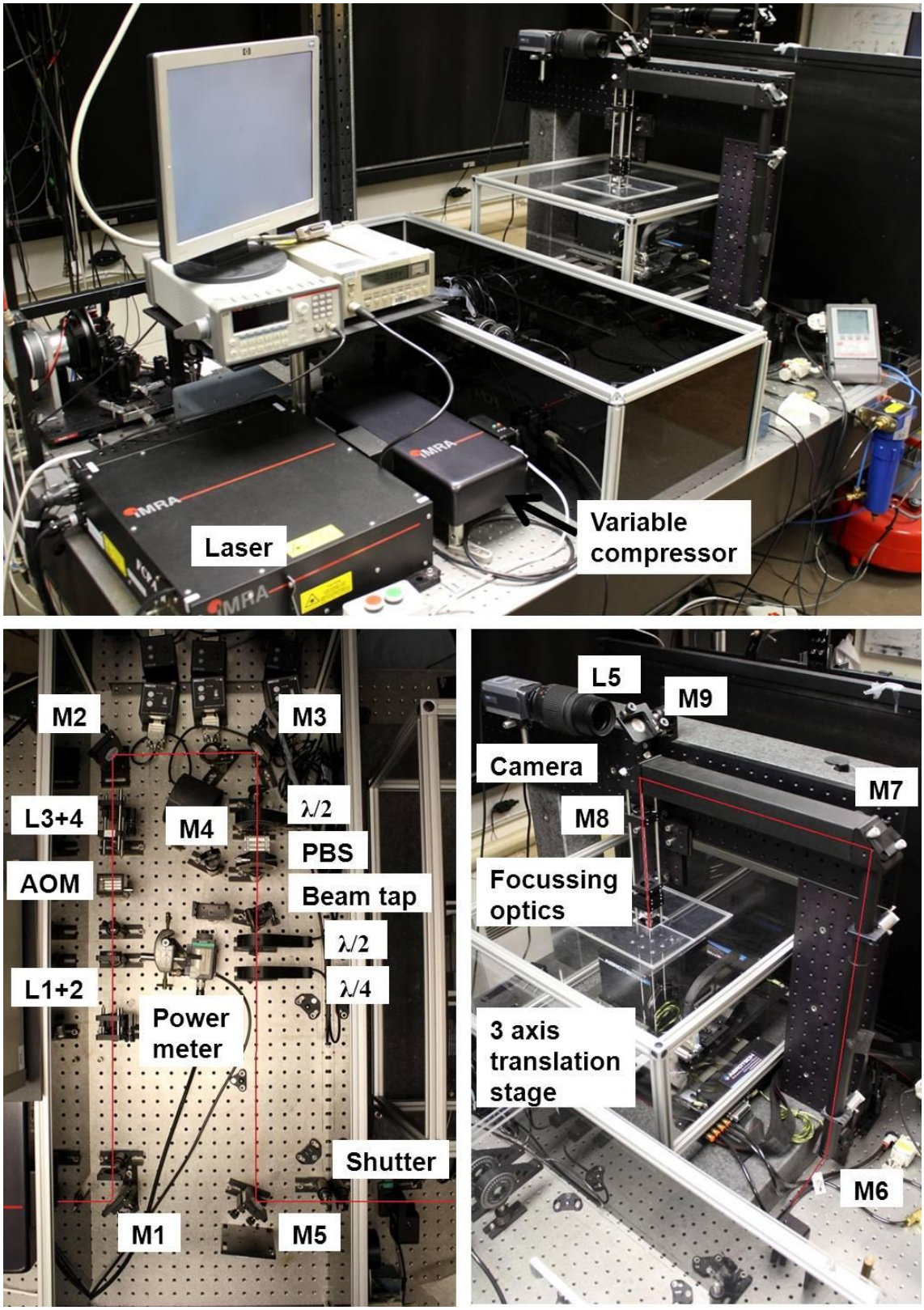

Figure 6.4. The inscription set-up used to create the fan-out devices where M1-M9 are mirrors, L1-L5 are lenses, AOM – acousto-optic modulator, PBS – polarising beam splitter, λ/2 – half wave-plate and λ/4 – quarter wave-plate.

6.2.4. Fan-out fabrication

The first step of fabricating the fan-out device is to determine the inscription parameters through waveguide characterisation. The material chosen in which to fabricate the fan-out was Corning Eagle-2000 glass. Waveguides were written using a 0.4NA microscope objective, a repetition rate of 500 kHz, a pulse duration of 460 fs with circular polarisation. These parameters were determined from previous work carried out in the NLO group. Twenty five scans spaced at 0.33 µm were used to create the single mode waveguides at 1550 nm. To determine the pulse energy and translation speed, a large number of straight waveguides were written with varying translation speeds and powers. These waveguides were then tested using 1550 nm light to check if they were single mode; the insertion loss was then measured for the waveguides operating in single mode. The region of the parameter scan where the lowest insertion loss and single mode operation occurred was then expanded for a second time with smaller power increments to find the lowest loss parameters possible. These were found to be at a translation speed of 4 $mm.s^{-1}$ with a pulse energy of 186 nJ. If the objective lens is removed or altered between inscriptions the parameters need to be determined again as the back aperture of the objective might not be filled to the same extent as previously, resulting in changes in the effective numerical aperture to with the modified region is very sensitive. The computer program to draw the three dimensional waveguides in the fan-out device was written by Dr Graeme Brown of Optoscribe. It was designed to have the same 80 µm square spacing as the MCF on one side of the chip and the other side of the chip had the same spacing as a commercial four fibre v-groove array as shown in Figure 6.5.

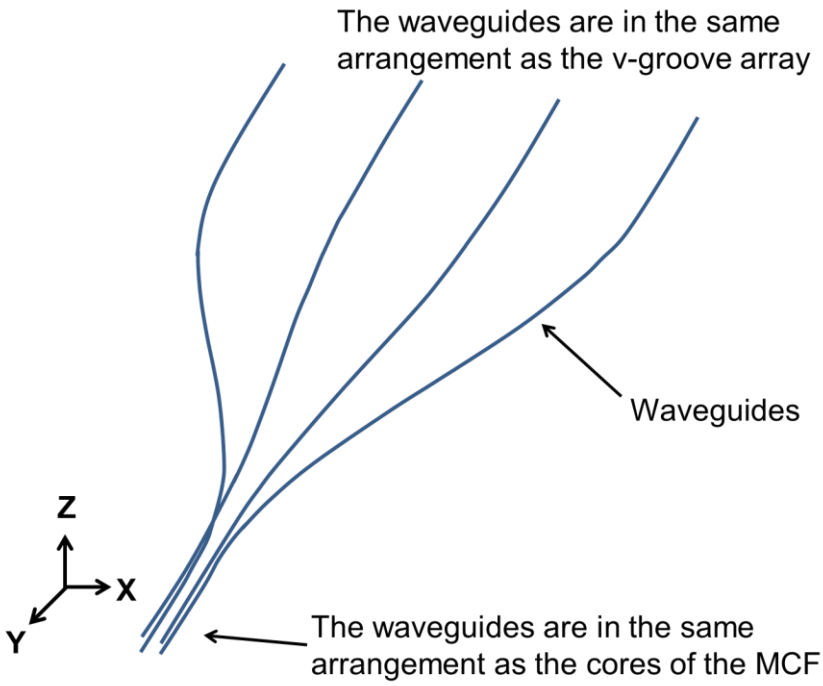

Figure 6.5. Illustration of the waveguides in the fan-out device. The waveguides have the same arrangement and separation as the MCF at the bottom end of the illustration and the same separation as a 4 fibre v-groove array at the top end.

After the waveguides in the fan-out were fabricated on a 10 mm sample and the ends were ground back and polished, the insertion loss of each channel was measured at 1550 nm. The insertion loss measurement was carried out by first taking a reference measurement, connecting a SMF-28 fibre between the pump source and the detector, using two pigtails spliced together to securely attach the fibre to ensure even coupling into the detector and into the fibre throughout the measurements. After the reference measurement was taken, the fibre was broken at the splice point and recleaved; the fan-out was then positioned between the fibre ends and aligned to gain the highest output. The insertion loss is calculated as the reference measurement minus the highest output achieved through the fan-out device. The insertion losses at 1550 nm for the fan-out device were found to be 1.1 dB for channel 1, 1.2 dB for channel 2, 1.05 dB for channel 3 and 1.3 dB for channel 4. The channels are labelled as shown in Figure 6.6. These values are higher than typical devices offered by Optoscribe with insertion losses of < 1 dB, typically 0.7 dB per channel; however they are low enough for our application and to show the feasibility of the device [48].

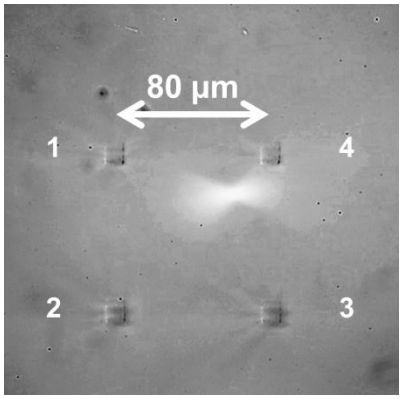

Figure 6.6. The output side of the fan-out device showing the waveguides with the same separation and orientation as the MCF, the channels are labelled 1-4 for reference.

The fan-out device was then attached to the 4 fibre v-groove array. Two fibre optic switches, both JDS Uniphase SB series, were used to move between two of the channels of the v-groove without disconnecting the connectors and changing the reference measurement. The outer channels 1 and 2 were put on one switch and 3 and 4 on the other switch, the second output of the tuneable laser source was used for the second switch. The output of each channel was measured at the facet of the v-groove array. This was used as the new reference measurement. The fan-out device was then placed after the v-groove array and the output was monitored on the camera whilst channels 1 and 4 were coupled into, channels 1 and 4 are the furthest apart on the linear 4x1 v-groove array therefore if they are at the correct roll position the centre channels will also be in line. To find the correct roll position, the v-groove array was moved up and down and side from side to see if the outputs go on and off at the same time or if they 'blink' at different rates. The roll was then adjusted until the outputs go on and off at the same time, as this indicates that the outputs from the v-groove array and the inputs to the fan-out are aligned closely in the same plane. The insertion loss for each channel was then measured and the pitch and yaw directions of the v-groove array was optimised to produce the lowest insertion loss, UV curing gel was used as index matching gel to remove loss due to the air gap and Fresnel reflections from the interface. Once the position of the lowest insertion loss was found the v-groove array was UV cured to the fan-out device through exposing the bond to the output of a UV lamp from Omnicare (model number S1000-1B) for 6 minutes. This forms a strong bond that will become permanent after approximately 3 days at room temperature.

To produce a stable bond between the MCF and the fan-out, a v-groove is needed to hold the MCF to increase the surface area of the bond and create a robust device. As the MCF is a non-standard size and shape, commercial v-grooves cannot be used, therefore the ULI process was used to create a custom design of v-groove that could then be etched to produce v-grooves as shown in Figure 6.7. When the inscription pulse energy is increased to a value higher than the refractive index modification regime, evenly spaced nano-sized planes are formed in the modified region of the sample, these being known as nanogratings [124]. These nanostructures were first described in 1999 [125], and were later found to be strongly dependant on the polarisation of the incident laser pulses [126]. The orientation of the nanogratings are orthogonal to the electric field vector of the laser beam, which when combined with chemical etching this allows control over the etching selectivity such as the speed of the etch. Dr Graeme Brown designed and etched the MCF v-groove shown in Figure 6.7. The etching is carried out in a solution of hydrofluoric acid that is diluted to 5 %.

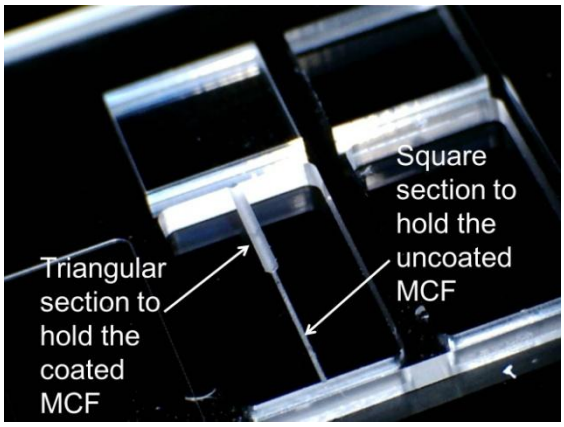

Figure 6.7. The custom made MCF v-groove. The square section ensures the MCF is held so that the cores are aligned in a square to aid with attachment to the fan-out.

The v-groove was designed to have a square section with a width of approximately 190 µm. This is bigger than the square sides of the uncoated MCF but smaller than the diagonal ensuring that the MCF could only be held in the v-groove in one orientation as shown in Figure 6.8. The MCF has an acrylic coating with a circular cross section with a diameter of approximately 315 µm, a triangular groove was designed to hold this section in the v-groove. To hold the MCF in place it was UV cured whilst the output

was imaged to ensure the fibre remained located square in the block. A plane block of glass was also glued on top of the MCF to strengthen it further. The end facet of the v-groove was polished back with care to produce the clean finish as shown in Figure 6.8.

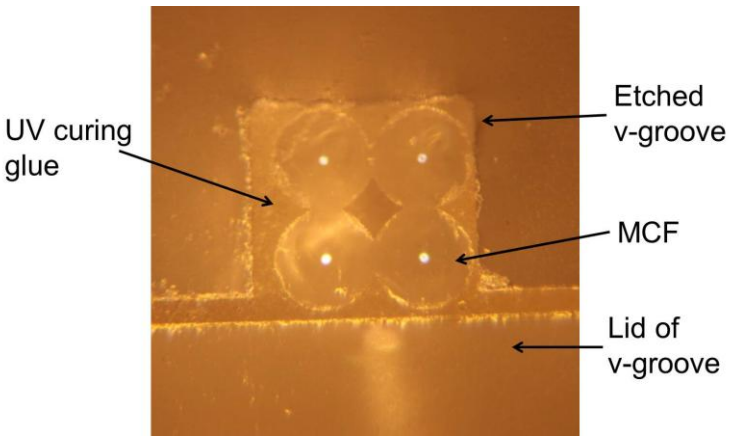

Figure 6.8. The output end of the custom made v-groove after polishing with light coupled into each core of the MCF.

Once the MCF was glued into the v-groove, it was attached to the fan-out, as before the insertion loss was measured and the fan-out device and MCF were aligned in the x, y and z directions and by using the pitch, roll and yaw of the alignment stages. The alignment was initially carried out by finding the optimum alignment position for each core and measuring the insertion loss of the other cores at this position. It was noted that the position of one of the cores was slightly off axis in comparison to the other cores. As the MCF device will be used for interferometric optical trapping the requirement for even coupling to each core has higher priority than an overall low insertion loss. Therefore the MCF was aligned until even coupling was achieved between the cores, the MCF was then UV cured to the fan-out device to create a permanent bond. After curing the total insertion loss measured through the whole device from the FC/APC connectorised 4x1 v-groove array through the fan-out chip and the MCF was measured at 1550 nm as 1.85 dB for channel 1, 1.77 dB for channel 2, 1.39 dB for channel 3 and 1.79 dB for channel 4.

To couple light into each core of the MCF simultaneously a 1 x 4 fibre splitter was used with a 25:25:25:25 split (from Thorlabs, model number FCQ1315-APC). To achieve

high output power, a tuneable laser source from Anritsu (model number MG9638A) with its output set at 1550 nm was amplified using an EDFA borrowed from Dr Xu Wang, from Amonics (model number AEDFA-23-R-FA) up to 205 mW of power was available after amplification from the EDFA. This resulted in a maximum output of 122 mW measured from the lensed MCF through the fan-out device, the 1x4 splitter a 1550 nm SMF-28 patchcord and five fibre connectors as demonstrated in Figure 6.9. This gives a total loss of 2.25 dB through the entire system at 1550 nm.

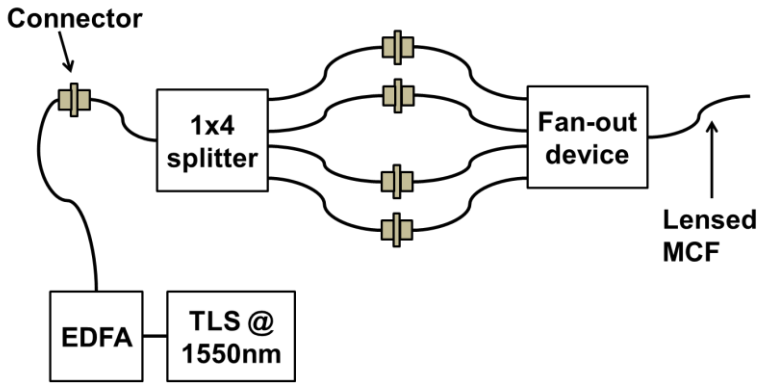

Figure 6.9. The tuneable laser source (TLS) is amplified by the EDFA before passing through the 1x4 fibre splitter to couple light evenly into each core of the MCF through the fan-out device creating a completely integrated device.

6.3. Fan-out at 1047 nm

If the fan-out device is used at 1047 nm, this will allow for the creation of a "turn-key" optical trapping device at a wavelength where biological cells can be trapped without causing damage due to a high temperature increase. When the fan-out that had been created for single mode operation at 1550 nm is used at 1047 nm a higher loss of 5.56 dB was measured when 360 mW was coupled into a single mode fibre pigtail from Thorlabs (model number 1060XP) this resulted in a maximum power of 100 mW at the output of the lensed MCF through a 1x4 splitter that is single mode at 1047 nm from Thorlabs (model number FCQ1064-APC) and the same fan-out as before and five fibre connectors. As the MCF has a cut of wavelength of 1 μm, it is single mode at 1047 nm, therefore the output from the MCF connected to the fan-out device will be single mode.

An attempt was made to create a fan-out with single mode waveguides at 1047 nm however high losses equivalent to the same as using the existing fan-out were achieved for the straight waveguides. It was noted that the loss would be higher for a fully integrated fan-out created with those waveguides that would be too high to produce adequate power at the end of the lensed MCF to produce trapping with the current laser power limitations therefore the decision was made to use the already existing fan-out device. Single mode waveguides at 1 µm are currently being investigated in the NLO group; it is reasonable to expect that a single mode fan-out operating at 1 µm could be fabricated in the future.

The interference fringes produced from the four cores output of the lensed MCF at 1047 nm was shown to be unstable. The interference pattern kept drifting, in a way similar to the patterns witnessed when the input polarisation was varied in Chapter 5, (Section 5.3, Figure 5.6). Attempts were made to stabilise the fringes such as thermally isolating the fan-out device by containing it in insulation foam as shown in Figure 6.10. This was shown to have little effect on the instability of the fringes at 1047 nm.

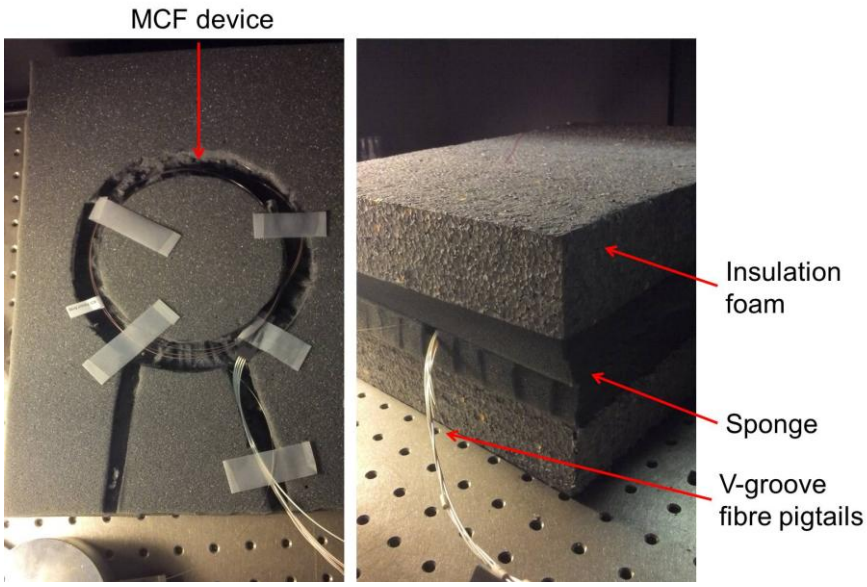

Figure 6.10. To insulate the fan-out device from environmental disturbances such as temperature change it was contained inside pieces of insulting foam and sponge.

The instability of the fringes caused low visibility, as shown in Figure 6.11, as the interference pattern kept drifting this also caused difficulty in capturing an image that resembles the lattice fringe pattern that is suitable for trapping multiple in two dimensions and this could also add to the reduced visibility of the fringes.

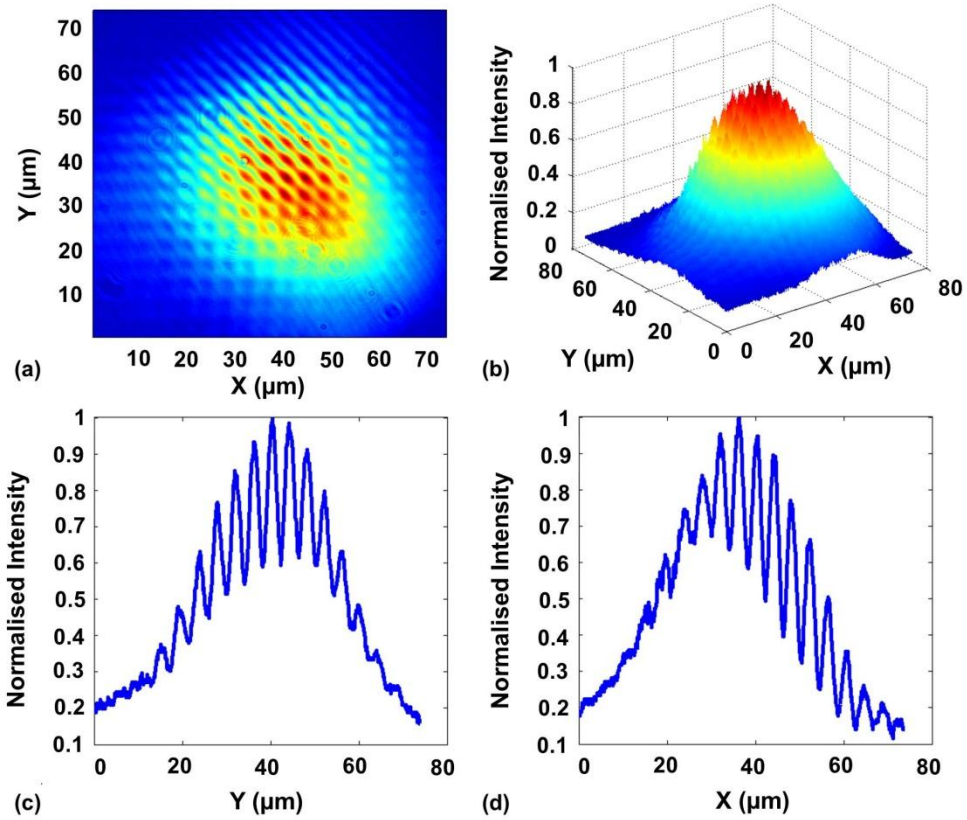

Figure 6.11. Interference fringes produced at the crossing point of the lensed MCF when all four cores are coupled into using a multimode fan-out device at 1047 nm. (a) Two dimensional intensity plot of the fringe pattern, (b) three dimensional normalised intensity plot of interference pattern, (c) the cross section through the centre of the normalised interference pattern in the x direction and (d) the cross section through the centre of the normalised interference pattern in the y direction.

The image shown in Figure 6.11 (a) shows that all four cores are not perfectly aligned over one another, this was due to difficulties in the lensing as a result of prolonged use of the fusion splicer and the electrodes starting to fail and also the slight asymmetry in the core spacing of the MCF. However even with the slight offset, the Gaussian shape of the curves can be seen and the fringes formed are as desired. The cross section of

Figure 6.11 (b) shown in Figure 6.11 (c) and (d) shows that the visibility of the fringes is less than that achieved when coupling into the MCF using the DOE. Over 80 % visibility was achieved using the DOE whereas the visibility achieved using the fan-out at 1047 nm is around 30 - 40 %. The fringe spacing of approximately 3 µm was found to be in agreement with the previous lensed MCF results demonstrated in Chapter 5. These images in Figure 6.11 were produced by exporting an image of the interference pattern into MATLAB and calibrated using a graticule that gave a calibration of 0.087 $\mu m.pixel^{-1}$ for images taken using a x60, 0.65NA aspheric objective lens from Newfocus (model number 5721) and a Thorlabs, high resolution USB CCD camera (model number DCU224C). The data from the image was normalised then plotted in two and three dimensional graphs. The highest intensity peak was then found and cross sections were taken along both the x and y directions of the fringe pattern.

Even though the output from the MCF is single mode at 1047 nm, the fibre used in the v-groove array is SMF-28 and therefore this and the waveguides in the fan-out device are multimode when coupled with 1047 nm light. It is therefore suspected that the instability of the fringes is due to the multimodal interactions in these waveguides. The modes in the v-groove array and the fan-out will be changing. As a consequence the coupling to the MCF is varying, resulting in poor visibility of the fringes and instability of the interference pattern. To improve this, single mode fibre and single mode waveguides should be used throughout the fan-out device; to examine if this would result in stable fringes, the output of the fan-out devices at 1550 nm was investigated.

6.4. Single mode fan-out at 1550 nm

When 1550 nm light is coupled into the fan-out device as illustrated in Figure 6.9 single mode operation is achieved throughout the device. This results in an increase in stability of the output in comparison to using the fan-out at 1047nm. The interference fringes still swept gradually but could be controlled to a certain degree through positioning of the input fibres to the v-groove array, allowing the pattern to remain stable for about 30 seconds that would be suitable to be used in optical trapping. The visibility of the fringes is shown to be greater than 80 % as demonstrated in Figure 6.12; this is due to single mode operation and equal coupling into each core of the MCF

through the fan-out device. As the visibility of the fringes is much greater at 1550 nm than at 1047 nm, it shows that the multimodal effects in the v-groove and fan-out cause the low visibility and instability of the fringes at 1047 nm. At 1550 nm the fringe separation is greater than at 1047 nm with a period of 5.2 µm at a distance approximately 300 ± 25 µm from the end of the fibre.

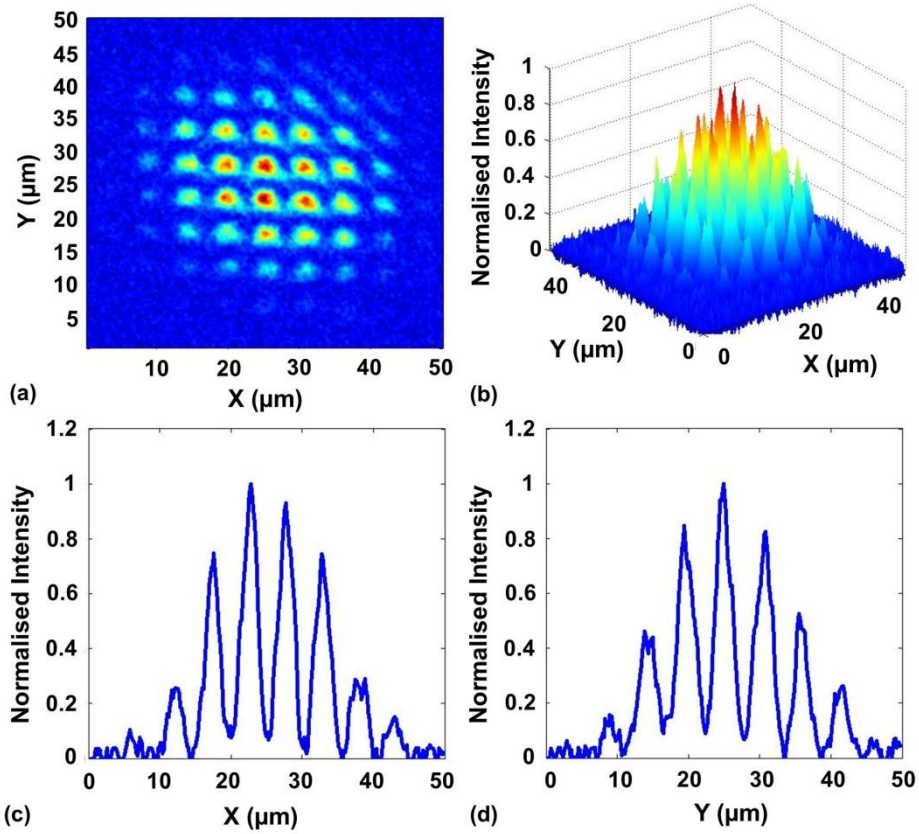

Figure 6.12. Interference fringes produced at the crossing point of the lensed MCF when all four cores are coupled into using a single mode fan-out device at 1550 nm. (a) Two dimensional intensity plot of the fringe pattern, (b) three dimensional normalised intensity plot of interference pattern, (c) the cross section through the centre of the normalised interference pattern in the x direction and (d) the cross section through the centre of the normalised interference pattern in the y direction.

The visibility of the fringes as demonstrated in Figure 6.12 (c) and (d) is greater than 80 %. This is comparable to the visibility achieved when coupling into the MCF at 1047 nm using the DOE. This shows that using a completely single mode device can produce high visibility of the fringes that could be suitable for optical trapping. This would be a completely integrated device with no free space optical components; therefore no alignment of the trapping device would be carried out by the user apart from alignment of the sample chamber, allowing for a device that could be used by non-optical personnel. To correct for the sweeping of the fringes still seen at 1550 nm, polarising maintaining fibres and waveguides could be used throughout the device. The use of a polarisation controller on each input fibre to the fan-out device could be implemented to achieve further manipulation of the trapped particles. When polarisation controllers were used in the input fibres to the fan-out in the current device, the appearance of the fringes could be altered but due to the instability of the fringes the pattern did not remain in the desired position. These images in Figure 6.12 were produced by exporting an image of the interference pattern into MATLAB and calibrated using the MFD of a Corning SMF-28 fibre that gave a calibration of 0.163 $\mu m.pixel^{-1}$ for images taken using a x60, 0.65NA aspheric objective lens from Newfocus (model number 5721) and a IR camera from Applied Scintillation Technologies (model number CamIR1550).

6.5. Simulations for four core interference at 1550 nm

To examine the interactions between the four core outputs of the lensed MCF at a wavelength of 1550 nm, the same BeamPROP model as used for the dual core interference and the interference from four cores at 1047 nm was used. The model has a lens with a radius of curvature of 130 µm and a diameter of 200 µm it is placed on top of a 150 µm long section of fibre with 7 µm diameter cores with a refractive index of 1.47 that are arranged in a square spaced 80 µm apart and surrounded by a cladding with a diameter of 200 µm and refractive index of 1.46. The sample chamber is included in the model as a 100 µm thick glass section with a refractive index of 1.45 followed by an 80 µm thick water section with a refractive index of 1.33. In this model, in comparison to the model for 1047 nm wavelength the sample chamber is now positioned 150 µm from the end of the fibre where as it was positioned 90 µm away in

the 1047 nm model. The results from the model are shown in Figure 6.13 and gave a crossing point at a distance of 300 µm from the end of the fibre with a fringe spacing of 4.84 µm. These values agree with the experimental results of a crossing point at approximately 300 µm from the end of the fibre with a fringe spacing of 5.2 µm, showing that this simple model accurately describes the effects of the lensing of the MCF even at different wavelengths.

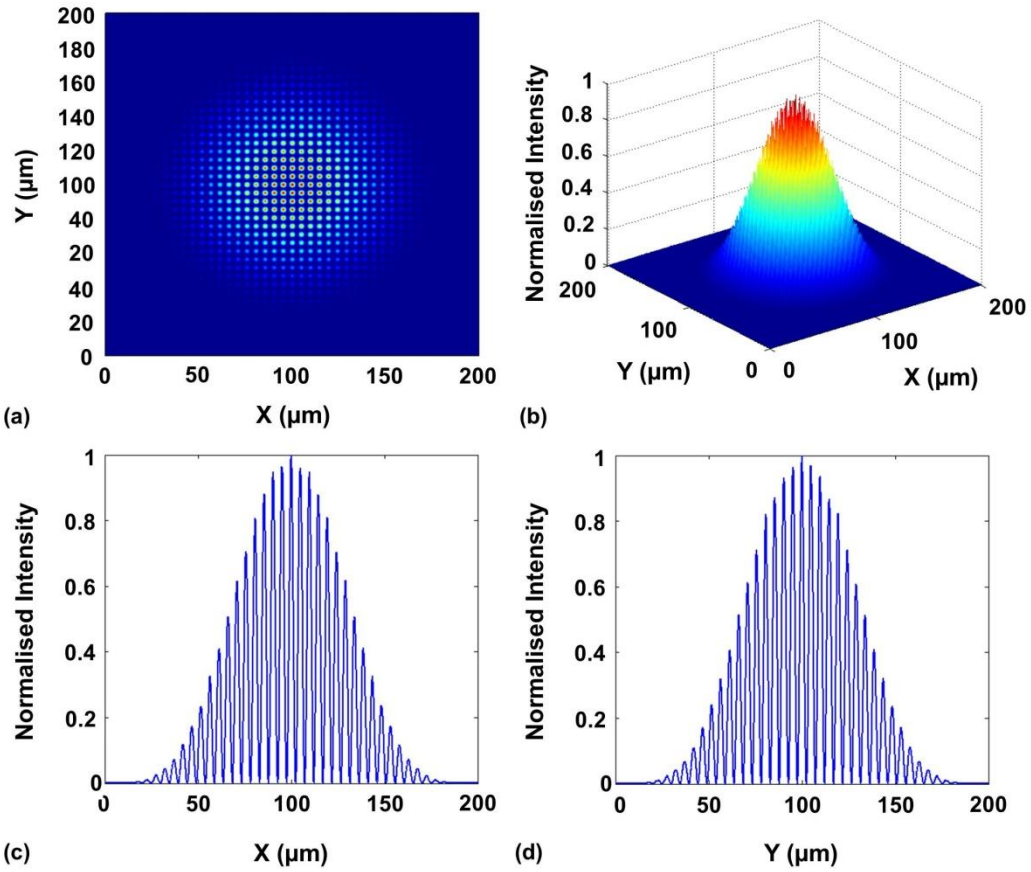

Figure 6.13. (a) The simulated normalised intensity plot of the overlap region for four cores at a wavelength of 1550 nm, (b) the simulated normalised intensity plot of the interference fringes in three dimensions at 1550 nm, (c) a cross section along the x direction through the highest intensity point and (d) a cross section along the y direction through the highest intensity point.

The simulated results demonstrated in Figure 6.13 agree with the experimental in the distance to the crossing point of 300 µm, and are within error of the fringe spacing values for four core interference from the lensed MCF at 1550 nm wavelength with a

simulated value of 4.84 µm compared to the experimental value of 5.2 µm. The cross section through the highest point of Figure 6.13 (a) and (b) is shown in Figure 6.13 (c) and (d). This shows that the visibility of the fringes is 100 %; this is because the model cannot accurately describe the effects from the fan-out device and the added polarisation component from the fibre as demonstrated in the experiment. These results show that without the polarisation component from the fibre 100 % visibility of the fringes could be achieved possibly by using polarisation maintaining fibres and waveguides.

6.6. Thermal effects at 1550 nm

At 1550 nm the absorption coefficient of water is $\propto_{abs}$ = 10.94 cm^{-1} compared to $\propto_{abs}$ = 0.17 cm^{-1} at 1047 nm [74]. This results in optical absorption induced thermal effects that cause convection driven drag forces that cannot be ignored when considering optical trapping. The increase in the absorption coefficient of water at 1550 nm results in a temperature increase due to the central peak in the interference pattern of the output from the four cores of ΔT_{Trap} ~ 7 K; at 1047 nm the temperature increase due to the central peak is ΔT_{Trap} = 0.04 K; the increase of temperature at 1550 nm is nearly 200 time more than at 1047nm. This was calculated from the following equation [127].

$$\Delta T_{Trap} = \frac{\propto_{abs} P_l}{2\pi K} \ln\left(\frac{D}{W}\right) \tag{6.3}$$

where P_l is the laser power of the central peak, D is the thickness of the sample chambers = 80 µm, W is the beam radius of the central peak and K is the thermal conductivity of water = 0.6 $W.m^{-1}.K^{-1}$. To calculate the laser power in the central peak and its beam radius, a MATLAB code was used to find the total percentage of power contained in the central peak and the $1/e^2$ value that defines the beam waist of a Gaussian profile. The laser power emitted from the end of the lensed fibre was 125 mW, the power contained in the central peak at 1550 nm was found to be P_l = 6.67 mW and the beam radius is W = 2.16 µm. At 1047 nm the power contained in the central peak is P_l = 1.94 mW and the beam radius is W = 1.36 µm.

When trapping biological particles, a low temperature rise due to the laser beam is desired, as biological processes within the cell can be altered due to the temperature of its surroundings and could also lead to cell death. For measuring cell-to-cell interactions, the temperature increase should not be greater than 2 K as this may skew the results of the study. Therefore 1550 nm may not be used to examine cell-to-cell interactions by trapping cells in close proximity. At 1047 nm there is a small temperature rise of 0.04 K that would not affect the cells behaviour as much than if using 1550 nm, where the temperature increase is ~7 K.

6.7. Optical trapping at 1550 nm

Trapping using 1550 nm laser light is known as optothermal trapping due to the added thermal effects. Optothermal trapping has previously been demonstrated by researchers lead by Andrew Poon at The Hong Kong University of Science and Technology using both a single beam [128] and multimode interference techniques [129]. Using a single laser beam at 1550 nm, it was shown that the strong water absorption can thermally induce a localised flow within the sample chamber that can exert a Stokes' drag force on the particles that compliments the optically induced gradient force. The thermal effects were shown to assist in the long range capturing of 6 μm polystyrene microspheres, where a particle was captured from a distance of 176 μm away from the tweezing beam; this was shown to be due to the effects of the Stokes' drag force as the capture range is much bigger than the 5 μm beam radius [128]. Using the optothermal tweezers, particles were shown to be separated into two distinct layers separated by 90 μm due to thermalphoretic repulsion from the highest temperature region close to the laser focus as shown in Figure 6.14. In the lower layer the particles are attracted towards and disappear at the focal axis of the tweezing beam, whereas in the upper layer the particles emerge at and are repealed away from the focal axis.

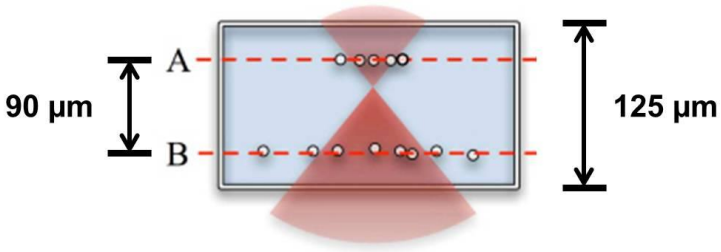

Figure 6.14. Particles can be separated into two distinct layers due to thermal effects caused by the optothermal tweezer. This image has been taken from [128].

The same group have also demonstrated two dimensional optical trapping using multimodal interference at a wavelength of 1565 nm [129]. Two dimensional arrays of traps were formed from a large core (100 µm), square silicon-on-insulator multimode interference waveguides that shaped the input optical beam into arrays of optical traps. The output from the multimode interference waveguide was focused into a 50 µm pattern array inside a sample chamber containing 1 µm or 2.2 µm polystyrene particles composed of two coverslips separated by gel containing 18 µm diameter particles. The 1565 µm light was coupled into the multimode interference waveguide; different lengths of waveguides were shown to vary the output pattern as shown in Figure 6.15.

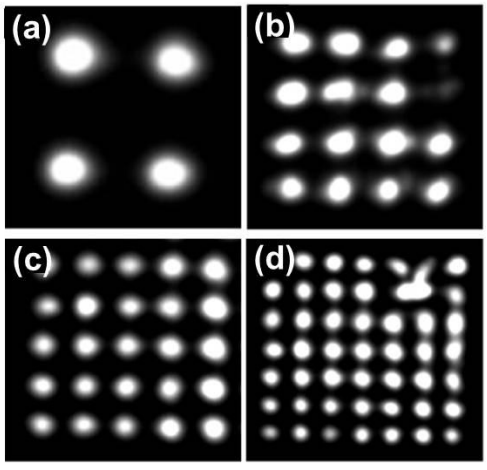

Figure 6.15. Trapping arrays produced from different lengths of waveguides, (a) output from a 11mm long waveguide, (b) output from a 5.5 mm long waveguide, (c) output from a 4.5 mm long waveguide and (d) output from a 3 mm long waveguide. This figure has been taken from [129].

The optically-induced thermal effects were shown to assist the trapping by levitating the particle. As demonstrated in their previous paper [128], in the horizontal direction (i.e. across the array) the convection flow fluidic force helps collect the particles in the optical trap which are then trapped by the optical gradient force. In the vertical direction the convection flow fluidic drag force lifts the particle from the floor of the sample chamber while the optical scattering force and the optical gradient force in the vertical direction depends on the particles position relative to the beams focal plane. It was shown that in order to limit the vertical flow rate, the optical absorption needs to be minimised; therefore the authors used an 18 µm thick sample chamber. In this demonstration the flow rate was shown to only sweep the particles horizontally without raising them up to the top of the sample chamber. With their device they were shown to trap 2.2 µm polystyrene microspheres in separate traps at the bottom of the sample chamber as shown in Figure 6.16 (a) and clusters of 1 µm polystyrene microspheres in separate optical traps as shown in Figure 6.16 (b).

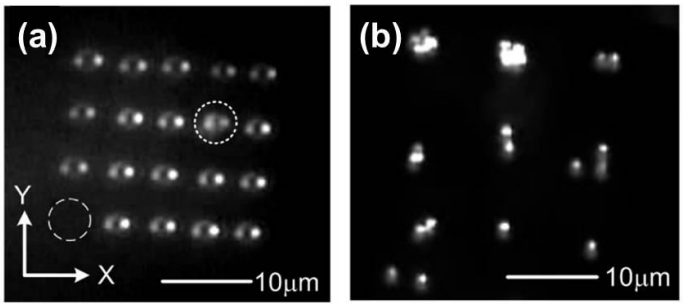

Figure 6.16. (a) 2 µm polystyrene microspheres trapped in separate optical traps and (b) 1 µm polystyrene microspheres trapped in separate clusters. This figure has been taken from [129].

6.7.1. Optical trapping at 1550 nm using interference from a MCF

Having previously demonstrated two-dimensional optical trapping using the lensed MCF at 1047 nm in Chapter 5, 1550 nm light was coupled into the MCF using the fan-out device described as in Section 6.4. The single mode operation of the fan-out at 1550 nm produced high visibility fringes and an array of peaks similar to those produced at 1047 nm using the DOE that successfully demonstrated two dimensional

optical trapping. At 1550 nm, the additional thermal effects due to the higher absorption coefficient of water result in convection flow fluidic drag forces and an increase of temperature of ~7 K when 125 mW of light is measured at the output of the MCF, this may cause the particles to move around more in the thermal currents and not be able to be optically trapped in the current set-up.

To examine our lensed MCF for optothermal trapping, we coupled 1550 nm light into each core of the MCF using the fan-out device as described in Figure 6.9. This produces an interference pattern in the far field where high contrast interference fringes with a spacing of approximately 5.2 µm are produced as shown in Figure 6.12. Using the same sample chamber as the previous optical trapping experiments described in Chapters 4 and 5 composing of two coverslips separated by and 80 µm vinyl spacer, attempts were made to trap polystyrene microspheres with diameters of 2 µm, 3 µm and 4.5 µm. As can be seen from Figure 6.17 the low resolution of 720 x 576 pixels and the response of the camera made it difficult to image the microspheres when they moved over the top of the interference pattern making it impossible to determine whether trapping occurs.

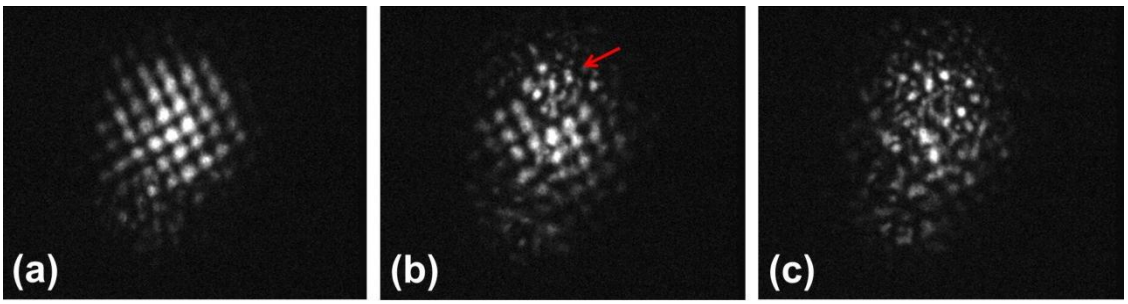

Figure 6.17. (a) The interference pattern produced at the crossing point of the four cores output from the lensed MCF at 1550 nm, (b) 3 µm microspheres start to move into the interference pattern as indicated by the red arrow and (c) as the population of microspheres increase it is difficult to determine whether the microspheres are trapped as the quality of the images is reduced due to scattering of light off of the microspheres.

As can be seen from Figure 6.17 (a), high contrast interference fringes are produced when the lensed MCF is coupled into with 1550 nm light using the single mode fan-out

device. However when the microspheres move over the interference pattern they block the 1550 nm light from the pattern and it becomes difficult to see whether the particles are aligned in the high intensity regions. Attempts were made to side-illuminate with a 460 nm LED and image using a visible camera, but this meant that the cameras needed to be changed during the experiment and that the position of the imaging lens needed to be varied for the different wavelengths. As the imaging set-up was constructed using cage plates to have the fibre pointing vertically, as shown in Figure 6.18, so that the thermal effects act against gravity as demonstrated in previous optothermal traps [128, 129]. The imaging objective was positioned on a mount that could only move in the z direction as x, y and z cage plate mounts could not be acquired. It was noted that although the plane of microspheres could be imaged, it was difficult to tell whether the same position as the interference pattern was as both could not be seen at the same time.

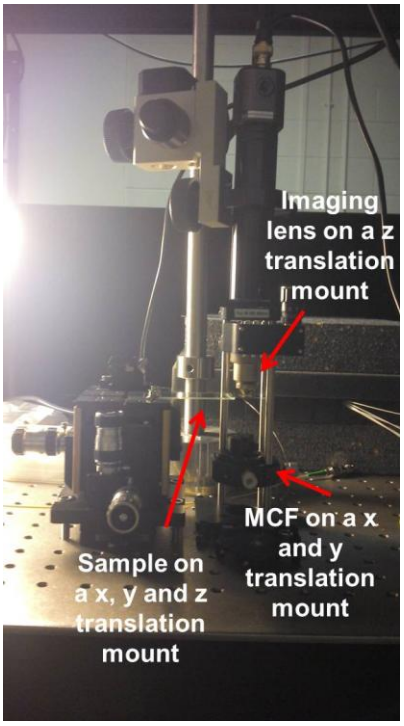

Figure 6.18. The experimental set up for thermal trapping showing fibre is pointed vertically upwards on a x and y translation cage mount with the lens on a z translation cage mount.

Alternatively, as our sample chamber is 80 µm thick in comparison to the 18 µm thick sample chamber used by Lei and Poon for their multimodal interference trapping array

[129], there may be convection flow fluidic drag forces that are pushing the particles to the top of the sample chamber and out of the imaging plane. The power contained in the interference pattern was reduced to decrease the temperature change and decrease the convection flow fluidic drag forces however trapping could still not be seen using 1550 nm and the lensed MCF in the current imaging set up. A future experiment could be carried out using a thinner sample chamber to reduce these forces and hopefully achieve optothermal trapping at 1550 nm using the lensed MCF device.

Prolonged use of the fusion splicer to create the lenses at the end of the MCF has been shown to reduce the temperature the electrodes reach, which reduces the lensing capability of the fusion splicer. To achieve the same lensing as previously demonstrated a 14 second arc needs to be repeated around 3 times in comparison to the single time used at the beginning of this research. However this also allows for weaker lenses to be created with longer focal lengths and larger fringe spacings as shown in Figure 6.19.

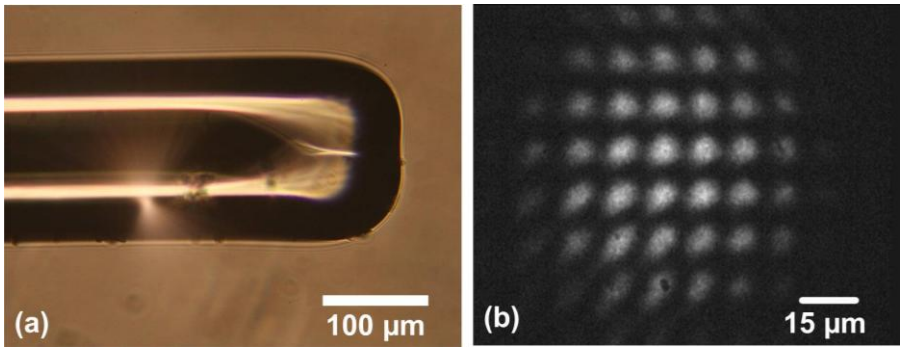

Figure 6.19. (a) The weaker lensed MCF that produces an interference pattern with a larger fringe spacing and (b) the interference pattern at 1550 nm using the weaker lensed MCF.

The weaker lensed MCF produces a fringe spacing of approximately 11.2 µm at the crossing point of four cores output at 1550 nm with each core coupled using the single mode fan-out device. The crossing point is approximately 400 ± 25 µm from the end of the fibre. The image was taken using a x60, 0.65NA aspheric objective lens from Newfocus (model number 5721) and a IR camera from Applied Scintillation

Technologies (model number CamIR1550) it was calibrated using the MFD of a Corning SMF-28 fibre that gave a calibration of 0.163 µm.pixel^{-1}. The output image shown in Figure 6.19 (b) was exported into MATLAB, to find the visibility of the fringes as shown in Figure 6.20.

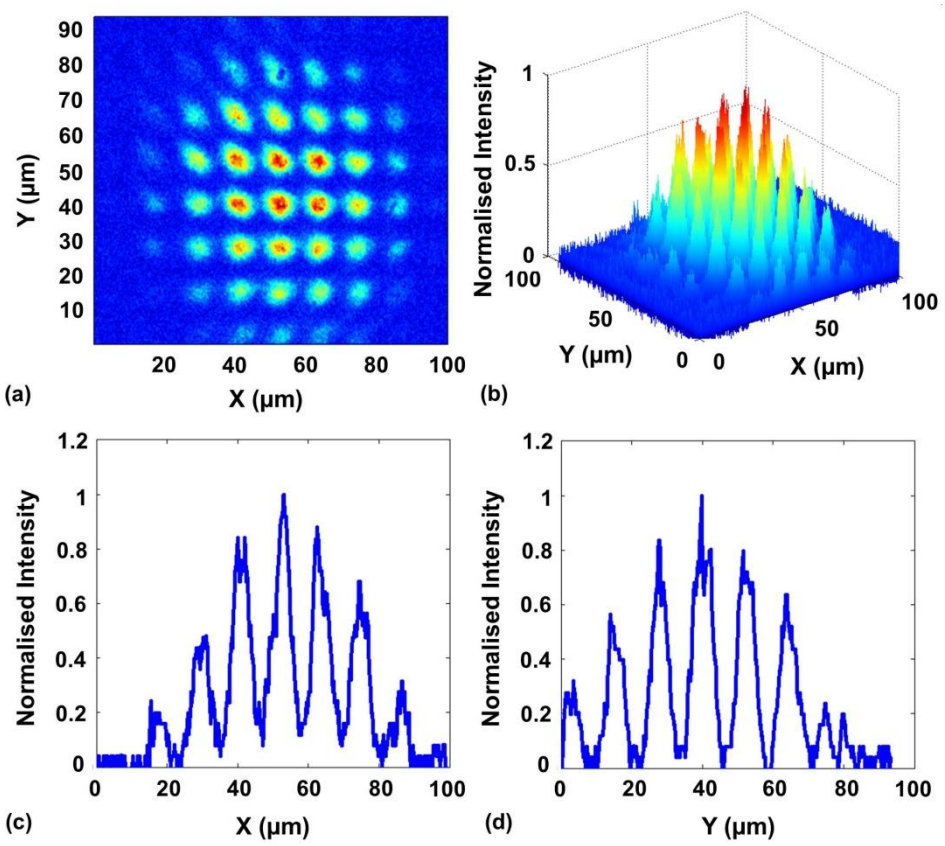

Figure 6.20. Interference fringes produced at the crossing point of the weaker lensed MCF when all four cores are coupled into using a single mode fan-out device at 1550 nm. (a) Two dimensional intensity plot of the fringe pattern, (b) three dimensional normalised intensity plot of interference pattern, (c) the cross section through the centre of the normalised interference pattern in the x direction and (d) the cross section through the centre of the normalised interference pattern in the y direction.

As can be seen from Figure 6.20 (c) and (d) the visibility of the fringes is greater than 80 %, comparable with the results from the lensed MCF as shown in Figure 6.12. This image was then used to calculate the percentage of power contained in the central peak using another MATLAB code, when 125 mW of power is emitted from the end of the

MCF, 5.93 mW is contained in the central peak that has a beam radius of 4.89 µm. The temperature change due to the central peak was calculated using equation 6.3 as ΔT_{Trap} = 4.81 K, this is a decrease of 69 % in comparison to the temperature rise due to the central peak of the lensed MCF. This lower temperature rise will result in a lower convection flow fluidic drag force.

A solution of 4.5 µm polystyrene microspheres were held in the 80 µm thick sample chamber and positioned between the MCF and the imaging lens as shown in Figure 6.18. The sample chamber was then translated in the z direction until the microspheres were imaged in the same plane as the interference pattern. Using the weaker lensed MCF that produces an interference pattern with larger beam spots and a larger fringe spacing, optical trapping was demonstrated as shown in Figure 6.21, using a wavelength of 1550 nm coupled into the four cores of the MCF using a single mode fan-out device.

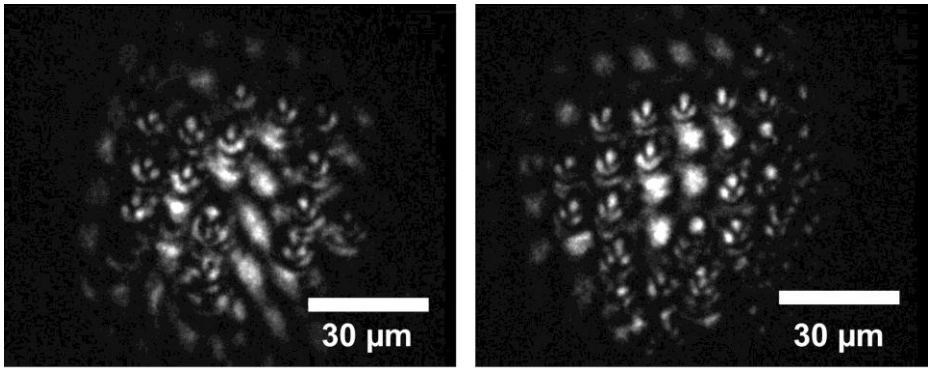

Figure 6.21. 4.5 µm polystyrene microspheres are trapped in the high intensity regions of the interference pattern produced at the crossing point from the four cores output of the weaker lensed MCF at 1550 nm.

Using the larger spot size and fringe spacing, it was easier to image the microspheres with the same imaging system as for images shown in Figure 6.17. This clearly shows that optical trapping is achievable using interference patterns from the lensed MCF when each core is coupled into using the single mode fan-out device. These results show that if a single mode fan-out device is created for 1047 nm operation, microspheres and cells could be trapped using a lensed MCF device that is fully integrated and contains no optical alignment.

6.8. Conclusions

An ultrafast laser inscribed fan-out device has been fabricated to couple light into each core of the four core multicore fibre creating a completely integrated device with no free space optical components that could be used in non-research facilities. When single mode operation of the fan-out device was demonstrated at 1550 nm, fringes with a visibility greater that 80 % were demonstrated, showing that optical trapping comparable to the results achieved using the DOE could be realised if a fan-out device is fabricated for single mode operation at 1047 nm. Optical trapping using the current fan-out device was not achieved at 1047 nm, even though the MCF was operating in single mode at 1047 nm the multimode propagation in the fibres in the v-groove array and the waveguides in the fan-out caused changes to the coupling into the MCF resulting in poor visibility of the fringes and drifting in the output interference pattern.

Due to the increase in the absorption coefficient of water, a maximum temperature increase at the central peak of the interference pattern was calculated as ΔT_{Trap} = 6.99 K at 1550 nm compared to ΔT_{Trap} = 0.04 K at 1047 nm when 125 mW of optical power is measured at the output of the MCF. The increase in the absorption coefficient of water also induces a convection flow fluidic drag force when 1550 nm light is used; in optical trapping this drag force lifts the microspheres to the top of the sample chamber. It can be reduced by using a thinner sample chamber, decreasing the temperature increase by using a lower laser power, or using a larger spot size and fringe spacing. Optical trapping was not demonstrated at 1550 nm using the lensed MCF with a fringe spacing of 5.2 μm at a distance of 300 μm from the end of the fibre; however when a weaker lens was used that produces a fringe spacing of 11.2 μm at a distance of 400 μm from the end of the fibre, two dimensional optical trapping was shown. The maximum temperature increase due to the central interference peak with the weaker lensed MCF was calculated as ΔT_{Trap} = 4.81 K. This lower temperature increase also indicates a lower convection drag force would be produced by the optically induced water absorption. This allowed 4.5 μm polystyrene microspheres to be trapped in the high intensity regions of the interference pattern produced from four core interference from the weaker lensed MCF when the cores were coupled into using a single mode fan-out device. These results show that if a single mode fan-out device is fabricated for 1047

nm a fully integrated multiple particle trapping device can be created and used for trapping microspheres or biological particles and cells for applications such as studying cell to cell interactions.

The same model previously used to examine the output from the lensed MCF at a wavelength of 1047 nm was used at for 1550 nm. The results showing a fringe spacing of 4.84 µm at a distance of 300 µm from the end of the fibre are in agreement with experimental results of a fringe spacing of 5.2 µm at a distance of 300 µm from the end of the fibre. These results show that even though the internal structure of the cores due to the lensing process is not known, the simple model can accurately describe the effects of the lensed MCF.

The results demonstrated in this chapter show the prospect of a "turn-key" MCF trapping system. At present the fan-out is not singlemode at the optimum wavelength resulting in the optical power coupling into the cores of the MCF to fluctuate; resulting in an unstable fringe pattern at the output. However, coupling into the cores of the MCF using the DOE resulted in a stable fringe pattern in which optical trapping of microspheres and *E. coli* bacteria was demonstrated. Using an optimised fan-out device at 1550 nm we successfully demonstrated a multiple particles trapping "turn-key" device. Therefore it is reasonable to expect that a system is feasible using low loss waveguides at 1047 nm, to optically trap microspheres and biological particles with a lensed MCF device.

Chapter 7. Conclusions and Future Work

7.1. Conclusions

The work reported in this thesis has focused on creating a multiple particle optical trapping device using a multicore fibre. Chapter 4 introduces the lensed four core multicore fibre used throughout the experiments discussed in this thesis; dual core interference from the lensed MCF is demonstrated to show multiple optical trapping in one dimension along the interference fringes. Chapter 5 explored this trapping device further by coupling light evenly into all four cores of the MCF using a diffractive optical element to produce an array of peaks in the interference pattern that were demonstrated to optically trap multiple microspheres and *E. coli* cells, showing that lensed MCF can be used in biological applications. Finally, Chapter 6 demonstrates work towards creating a fully optically integrated trapping probe using an ultrafast laser inscribed fan-out device to couple light into each core of the MCF. Single mode operation of the device was demonstrated at 1550 nm and two dimensional optical trapping was demonstrated at 1550 nm using a weaker lensed MCF device. The following will summarise the work presented in each chapter.

Chapter 4 presents the fusion splicer lensing process used to functionalise the MCF, creating a crossing point in the far field output where interference fringes are formed. This technique was shown to be a robust technique that utilises equipment commonly found in optical laboratories thus not incurring any additional fabrication facilities such as clean rooms etc. In comparison to other methods previously used for optical trapping fibres such as ion beam milling, two photon lithography, chemical etching and fibre polishing the use of a conventional fusion splicer provides repeatable results with high quality scatter free surfaces with a large reduction in fabrication costs and time.

The lensed MCF was demonstrated for dual core coupling by coupling into the diagonal cores using a beam splitter, steering mirrors and a common x20, 0.54NA microscope objective. At the far field output approximately 250 µm from the end of the MCF the output from the cores overlap and produce interference fringes with a spacing of 2 ± 0.3 µm in air that increases to a fringe spacing of 4.3 µm at a distance of approximately 500

μm from the end of the fibre when it is immersed in water. The lensed MCF was modelled using BeamPROP firstly using dimensions based on the external structure of the lensed MCF. This yielded results that showed the fringe spacing and the distance to the crossing point increased when the fibre was placed in water in comparison to air, however the values of these were not within the experimental error range so a second model was designed by increasing the radius of curvature of the lens until the results showed agreement with the experimental results. This second model gave a fringe spacing of 1.77 μm at a distance of 220 μm from the end of the MCF which is in an acceptable error range of the experimental data. The first model showed discrepancies in the fringe spacing and distance to the crossing point as the internal structure of the cores due to the lensing process is unknown, an experiment carried out to determine the central positions of the cores showed that after lensing each core was tapered towards the centre of the fibre by approximately 5 μm though it is thought that the main lensing property of the fibre is due to the external shape of the fibre at the output of the cores.

The linear interference fringes produced at the crossing point were used to optically trap polystyrene microspheres with diameters of 1.3 μm, 2 μm and 3 μm in the high intensity regions of the fringes. This was the first demonstration of using a fibre for interferometric optical trapping. The 2 μm diameter microspheres were chosen for further experiments to show that the trapping was due to the interference fringes as when the fringes were removed the particles could move freely in all directions but when the fringes were present the particles line up along the fringes. The linear interference fringes produce strong gradient forces across the fringes with a weaker gradient force along the fringes, this separates the particles across the fringes but the particles collect side by side in the high intensity regions in the centre of the fringe. These results were published in Optics Express in 2012 [130].

Chapter 5 presents results using all four cores of the lensed MCF, each core was coupled into using a custom made diffractive optical element that was designed to produce four highly uniform beams with the same spacing and orientation as the cores of the MCF. The use of a DOE to couple light into each core provides a compact system without the need for beam splitters and multiple steering mirrors. The output from the four cores of lensed MCF produces a high contrast lattice fringe pattern

approximately 250 μm from the end of the fibre with a fringe spacing of approximately 2.75 μm. The uniformity of coupling into each core produces high visibility of the fringes of greater than 80 % creating strong optical traps. Across the interference pattern high intensity peaks are produced that were used to optically trap polystyrene microspheres with diameters of 1.3 μm, 2 μm and 3 μm at equal spatially separated sites across the lattice pattern. Each of the intensity peaks act as individual optical traps suitable for trapping individual particles. The lensed MCF was also used to optically trap *E. coli* bacterial cells, this demonstrates that the lensed MCF device is suitable for trapping multiple biological cells in close proximity and is suitable for cell sensing applications such as examining cell to cell interactions.

The same BeamPROP model used to examine the output due to dual core interference from the lensed MCF in Chapter 4 was used to study the output from all four cores. The results gave a fringe spacing of 2.75 μm at a crossing point 245 μm from the end of the MCF. These results agree with the experimental results showing that the model accurately describes the effects of lensing the end of the MCF even if the effects of the lensing procedure on the cores is not fully known.

The appearance of the interference fringes could also be transformed into a variety of different trapping patterns through the rotation of a half wave-plate positioned at the input to the DOE. Manipulation of 2 μm polystyrene microspheres was demonstrated by rotating the half wave-plate from a position that produced one dimensional trapping fringes at the output, to a position that produced two dimensional trapping arrays of intensity peaks. This could be useful in the manipulation of optically trapped cells by controlling their separation in cell to cell interaction studies or in cell sorting applications where the motion of the particles can be controlled along the high intensity regions of the fringes. The results presented in Chapter 5 were published in Optics Express in 2013 [112].

Chapter 6 presents results using an ultrafast laser inscribed fan-out device when used at both 1047 nm and at 1550 nm. The use of a fan-out device creates a completely integrated optical device that does not rely on any alignment, producing a device that could be used out with an optical research environment. Ultrafast laser inscription is a

three dimensional waveguide writing technique that allows custom devices to be fabricated for any multicore fibre arrangement.

Single mode operation of the fan-out device was demonstrated at 1550 nm, when all four cores were coupled into, fringes with a visibility greater that 80 % was demonstrated this is comparable to the fringes produced using the DOE at a wavelength of 1047 nm. These results show that if a completely single mode device can be fabricated at 1047 nm, optical trapping similar to using the DOE can be achieved in an entirely optically integrated device. Optical trapping was not achieved at 1047 nm with the current fan-out device due to multimodal effects originating from the fibre in the v-groove array and the fan-out. Even though the MCF was operating in single mode at 1047 nm, the fibre in the v-groove and the waveguides in the fan-out were operating in multimode, this caused changing to the coupling into the MCF that resulted in poor visibility of the fringes at drifting of the output interference pattern.

The same BeamPROP model as previously demonstrated was used to show the effects of the lensing at a wavelength of 1550 nm, the results showed that fringe spacing of 4.84 µm is produced at a distance of 300 µm from the end of the MCF. These results are within a reasonable error of the experimental results of a fringe spacing of 5.2 µm at a distance of 300 ± 25 µm from the end of the fibre. These results show that the model can accurately describe the effects of lensing the MCF even at varying wavelengths.

The increase in the absorption of water coefficient at 1550 nm compared to 1047 nm results in an increase of temperature due to the central intensity peak of the interference pattern of ΔT_{Trap} = 6.99 K at 1550 nm compared to ΔT_{Trap} = 0.0356 K at 1047 nm when 125 mW of light is measured at the output of the MCF. This increase in temperature also induces a convection flow fluidic drag force that lifts the microsphere to the top of the sample chamber during optical trapping when the trapping beam enters the sample chamber from below. The convection flow fluidic drag force can be reduced by using a thinner sample chamber or by reducing the temperature increase by reducing the power of the trapping laser or using a larger spot size and fringe spacing. Optical trapping was not demonstrated using the lensed MCF at 1550 nm that produced a crossing point approximately 300 ± 25 µm from the end of the fibre with a fringe

spacing of 5.2 µm. However when a weaker lens was created at the end of the MCF that produced a crossing point approximately 400 ± 25 µm from the end of the MCF with a fringe spacing of 11.2 µm two dimensional interferometric optical trapping was demonstrated. The weaker lensed MCF produced larger spot sizes, this decreased the maximum temperature increase due to the central intensity peak of the interference pattern to ΔT_{Trap} = 4.81 K, this lower temperature indicates that the convection flow fluidic drag force would also reduce. Using the weaker lensed MCF, 4.5 µm polystyrene microspheres were trapped in the high intensity regions of the interference pattern when each core of the MCF was coupled into using an ultrafast laser inscribed fan-out device. These results show that if a single mode fan-out device is fabricated at 1047 nm, two dimensional interferometric optical trapping should be achievable using a completely optically integrated MCF device.

7.2. Future work

7.2.1. Single mode fan-out device at 1047 nm

The successful demonstration of optically trapping multiple particles using a single mode fan-out device at 1550 nm shows that if a fan-out device is fabricated for single mode operation at 1047 nm, the optical trapping of biological cells could be achieved using a optically integrated MCF trapping device. This would allow the device to be used in non-optical research environments such as biology laboratories where it could be used as a tool to trap multiple cells in close proximity to study cell to cell interactions such as quorum sensing and biofilm formation. If polarisation maintaining waveguides are fabricated in the fan-out and polarisation maintaining fibre used throughout the trapping device the interference pattern at the output would not drift therefore more stable trapping could be achieved. Using polarisation controllers on the input fibres of the v-groove array would allow for active manipulation of the trapped particles to be carried out.

7.2.2. Stronger lensed MCF

A stronger lens at the end of the MCF will produce stronger gradient forces and stronger confinement of the trapped particles. This could be achieved using a higher power fusion splicer such as a Vytran splicer. If a lens with a large angle of refraction is produced at the end of the MCF this would increase the axial gradient forces and could produce three dimensional trapping. The number of trapping sites would be reduced as would the distance between the end of the fibre and the optical trapping site; therefore this would limit its application in measuring cell to cell interactions. However if a three dimensional optical trapping device can be fabricated using a fusion splicer this would greatly reduce the cost and fabrication time of current three dimensional fibre optical tweezers that have been created using ion beam milling [27] and two photon lithography [28]. The four core MCF could be tapered then lensed to create a three dimensional trap. This has been demonstrated using a two core MCF by Zhang et al., in 2012 [104], the use of a four core MCF will create further confinement of the trapped particle.

7.2.3. Study of different lensed MCF's

Throughout this thesis only one type of MCF was investigated. The Gemini four core fibre used throughout these experiments was larger than standard optical fibres and was a non-standard shaped. This meant that the MCF could not be cleaved in a fibre cleaver instead it had to be cleaved by hand using a fibre scribe, this resulted in successful cleaves around 30 % of the time. Therefore if a circular fibre with a smaller diameter is used a standard cleaver could be used resulting in a quicker fabrication time. A study could be carried out on different four core MCF to see how different core spacing can achieve different fringe spacing and the different strengths of lenses that could be created. If interference peaks are produced with a fringe spacing greater than 10 μm this could be used to study cell to cell interactions between mammalian cells.

If different MCFs with a variety of core numbers and arrangements are used, different fringe patterns could be produced these will allow multiple particles and cells to be trapped in various configuration. If the MCF has a central core, optical traps could be created from interference from the outer cores and the central core could be used for

sensing studies by using a different wavelength in the central core that won't interfere with the interference pattern.

Appendix A. Optical Trapping Videos

As an addition to this thesis, videos showing the optical trapping of microspheres and particles using the lensed MCF are supplied. Image stills from these videos are already included in the main body of this thesis, contained within this appendix are descriptions of the videos, including where in the thesis the images in the video are presented.

A1. Dual core interference trapping

This video corresponds to Chapter 4, Figure 4.22 and shows 2 μm polystyrene microspheres trapped in the linear fringes produced from dual core interference from the lensed MCF. During the video one of the beams is blocked, destroying the fringes, the particles can be seen to drift from their trapped positions in all directions. Once the beam is unblocked and the fringes reappear and the particles realign along the fringes, trapped in the areas of high intensity.

A2. Four core interferometric optical trapping of microspheres

This video corresponds to Chapter 5, Figure 5.11 and shows 2 μm polystyrene microspheres trapped in two dimensions in the intensity peaks produced from interference from the output of the lensed MCF when all four cores are coupled into using the DOE. During the video the fringes are destroyed by perturbing the fibre. This allows the particles to move from their trapped positions, when the fringes reappear the particles are immediately trapped in the high intensity regions of the fringe pattern.

A3. Active manipulation of optically trapped microspheres

This video corresponds to Chapter 5, Figure 5.12 and shows the active manipulation of optically trapped microspheres by changing the input polarisation to the MCF using a half wave-plate. Initially, the half wave-plate is at a position that produces linear interference fringes at the output of the MCF, 2 μm polystyrene microspheres trapped along the interference fringes. They can be seen to be closer together in the vertical

direction than the horizontal direction. Approximately 6 seconds into the video the half wave-plate is rotated to a position that produces a two dimensional lattice fringe pattern at the output from the four cores of the MCF. When the half wave-plate is rotated the particles can be seen to move to the high intensity position of the interference array and are spatially separated both vertically and horizontally.

A4. Two dimensional optical trapping of *E. coli* bacterial cells

This video corresponds to Chapter 5, Figure 5.13 (b), *E. coli* cells are trapped in the high intensity regions of the interference pattern produced at the output from the four cores of the MCF when it is coupled into using the DOE. In the video the interference pattern produced by the laser cannot be seen as an IR filter is used to block the 1047 nm light. The *E.coli* cells are imaged by side illumination using a 460 nm LED.

A5. Two dimensional trapping at 1550 nm using a weaker lensed MCF and the fan-out device

This video corresponds to Chapter 6, Figure 6.21 (b), 4.5 μm polystyrene microspheres are trapped in the high intensity regions of the fringe pattern formed from the output of the weaker lensed MCF when all four cores are coupled into with 1550 nm light using the single mode fan-out device. Approximately 21 seconds into the video the fringe pattern drifts however the microspheres briefly move out of their traps until the original interference pattern returns and they move back into their traps.

References

1. A. C. S. v. Heel, "A new method of transporting optical images without aberations," Nature **173**, 39 (1954).
2. H. H. Hopkins and N. S. Kapany, "A flexible fibrescope, using static scanning," Nature **173**, 39-41 (1954).
3. T. H. Maiman, "Stimulated optical radiation in ruby," Nature **187**, 493 (1960).
4. "Technical demographics," Electron. Commun. Eng. **7**, 265-271 (1995).
5. K. C. Kao and G. A. Hockham, "Dielectric-fibre surface waveguides for optical frequencies," Proc. IEE **113**, 1151-1158 (1966).
6. "The Nobel Prize in Physics 2009" (Nobel Prize, 2009), retrieved 5th November 2013, http://www.nobelprize.org/nobel_prizes/physics/laureates/2009/.
7. J. Hecht, "Ch. 14: Three generations in five years," in *City of light - the story of fiber optics* (Oxford University Press, 1999).
8. J. Hecht, "Ch. 15: Submarine cables - covering the ocean floor with glass," in *City of light - the story of fiber optics* (Oxford University Press, 1999).
9. R. J. Mears, L. Reekie, I. M. Jauncey, and D. N. Payne, "Low-noise erbium-doped fiber amplifier operating at 1.54-mu-m," Electron. Lett. **23**, 1026-1028 (1987).
10. P. Trischitta, M. Colas, M. Green, G. Wuzniak, and J. Arena, "The TAT-12/13 cable network," IEEE Commun. Mag. **34**, 24-28 (1996).
11. "TAT-14 Cable System" (Sprint Nextel, 2009), retrieved 5th November 2013, https://www.tat-14.com/tat14/.
12. "Construction Project Express" (Hibernia Networks), retrieved 5th December 2013, www.hiberniaatlantic.com/construction.html.
13. D. J. Richardson, J. M. Fini, and L. E. Nelson, "Space-division multiplexing in optical fibres," Nat. Photonics **7**, 354-362 (2013).
14. R. J. Essiambre and R. W. Tkach, "Capacity Trends and Limits of Optical Communication Networks," P. IEEE **100**, 1035-1055 (2012).
15. J. M. Dudley, L. P. Barry, P. G. Bollond, J. D. Harvey, and R. Leonhardt, "Simultaneous measurement of the dispersion and nonlinearity of standard fibre using frequency resolved optical gating," in *Integrated Optics and Optical Fibre Communications, 11th International Conference on, and 23rd European Conference on Optical Communications (Conf. Publ. No.: 448)*, 1997), 307-310 vol.303.
16. P. J. Winzer, "Energy-Efficient Optical Transport Capacity Scaling Through Spatial Multiplexing," IEEE Photonic. Tech. L. **23**, 851-853 (2011).
17. F. Yaman, N. Bai, B. Zhu, T. Wang, and G. Li, "Long distance transmission in few-mode fibers," Opt. Express **18**, 13250-13257 (2010).
18. N. Bozinovic, Y. Yue, Y. Ren, M. Tur, P. Kristensen, H. Huang, A. E. Willner, and S. Ramachandran, "Terabit-Scale Orbital Angular Momentum Mode Division Multiplexing in Fibers," Science **340**, 1545-1548 (2013).
19. M. Koshiba, K. Saitoh, and Y. Kokubun, "Heterogeneous multi-core fibers: proposal and design principle," IEICE Electron. Express **6**, 98-103 (2009).
20. T. Hayashi, T. Taru, O. Shimakawa, T. Sasaki, and E. Sasaoka, "Design and fabrication of ultra-low crosstalk and low-loss multi-core fiber," Opt. Express **19**, 16576-16592 (2011).
21. H. Takara, A. Sano, T. Kobayashi, H. Kubota, H. Kawakami, A. Matsuura, Y. Miyamoto, Y. Abe, H. Ono, K. Shikama, Y. Goto, K. Tsujikawa, Y. Sasak, I. Ishida, K. Takenaga, S. Matsuo, K. Saitoh, M. Koshiba, and T. Morioka, "1.01-Pb/s (12 SDM/222 WDM/456 Gb/s) crosstalk managed transmission with 91.4-b/s/Hz aggregate spectral efficiency," in *ECOC*, (2012), p. Postdeadline paper Th3.C.1
22. D. Qian, E. Ip, M. Huang, M. Li, A. Dogariu, S. Zhang, Y. Shao, Y. Huang, Y. Zhang, X. Cheng, Y. Tian, P. N. Ji, A. Collier, Y. Geng, J. Liñares, C. Montero, V. Moreno, X.

Prieto, and T. Wang, "1.05Pb/s Transmission with 109b/s/Hz spectral efficiency using hybrid single and few mode cores," in *FIO*, (2012), p. Postdeadline paper FW6C.3.
23. G. Zhang, Q. Zhang, Y. L. Shen, Q. L. Zhou, L. L. Hu, J. R. Qiu, and D. P. Chen, "Phase locking of a compact Nd-doped phosphate multicore fiber laser," Laser Phys. **21**, 410-413 (2011).
24. H. T. Bookey, J. Lousteau, A. Jha, N. Gayraud, R. R. Thomson, N. D. Psaila, H. Li, W. N. MacPherson, J. S. Barton, and A. K. Kar, "Multiple rare earth emissions in a multicore tellurite fiber with a single pump wavelength," Opt. Express **15**, 17554-17561 (2007).
25. G. M. H. Flockhart, W. N. MacPherson, J. S. Barton, J. D. C. Jones, L. Zhang, and I. Bennion, "Two-axis bend measurement with Bragg gratings in multicore optical fiber," Opt. Lett. **28**, 387-389 (2003).
26. N. Ortega-Quijano, F. Fanjul-Velez, and J. L. Arce-Diego, "Optical crosstalk influence in fiber imaging endoscopes design," Opt Commun **283**, 633-638 (2010).
27. C. Liberale, P. Minzioni, F. Bragheri, F. De Angelis, E. Di Fabrizio, and I. Cristiani, "Miniaturized all-fibre probe for three-dimensional optical trapping and manipulation," Nat. Photonics **1**, 723-727 (2007).
28. C. Liberale, G. Cojoc, F. Bragheri, P. Minzioni, G. Perozziello, R. La Rocca, L. Ferrara, V. Rajamanickam, E. Di Fabrizio, and I. Cristiani, "Integrated microfluidic device for single-cell trapping and spectroscopy," Sci. Rep. **3**, 1258 (2013).
29. N. Ma, F. Gunn-Moore, and K. Dholakia, "Optical transfection using an endoscope-like system," J. Biomed. Opt. **16**, 028002 (2011).
30. M. Reicherter, T. Haist, E. U. Wagemann, and H. J. Tiziani, "Optical particle trapping with computer-generated holograms written on a liquid-crystal display," Opt. Lett. **24**, 608-610 (1999).
31. E. R. Dufresne and D. G. Grier, "Optical tweezer arrays and optical substrates created with diffractive optics," Rev. Sci. Instrum. **69**, 1974-1977 (1998).
32. A. E. Chiou, W. Wang, G. J. Sonek, J. Hong, and M. W. Berns, "Interferometric optical tweezers," Opt Commun **133**, 7-10 (1997).
33. A. Yariv, *Optical Electronics in Modern Communications - 5th Edition*, 5th Edition ed. (Oxford University Press, Inc., New York, 1997).
34. A. Ghatak and K. Thyagarajan, *Introduction to Fiber Optics* (Cambridge University Press, Cambridge, United Kingdom, 1998).
35. J. M. Senior, *Optical Fiber Communications - Principles and Practice* (Prentice Hall International (UK) Ltd., Hertfordshire, United Kingdom, 1985).
36. W. Klaus, (personal communication, 12/07/2013, National Institute of Information and Communication Technology (NICT), Japan).
37. K. Saitoh, M. Koshiba, K. Takenaga, and S. Matsuo, "Crosstalk and Core Density in Uncoupled Multicore Fibers," IEEE Photonic. Tech. L. **24**, 1898-1901 (2012).
38. H. Takahashi, T. Tsuritani, E. L. T. de Gabory, T. Ito, W. R. Peng, K. Igarashi, K. Takeshima, Y. Kawaguchi, I. Morita, Y. Tsuchida, Y. Mimura, K. Maeda, T. Saito, K. Watanabe, K. Imamura, R. Sugizaki, and M. Suzuki, "First demonstration of MC-EDFA-repeatered SDM transmission of 40 x 128-Gbit/s PDM-QPSK signals per core over 6,160-km 7-core MCF," Opt. Express **21**, 789-795 (2013).
39. "Chiral Photonics", retrieved 10th December 2013, http://www.chiralphotonics.com.
40. "Optoscribe", retrieved 10th December 2013, http://optoscribe.com/.
41. W. Klaus, J. Sakaguchi, B. J. Puttnam, Y. Awaji, N. Wada, T. Kobayashi, and M. Watanabe, "Free-Space Coupling Optics for Multicore Fibers," IEEE Photonic.Tech. L. **24**, 1902-1905 (2012).
42. J. Sakaguchi, B. J. Puttnam, W. Klaus, Y. Awaji, N. Wada, A. Kanno, T. Kawanishi, K. Imamura, H. Inaba, K. Mukasa, R. Sugizaki, T. Kobayashi, and M. Watanabe, "305 Tb/s Space Division Multiplexed Transmission Using Homogeneous 19-Core Fiber," J. Lightwave Technol. **31**, 554-562 (2013).
43. "PROFA" (Chiral Photonics, 2013), retrieved 22nd October 2013, 2013, http://www.chiralphotonics.com/Web/docs/PROFA_presentation.pdf.

44. B. Zhu, T. F. Taunay, M. F. Yan, J. M. Fini, M. Fishteyn, E. M. Monberg, and F. V. Dimarcello, "Seven-core multicore fiber transmissions for passive optical network," Opt. Express **18**, 11117-11122 (2010).
45. R. R. Thomson, H. T. Bookey, N. D. Psaila, A. Fender, S. Campbell, W. N. MacPherson, J. S. Barton, D. T. Reid, and A. K. Kar, "Ultrafast-laser inscription of a three dimensional fan-out device for multicore fiber coupling applications," Opt. Express **15**, 11691-11697 (2007).
46. T. Watanabe, M. Hikita, and Y. Kokubun, "Laminated polymer waveguide fan-out device for uncoupled multi-core fibers," Opt. Express **20**, 26317-26325 (2012).
47. C. B. Schaffer, A. Brodeur, and E. Mazur, "Laser-induced breakdown and damage in bulk transparent materials induced by tightly focused femtosecond laser pulses," Meas. Sci. Technol. **12**, 1784 (2001).
48. Optoscribe, "3D Optofan Series 4/7 Channel devices" (2013), retrieved 1st November 2013, http://optoscribe.com/wp-content/uploads/2013/09/OPTOSCRIBE-4-and-7-Multicore-fiber-fanout.pdf.
49. A. S. Kurkov, S. A. Babin, I. A. Lobach, and S. I. Kablukov, "Mechanism of mode coupling in multicore fiber lasers," Opt. Lett. **33**, 61-63 (2008).
50. P. S. Westbrook, K. S. Abedin, T. F. Taunay, T. Kremp, J. Porque, E. Monberg, and M. Fishteyn, "Multicore fiber distributed feedback lasers," Opt. Lett. **37**, 4014-4016 (2012).
51. J. T. Kringlebotn, J. L. Archambault, L. Reekie, and D. N. Payne, "Er3+:Yb3+-codoped fiber distributed-feedback laser," Opt. Lett. **19**, 2101-2103 (1994).
52. J. Canning, "Fibre gratings and devices for sensors and lasers," Laser Photonics Rev. **2**, 275-289 (2008).
53. M. J. Gander, W. N. MacPherson, R. McBride, J. D. C. Jones, L. Zhang, I. Bennion, P. M. Blanchard, J. G. Burnett, and A. H. Greenaway, "Bend measurement using Bragg gratings in multicore fibre," Electron. Lett. **36**, 120-121 (2000).
54. B. Lee, "Review of the present status of optical fiber sensors," Opt. Fiber Technol. **9**, 57-79 (2003).
55. G. A. Cranch, G. M. H. Flockhart, W. N. MacPherson, J. S. Barton, and C. K. Kirkendall, "Ultra-high-sensitivity two-dimensional bend sensor," Electron. Lett. **42**, 520 (2006).
56. C. G. Askins, G. A. Miller, and E. J. Friebele, "Bend and twist sensing in a multi-core optical fiber," in *IEEE Lasers and Electro-Optics Society, 2008. LEOS 2008. 21st Annual Meeting of the*, 2008), 109-110.
57. S. Dochow, I. Latka, M. Becker, R. Spittel, J. Kobelke, K. Schuster, A. Graf, S. Brückner, S. Unger, M. Rothhardt, B. Dietzek, C. Krafft, and J. Popp, "Multicore fiber with integrated fiber Bragg gratings for background-free Raman sensing," Opt. Express **20**, 20156-20169 (2012).
58. T. Meyer, N. Bergner, C. Bielecki, C. Krafft, D. Akimov, B. F. M. Romeike, R. Reichart, R. Kalff, B. Dietzek, and J. Popp, "Nonlinear microscopy, infrared, and Raman microspectroscopy for brain tumor analysis," J. Biomed. Opt. **16**, 021113-021113-021110 (2011).
59. Z. Huang, H. Zeng, I. Hamzavi, D. I. McLean, and H. Lui, "Rapid near-infrared Raman spectroscopy system for real-time in vivo skin measurements," Opt. Lett. **26**, 1782-1784 (2001).
60. K. Bulut and M. N. Inci, "Three-dimensional optical profilometry using a four-core optical fibre," Opt. Laser Technol. **37**, 463-469 (2005).
61. A. Novack, D. D'Annunzio, E. D. Cubuk, N. Inci, and L. Molter, "Three-dimensional phase step profilometry with a multicore optical fiber," Appl. Opt. **51**, 1045-1048 (2012).
62. N. M. Sohn, M. N. Inci, and L. A. Molter, "Two Dimensional Force and Longitudinal Twisting Measurements with a Four-Core Optical Fiber Sensor," in *Workshop on Specialty Optical Fibers and their Applications*, (Optical Society of America, 2013), W3.14.

63. N. Ortega-Quijano, F. Fanjul-Vélez, and J. L. Arce-Diego, "Optical crosstalk influence in fiber imaging endoscopes design," Opt Commun **283**, 633-638 (2010).
64. S. Schedin, G. Pedrini, H. J. Tiziani, and A. K. Aggarwal, "Comparative Study of Various Endoscopes for Pulsed Digital Holographic Interferometry," Appl. Opt. **40**, 2692-2697 (2001).
65. A. Ashkin, "Acceleration and Trapping of Particles by Radiation Pressure," Phys. Rev. Lett. **24**, 156-159 (1970).
66. A. Ashkin and J. M. Dziedzic, "Optical Levitation by Radiation Pressure," Appl. Phys. Lett. **19**, 283-285 (1971).
67. A. Ashkin, J. M. Dziedzic, J. E. Bjorkholm, and S. Chu, "Observation of a single-beam gradient force optical trap for dielectric particles," Opt. Lett. **11**, 288-290 (1986).
68. A. L. Stout, "Detection and characterization of individual intermolecular bonds using optical tweezers," Biophys. J. **80**, 2976-2986 (2001).
69. M. D. Wang, H. Yin, R. Landick, J. Gelles, and S. M. Block, "Stretching DNA with optical tweezers," Biophys. J. **72**, 1335-1346 (1997).
70. J. T. Finer, R. M. Simmons, and J. A. Spudich, "Single myosin molecule mechanics: piconewton forces and nanometre steps," Nature **368**, 113-119 (1994).
71. K. Sasaki, M. Koshioka, H. Misawa, N. Kitamura, and H. Masuhara, "Pattern formation and flow control of fine particles by laser-scanning micromanipulation," Opt. Lett. **16**, 1463-1465 (1991).
72. Polysciences, "Data sheet for Polybead polystyrene microspheres - technical data sheet 238", retrieved 2014, http://www.polysciences.com/SiteData/docs/TDS238/d060e1ed6379b508/TDS%20238.pdf.
73. J. E. Molloy and M. J. Padgett, "Lights, action: Optical tweezers," Contemp. Phys. **43**, 241-258 (2002).
74. M. R. Querry, D. M. Wieliczka, and D. J. Segelstein, "Refractive index of water," in *Handbook of optical constants of solids*, E. D. Palik, ed. (Academic Press, New York, 1991), pp. 1059-1077.
75. K. Sasaki, M. Koshioka, H. Misawa, N. Kitamura, and H. Masuhara, "Laser-Scanning Micromanipulation and Spatial Patterning of Fine Particles," Jap. J. Appl. Phys.2 **30**, L907-L909 (1991).
76. D. S. Viswanath, T. K. Ghosh, D. H. L. Prasad, N. V. K. Dutt, and K. Y. Rani, "Viscosity of Liquids - Theory, Estimation, Experiment and Data," (Springer Netherlands, 2007), pp. 163-176.
77. H. Misawa, K. Sasaki, M. Koshioka, N. Kitamura, and H. Masuhara, "Multibeam laser manipulation and fixation of microparticles," Appl. Phys. Lett. **60**, 310-312 (1992).
78. C. Mio, T. Gong, A. Terray, and D. W. M. Marr, "Design of a scanning laser optical trap for multiparticle manipulation," Rev. Sci. Instrum. **71**, 2196-2200 (2000).
79. K. Visscher, S. P. Gross, and S. M. Block, "Construction of multiple-beam optical traps with nanometer-resolution position sensing," IEEE J. Sel. Top. Quant. **2**, 1066-1076 (1996).
80. D. L. J. Vossen, A. van der Horst, M. Dogterom, and A. van Blaaderen, "Optical tweezers and confocal microscopy for simultaneous three-dimensional manipulation and imaging in concentrated colloidal dispersions," Rev. Sci. Instrum. **75**, 2960-2970 (2004).
81. E. R. Dufresne, G. C. Spalding, M. T. Dearing, S. A. Sheets, and D. G. Grier, "Computer-generated holographic optical tweezer arrays," Rev. Sci. Instrum. **72**, 1810-1816 (2001).
82. P. Korda, G. C. Spalding, E. R. Dufresne, and D. G. Grier, "Nanofabrication with holographic optical tweezers," Rev. Sci. Instrum. **73**, 1956-1957 (2002).
83. D. G. Grier, "A revolution in optical manipulation," Nature **424**, 810-816 (2003).
84. J. Liesener, M. Reicherter, T. Haist, and H. J. Tiziani, "Multi-functional optical tweezers using computer-generated holograms," Opt Commun **185**, 77-82 (2000).

85. J. E. Curtis, B. A. Koss, and D. G. Grier, "Dynamic holographic optical tweezers," Opt Commun **207**, 169-175 (2002).
86. J. Leach, G. Sinclair, P. Jordan, J. Courtial, M. Padgett, J. Cooper, and Z. Laczik, "3D manipulation of particles into crystal structures using holographic optical tweezers," Opt. Express **12**, 220-226 (2004).
87. G. Sinclair, P. Jordan, J. Courtial, M. Padgett, J. Cooper, and Z. Laczik, "Assembly of 3-dimensional structures using programmable holographic optical tweezers," Opt. Express **12**, 5475-5480 (2004).
88. M. M. Burns, J.-M. Fournier, and J. A. Golovchenko, "Optical Matter: Crystallization and Binding in Intense Optical Fields," Science **249**, 749-754 (1990).
89. A. N. Rubinov, V. M. Katarkevich, A. A. Afanas'ev, and T. S. Efendiev, "Interaction of interference laser field with an ensemble of particles in liquid," Opt Commun **224**, 97-106 (2003).
90. A. Casaburi, G. Pesce, P. Zemanek, and A. Sasso, "Two and three beam interferometric optical tweezers," Opt Commun **251**, 393-404 (2005).
91. E. Schonbrun, R. Piestun, P. Jordan, J. Cooper, K. D. Wulff, J. Courtial, and M. Padgett, "3D interferometric optical tweezers using a single spatial light modulator," Opt. Express **13**, 3777-3786 (2005).
92. J. Xavier, R. Dasgupta, S. Ahlawat, J. Joseph, and P. K. Gupta, "Controlled formation and manipulation of colloidal lattices by dynamically reconfigurable three dimensional interferometric optical traps," Appl. Phys. Lett. **101**, 201101 (2012).
93. W. Mu, G. Wang, L. Luan, G. C. Spalding, and J. B. Ketterson, "Dynamic control of defects in a two-dimensional optically assisted assembly," New J. Phys. **8**, 70 (2006).
94. B. N. Slama-Eliau and G. Raithel, "Three-dimensional arrays of submicron particles generated by a four-beam optical lattice," Phys. Rev. E **83**(2011).
95. A. Constable, J. Kim, J. Mervis, F. Zarinetchi, and M. Prentiss, "Demonstration of a fiber-optical light-force trap," Opt. Lett. **18**, 1867-1869 (1993).
96. E. R. Lyons and G. J. Sonek, "Confinement and bistability in a tapered hemispherically lensed optical fiber trap," Appl. Phys. Lett. **66**, 1584 (1995).
97. K. Taguchi, H. Ueno, T. Hiramatsu, and M. Ikeda, "Optical trapping of dielectric particle and biological cell using optical fibre," Electron. Lett. **33**, 413-414 (1997).
98. K. Taguchi, K. Atsuta, T. Nakata, and M. Ikeda, "Single laser beam fiber optic trap," Opt. Quant. Electron. **33**, 99-106 (2001).
99. Z. Hu, J. Wang, and J. Liang, "Manipulation and arrangement of biological and dielectric particles by a lensed fiber probe," Opt. Express **12**, 4123-4128 (2004).
100. R. Taylor and C. Hnatovsky, "Particle trapping in 3-D using a single fiber probe with an annular light distribution," Opt. Express **11**, 2775-2782 (2003).
101. Y. Gong, A. Y. Ye, Y. Wu, Y. J. Rao, Y. Yao, and S. Xiao, "Graded-index fiber tip optical tweezers: numerical simulation and trapping experiment," Opt. Express **21**, 16181-16190 (2013).
102. J. M. Tam, I. Biran, and D. R. Walt, "An imaging fiber-based optical tweezer array for microparticle array assembly," Appl. Phys. Lett. **84**, 4289 (2004).
103. L. Yuan, Z. Liu, J. Yang, and C. Guan, "Twin-core fiber optical tweezers," Opt. Express **16**, 4559-4566 (2008).
104. Y. Zhang, Z. Liu, J. Yang, and L. Yuan, "A non-contact single optical fiber multi-optical tweezers probe: Design and fabrication," Opt Commun **285**, 4068-4071 (2012).
105. E. Zetterlund, A. Loriette, C. Sterner, M. Eriksson, H. Eriksson-Quist, and W. Margulis, "Gemini fiber for interferometry and sensing applications," J. Sens. **2009**, 196380 (2009).
106. Crystran, "Silica Glass (SiO2)", retrieved 11th March 2014, http://www.crystran.co.uk/optical-materials/silica-glass-sio2.
107. X. Feng, W. H. Loh, J. C. Flanagan, A. Camerlingo, S. Dasgupta, P. Petropoulos, P. Horak, K. E. Frampton, N. M. White, J. H. Price, H. N. Rutt, and D. J. Richardson, "Single-mode tellurite glass holey fiber with extremely large mode area for infrared nonlinear applications," Opt. Express **16**, 13651-13656 (2008).

108. J. S. Liu, A. J. Caley, A. J. Waddie, and M. R. Taghizadeh, "Comparison of simulated quenching algorithms for design of diffractive optical elements," Appl. Opt. **47**, 807-816 (2008).
109. A. J. Caley, M. J. Thomson, J. Liu, A. J. Waddie, and M. R. Taghizadeh, "Diffractive optical elements for high gain lasers with arbitrary output beam profiles," Opt. Express **15**, 10699-10704 (2007).
110. M. P. MacDonald, G. C. Spalding, and K. Dholakia, "Microfluidic sorting in an optical lattice," Nature **426**, 421-424 (2003).
111. M. Righini, P. Ghenuche, S. Cherukulappurath, V. Myroshnychenko, F. J. García de Abajo, and R. Quidant, "Nano-optical Trapping of Rayleigh Particles and Escherichia coli Bacteria with Resonant Optical Antennas," Nano Lett. **9**, 3387-3391 (2009).
112. A. L. Barron, A. K. Kar, T. J. Aspray, A. J. Waddie, M. R. Taghizadeh, and H. T. Bookey, "Two dimensional interferometric optical trapping of multiple particles and Escherichia coli bacterial cells using a lensed multicore fiber," Opt. Express **21**, 13199-13207 (2013).
113. R. Mary, G. Brown, S. J. Beecher, F. Torrisi, S. Milana, D. Popa, T. Hasan, Z. P. Sun, E. Lidorikis, S. Ohara, A. C. Ferrari, and A. K. Kar, "1.5 GHz picosecond pulse generation from a monolithic waveguide laser with a graphene-film saturable output coupler," Opt. Express **21**, 7943-7950 (2013).
114. R. Mary, S. J. Beecher, G. Brown, R. R. Thomson, D. Jaque, S. Ohara, and A. K. Kar, "Compact, highly efficient ytterbium doped bismuthate glass waveguide laser," Opt. Lett. **37**, 1691-1693 (2012).
115. R. Mary, G. Brown, S. J. Beecher, R. R. Thomson, D. Popa, Z. Sun, F. Torrisi, T. Hasan, S. Milana, F. Bonaccorso, A. C. Ferrari, and A. K. Kar, "Evanescent-wave coupled right angled buried waveguide: Applications in carbon nanotube mode-locking," Appl. Phys. Lett. **103**, 221117 (2013).
116. J. R. Macdonald, S. J. Beecher, P. A. Berry, K. L. Schepler, and A. K. Kar, "Compact mid-infrared Cr:ZnSe channel waveguide laser," Appl. Phys. Lett. **102**, 161110 (2013).
117. D. Choudhury, W. T. Ramsay, R. Kiss, N. A. Willoughby, L. Paterson, and A. K. Kar, "A 3D mammalian cell separator biochip," Lab Chip **12**, 948-953 (2012).
118. L. V. Keldysh, "Ionization in the field of a strong electromagnetic wave," Soviet Physics JETP **20**, 1307-1314 (1965).
119. S. Nolte, J. Burghoff, M. Will, and A. Tuennermann, "Femtosecond writing of high-quality waveguides inside phosphate glasses and crystalline media using a bifocal approach," in *Commercial and Biomedical Applications of Ultrafast Lasers IV*, (2004), 164-171.
120. M. Ams, G. Marshall, D. Spence, and M. Withford, "Slit beam shaping method for femtosecond laser direct-write fabrication of symmetric waveguides in bulk glasses," Opt. Express **13**, 5676-5681 (2005).
121. R. Osellame, S. Taccheo, M. Marangoni, R. Ramponi, P. Laporta, D. Polli, S. De Silvestri, and G. Cerullo, "Femtosecond writing of active optical waveguides with astigmatically shaped beams," J. Opt. Soc. Am. B **20**, 1559-1567 (2003).
122. R. R. Thomson, A. S. Bockelt, E. Ramsay, S. Beecher, A. H. Greenaway, A. K. Kar, and D. T. Reid, "Shaping ultrafast laser inscribed optical waveguides using a deformable mirror," Opt. Express **16**, 12786-12793 (2008).
123. N. D. Psaila, R. R. Thomson, H. T. Bookey, A. K. Kar, N. Chiodo, R. Osellame, G. Cerullo, G. Brown, A. Jha, and S. Shen, "Femtosecond laser inscription of optical waveguides in Bismuth ion doped glass," Opt. Express **14**, 10452-10459 (2006).
124. R. Taylor, C. Hnatovsky, and E. Simova, "Applications of femtosecond laser induced self-organized planar nanocracks inside fused silica glass," Laser Photon. Rev. **2**, 26-46 (2008).
125. L. Sudrie, M. Franco, B. Prade, and A. Mysyrowicz, "Writing of permanent birefringent microlayers in bulk fused silica with femtosecond laser pulses," Opt Commun **171**, 279-284 (1999).

126. C. Hnatovsky, R. S. Taylor, E. Simova, P. P. Rajeev, D. M. Rayner, V. R. Bhardwaj, and P. B. Corkum, "Fabrication of microchannels in glass using focused femtosecond laser radiation and selective chemical etching," Appl. Phys. A **84**, 47-61 (2006).
127. P. Haro-González, W. T. Ramsay, L. M. Maestro, B. del Rosal, K. Santacruz-Gomez, M. del Carmen Iglesias-de la Cruz, F. Sanz-Rodríguez, J. Y. Chooi, P. R. Sevilla, M. Bettinelli, D. Choudhury, A. K. Kar, J. G. Solé, D. Jaque, and L. Paterson, "Quantum Dot-Based Thermal Spectroscopy and Imaging of Optically Trapped Microspheres and Single Cells," Small **9**, 2162-2170 (2013).
128. Y. Y. Liu and A. W. Poon, "Flow-assisted Single-beam Optothermal Manipulation of Microparticles," Opt. Express **18**, 18483-18491 (2010).
129. T. Lei and A. W. Poon, "Silicon-on-insulator multimode-interference waveguide-based arrayed optical tweezers (SMART) for two-dimensional microparticle trapping and manipulation," Opt. Express **21**, 1520-1530 (2013).
130. A. L. Barron, A. K. Kar, and H. T. Bookey, "Dual-beam interference from a lensed multicore fiber and its application to optical trapping," Opt. Express **20**, 23156-23161 (2012).